AWARD NUMBER: W81XWH-17-1-0009

TITLE: Integrin Regulation of Ferroptosis in Breast Cancer

PRINCIPAL INVESTIGATOR: Arthur M. Mercurio

CONTRACTING ORGANIZATION: University of Massachusetts Medical School

REPORT DATE: Nov 2019

TYPE OF REPORT: Final

PREPARED FOR: U.S. Army Medical Research and Materiel Command
                Fort Detrick, Maryland 21702-5012

REPORT DOCUMENTATION PAGE

1. REPORT DATE	2. REPORT TYPE	3. DATES COVERED
Nov 2019	Final	01/15/2017 – 07/14/2019

4. TITLE AND SUBTITLE	5a. CONTRACT NUMBER
Integrin Regulation of Ferroptosis in Breast Cancer	
	5b. GRANT NUMBER
	W81XWH-17-1-0009
	5c. PROGRAM ELEMENT NUMBER

6. AUTHOR(S)	5d. PROJECT NUMBER
Arthur M. Mercurio	
	5e. TASK NUMBER
	5f. WORK UNIT NUMBER
E-Mail: arthur.mercurio@umassmed.edu	

7. PERFORMING ORGANIZATION NAME(S) AND ADDRESS(ES)	8. PERFORMING ORGANIZATION REPORT NUMBER
University of Massachusetts Medical School Worcester, MA 01605	

9. SPONSORING / MONITORING AGENCY NAME(S) AND ADDRESS(ES)	10. SPONSOR/MONITOR'S ACRONYM(S)
U.S. Army Medical Research and Materiel Command Fort Detrick, Maryland 21702-5012	
	11. SPONSOR/MONITOR'S REPORT NUMBER(S)

12. DISTRIBUTION / AVAILABILITY STATEMENT

Approved for Public Release; Distribution Unlimited

13. SUPPLEMENTARY NOTES

14. ABSTRACT

The hypothesis being tested in this proposal is that breast cancer cells, especially metastatic cells, are prone to rapid increases in ROS and lipid peroxidation caused by adverse micro-environmental conditions and that these oxidative bursts could have deleterious consequences including ferroptosis. Ferroptosis is defined as an iron-dependent, non-apoptotic form of programmed cell death characterized by the accumulation of intracellular soluble and lipid reactive oxygen species (ROS). For this reason, breast tumor cells must acquire mechanisms to protect against oxidative bursts and ferroptosis to metastasize. Work accomplished during the second year of this proposal has demonstrated that matrix-detached breast carcinoma cells cluster spontaneously and that this clustering triggers an increase in lipid peroxidation that is sufficient to induce ferroptosis. We also found that clustering occurs by a mechanism that involves the cell adhesion protein PVRL4 (also known as Nectin-4). We found that this clustering process allows these cells to survive by stimulating a PVRL4/α6β4/Src signaling axis that sustains GPX4 expression and buffers against lipid peroxidation. These results indicate that ferroptosis induction depends on cell clustering in matrix-detached cells that lack α6β4 and imply that the fate of matrix-detached cells can be determined by the state of their cell–cell interactions.

15. SUBJECT TERMS
Breast cancer, Integrins, Ferroptosis, Cell Death, Metastasis, Lipid Peroxidation

16. SECURITY CLASSIFICATION OF:			17. LIMITATION OF ABSTRACT	18. NUMBER OF PAGES	19a. NAME OF RESPONSIBLE PERSON USAMRMC
a. REPORT	b. ABSTRACT	c. THIS PAGE	Unclassified	4	19b. TELEPHONE NUMBER *(include area code)*
Unclassified	Unclassified	Unclassified			

Table of Contents

1. INTRODUCTION

The goal of this Breakthrough Award application is to open a new direction in our understanding of the mechanisms that sustain the survival of breast tumor cells, a problem of paramount importance in the biology and therapy of breast cancer. Adverse conditions in the tumor microenvironment such as detachment from matrix (anoikis) and hypoxia result in cell death, and tumor cells must acquire mechanisms to resist such death to survive and progress to metastatic disease. Our interest in this area has been awakened by the discovery of a novel mode of programmed cell death termed ferroptosis, which is defined as an iron-dependent, non-apoptotic form of programmed cell death characterized by the accumulation of intracellular soluble and lipid reactive oxygen species (ROS). The overarching hypothesis to be tested is that breast cancer cells, especially metastatic cells, are prone to rapid increases in ROS and lipid peroxidation caused by adverse micro-environmental conditions and that these oxidative bursts could have deleterious consequences including ferroptosis. For this reason, breast tumor cells must acquire mechanisms to protect against oxidative bursts and ferroptosis to metastasize. One novel mechanism involves expression of the α6β4 integrin, which we postulated in the original application has the ability to regulate enzymes that buffer intracellular ROS and diminish lipid peroxidation.

Two specific aims were proposed to address our hypothesis. The first aim was to establish that the α6β4 integrin protects breast tumor cells against ferroptosis caused by adverse tumor microenvironments and the second aims was to determine the mechanism by which the α6β4 integrin protects tumor cells against ferroptosis. As reported below, we have made significant progress in achieving the goals that we outlined and the impact of the data that we have obtained has been strengthened by other developments in the field.

2. KEYWORDS
Breast cancer, Integrins, Ferroptosis, Cell Death, Metastasis, Lipid Peroxidation

3. ACCOMPLISHMENTS
What were the major goals of the project?
The major goals of the project were divided into two major tasks:

Task 1. Establish that the α6β4 integrin protects breast tumor cells against ferroptosis caused by adverse tumor microenvironments. Months 1-24.

Task 2. Determine the mechanism by which the α6β4 integrin protects tumor cells against ferroptosis. Months 6-24.

What was accomplished under these goals?
Task 1. Establish that the α6β4 integrin protects breast tumor cells against ferroptosis caused by adverse tumor microenvironments.

Task 2. Determine the mechanism by which the α6β4 integrin protects tumor cells against ferroptosis.

Both of these tasks were completed as evidenced by the publication of two manuscripts:

Brown et al., Journal of Cell Biology, 2017, 216:4287-4297. In our first manuscript, using the approaches outlined in the SOW, we established that ferroptosis resistance is mediated by the α6β4 integrin in breast cancer cell lines (see Figures 1 and 2 in the Brown et al. publication).

1a. Assay ferroptosis as a function of α6β4 expression in breast cancer cell lines. Using the approaches outlined in the SOW, we have established that ferroptosis resistance is mediated by the α6β4 integrin in breast cancer cell lines (see Figures 1 and 2 in the Brown et al. publication).

1c. Assay ferroptosis in PDX models of breast cancer. To address this task, we sorted a PDX model of triple-negative breast cancer into α6β4^{high} and α6β4^{low} populations by FACS. Subsequently, we assessed each population for sensitivity to ferroptosis using erastin. The results obtained demonstrated that the α6β4^{high} PDX cells are much more resistant to erastin-mediated ferroptosis than the α6β4^{low} low cells (see Figures 3C and 3D in the Brown et al. publication).

1e. <u>Assess the ability of matrix-detachment to induce ferroptosis</u>.   Completion of this task has resulted in a significant advancement in our understanding of the pathophysiological processes that trigger ferroptosis. We discovered that matrix-detachment of mammary epithelial and breast carcinoma cells results in death by ferroptosis unless they express the α6β4 integrin (see Figure 2 in the Brown et al. publication).

Brown et al., Journal of Biological Chemistry, 2018, 293:12741-12748.
We finalized this task in this second manuscript Specifically, we discovered that matrix-detached breast carcinoma cells cluster spontaneously and that this clustering triggers an increase in lipid peroxidation that is sufficient to induce ferroptosis (see Figures 1 and 2 in the Brown et al. publication).   We also found that clustering occurs by a mechanism that involves the cell adhesion protein PVRL4 (also known as Nectin-4). We found that this clustering process allows these cells to survive by stimulating a PVRL4/α6β4/Src signaling axis that sustains GPX4 expression and buffers against lipid peroxidation (see Figures 3-5 in the Brown et al. publication). These results indicate that ferroptosis induction depends on cell clustering in matrix-detached cells that lack α6β4 and imply that the fate of matrix-detached cells can be determined by the state of their cell–cell interactions.

Completion of these tasks provided the foundation for extending the project in a new direction to investigate the mechanism of ferroptosis resistance in breast cancer more rigorously in a third manuscript that was published recently.

Brown et al., Developmental Cell, 2019, 51:575-586.
More specifically, cells differ in their sensitivity to ferroptosis and a key challenge is to understand mechanisms that contribute to resistance. Using RNA-Seq to identify genes that contribute to ferroptosis resistance, we discovered that pro-ferroptotic stimuli including inhibition of the lipid hydroperoxidase GPX4 and detachment from the extracellular matrix (see above) induce expression of prominin2, a pentaspanin protein implicated in regulation of lipid dynamics. Prominin2 facilitates ferroptosis resistance in mammary epithelial and breast carcinoma cells. Mechanistically, prominin2 promotes the formation of ferritin-containing multi-vesicular bodies (MVBs) and exosomes that transport iron out of the cell, inhibiting ferroptosis. These findings revealed that ferroptosis resistance can be driven by a prominin2-MVB/exosome-ferritin pathway and have broad implications for iron homeostasis, intracellular trafficking and cancer. This mechanism of prominin2-mediated ferroptosis resistance has potential implications for efforts that seek to induce ferroptosis as a mode of anti-cancer therapy. For example, inhibiting GPX4 activity can selectively kill certain tumor cells via ferroptosis. Given that cells can acquire resistance to GPX4 inhibition by inducing prominin2, strategies that simultaneously block prominin2 expression or function may enhance sensitivity to GPX4 inhibitors. Indeed, analysis of the Broad Institute Cancer Therapeutics Response Portal resource indicates that high levels of prominin2 expression are significantly correlated with resistance to the GPX4 inhibitor ML210 across hundreds of cancer cells lines (https://portals.broadinstitute.org/ctrp/?featureName=PROM2). Given that prominin2 expression is correlated with poor clinical outcomes in several cancers, prominin2-mediated MVB formation and iron export may also be relevant to the emerging role of ferroptosis in tumor suppression.

What opportunities for training and professional development has the project provided?
Nothing to report

How were the results disseminated to communities of interest?
Nothing to report

What do you plan to do during the next reporting period to accomplish the goals?
This is a FINAL report

4. IMPACT

The findings that we have made with this award have significant implications for the therapeutic treatment of aggressive cancers. Although studies on the nature of cell death triggered by matrix-detachment have focused largely on apoptosis, it is becoming apparent that other modes of cell death can occur that involve elevated ROS levels. Our findings establish ferroptosis as one such ROS-mediated form of cell death. They also provide insight into the cell biological parameters that influence ferroptosis by revealing how the clustering of matrix-detached carcinoma cells can promote ferroptosis as opposed to apoptosis. On a broader level, the role of ferroptosis in eliminating matrix-detached carcinoma cells is timely and significant based on the recent realization that aggressive carcinoma cells with a mesenchymal phenotype are highly sensitive to ferroptosis unless they enable mechanisms that sustain GPX4 expression (Viswanathan et al., *Nature*, 2017, 547:453-457). A major effort is underway to develop effective GPX4 inhibitors (Hangauer et al. *Nature*, 2017, 551:247-250) but an understanding of why some breast tumor cells are resistant is critical to this endeavor. In this direction, this mechanism of prominin2-mediated ferroptosis resistance that we discovered has potential implications for efforts that seek to induce ferroptosis as a mode of anti-cancer therapy. For example, inhibiting GPX4 activity can selectively kill certain tumor cells via ferroptosis. Given that cells can acquire resistance to GPX4 inhibition by inducing prominin2, strategies that simultaneously block prominin2 expression or function may enhance sensitivity to GPX4 inhibitors. Indeed, analysis of the Broad Institute Cancer Therapeutics Response Portal resource indicates that high levels of prominin2 expression are significantly correlated with resistance to the GPX4 inhibitor ML210 across hundreds of cancer cells lines (https://portals.broadinstitute.org/ctrp/?featureName=PROM2). Given that prominin2 expression is correlated with poor clinical outcomes in several cancers, prominin2-mediated MVB formation and iron export may also be relevant to the emerging role of ferroptosis in tumor suppression.

5. CHANGES/PROBLEMS
Nothing to report.

6. PRODUCTS
The major product to report for this report are the three publications that were supported by this award:
Brown et al., Journal of Cell Biology, 2017, 216:4287-4297.
Brown et al., Journal of Biological Chemistry, 2018, 293:12741-12748.
Brown et al., Developmental Cell, 2019, 51:575-586.

7. PARTICIPANTS and OTHER COLLABORATING ORGANIZATIONS
What individuals worked on the project?
Arthur M. Mercurio   (No Change)
Caitlin W. Brown   (No Change)
John J. Amante   (No Change)

Has there been a change in the active support of PI or key personnel?
We are thankful that this Breakthrough enabled us to obtain a NIH R01 grant. This grant was awarded recently and will allow us to continue our studies on the regulation and function of ferroptosis in breast cancer with an emphasis on therapy.

1R01 CA218085-01A1 (Mercurio, PI)   07/11/18 – 06/30/23
NIH/NCI   *Integrin Regulation of Non-apoptotic Death in Breast Cancer*
The goal of this application is to understand mechanisms that enable breast tumor cells to survive under conditions that have the potential to kill them with an emphasis on ferroptosis.

What other organizations were involved as partners?
None

8. APPENDICES

We include 3 publications in the Appendix.

The α6β4 integrin promotes resistance to ferroptosis

Caitlin W. Brown, John J. Amante, Hira Lal Goel, and Arthur M. Mercurio

Department of Molecular, Cell and Cancer Biology, University of Massachusetts Medical School, Worcester, MA

Increases in lipid peroxidation can cause ferroptosis, a form of cell death triggered by inhibition of glutathione peroxidase 4 (GPX4), which catalyzes the reduction of lipid peroxides and is a target of ferroptosis inducers, such as erastin. The α6β4 integrin protects adherent epithelial and carcinoma cells from ferroptosis induced by erastin. In addition, extracellular matrix (ECM) detachment is a physiologic trigger of ferroptosis, which is evaded by α6β4. The mechanism that enables α6β4 to evade ferroptosis involves its ability to protect changes in membrane lipids that are proferroptotic. Specifically, α6β4-mediated activation of Src and STAT3 suppresses expression of ACSL4, an enzyme that enriches membranes with long polyunsaturated fatty acids and is required for ferroptosis. Adherent cells lacking α6β4 require an inducer, such as erastin, to undergo ferroptosis because they sustain GPX4 expression, despite their increase in ACSL4. In contrast, ECM detachment of cells lacking α6β4 is sufficient to trigger ferroptosis because GPX4 is suppressed. This causal link between α6β4 and ferroptosis has implications for cancer biology and therapy.

THE JOURNAL OF CELL BIOLOGY

Introduction

The ability of cells to resist death is a hallmark of tissue homeostasis and disease, especially cancer (Hanahan and Weinberg, 2011). With respect to cancer, resistance to chemotherapy-induced cell death is a problem of paramount importance (Safa, 2016). In addition, adverse conditions in the tumor microenvironment, such as detachments from matrix (anoikis), result in cell death, and tumor cells must acquire mechanisms to resist such death to survive and progress to metastatic disease (Buchheit et al., 2014). Our interest in this area has been awakened by the discovery of a novel mode of programmed cell death, termed ferroptosis. Ferroptosis is defined as an iron-dependent form of programmed cell death, which is characterized by lipid reactive oxygen species (ROS) accumulation that damages the plasma membrane by peroxidation of polyunsaturated fatty acids (Yang et al., 2016; Yang and Stockwell, 2016). At a mechanistic level, ferroptosis is triggered by the loss of activity for the lipid repair enzyme glutathione peroxidase 4 (GPX4), which catalyzes the reduction of lipid and other peroxides and is a target of several ferroptosis inducers (Yang et al., 2014). The antiporter system X_C^-, which imports cystine into the cell in exchange for glutamate, also has a critical role in protecting against ferroptosis because cysteine, the monomeric form of cystine, is converted to the antioxidant glutathione, which is a substrate for GPX4 (Yang and Stockwell, 2016). Molecules that inhibit system X_C^-, such as erastin, trigger ferroptosis, and they have proven to be useful for studying this process in detail (Dixon et al., 2012).

At present, the significance of ferroptosis in the context of epithelial and carcinoma biology is still emerging. The findings that ferroptosis inducers can inhibit the growth of tumor xenografts have heightened the cancer relevance of this mode of cell death (Yang et al., 2014; Kim et al., 2016). Although exciting, these findings do not provide insight into the mechanisms used by cells to evade ferroptosis or whether tumor cells encounter conditions that trigger ferroptosis and, consequently, whether they must acquire mechanisms to evade this process. The study that reported that p53-mediated tumor suppression involves ferroptosis (Jiang et al., 2015) provided some indication of the physiological relevance of this process in cancer. Ferroptosis also occurs in p53 mutant cells (Jiang et al., 2015) indicating that mechanisms other than loss of p53 function are involved in promoting resistance to ferroptosis.

Given the existing literature, we were intrigued by the possibility that integrin signaling protects cells from ferroptosis. We were particularly interested in the integrin α6β4 because several seminal studies have revealed that this integrin can protect epithelial and carcinoma cells from death in adverse conditions (Lipscomb and Mercurio, 2005; Giancotti, 2007), and it has been implicated in metastasis. In this study, we uncovered a key role for α6β4 in the evasion of ferroptosis, and we pursued the mechanisms involved.

Results

The integrin α6β4 promotes resistance to erastin-induced ferroptosis

Initially, we assessed the susceptibility of MCF-10A (immortalized breast epithelial cells) and SUM-159 (breast carcinoma
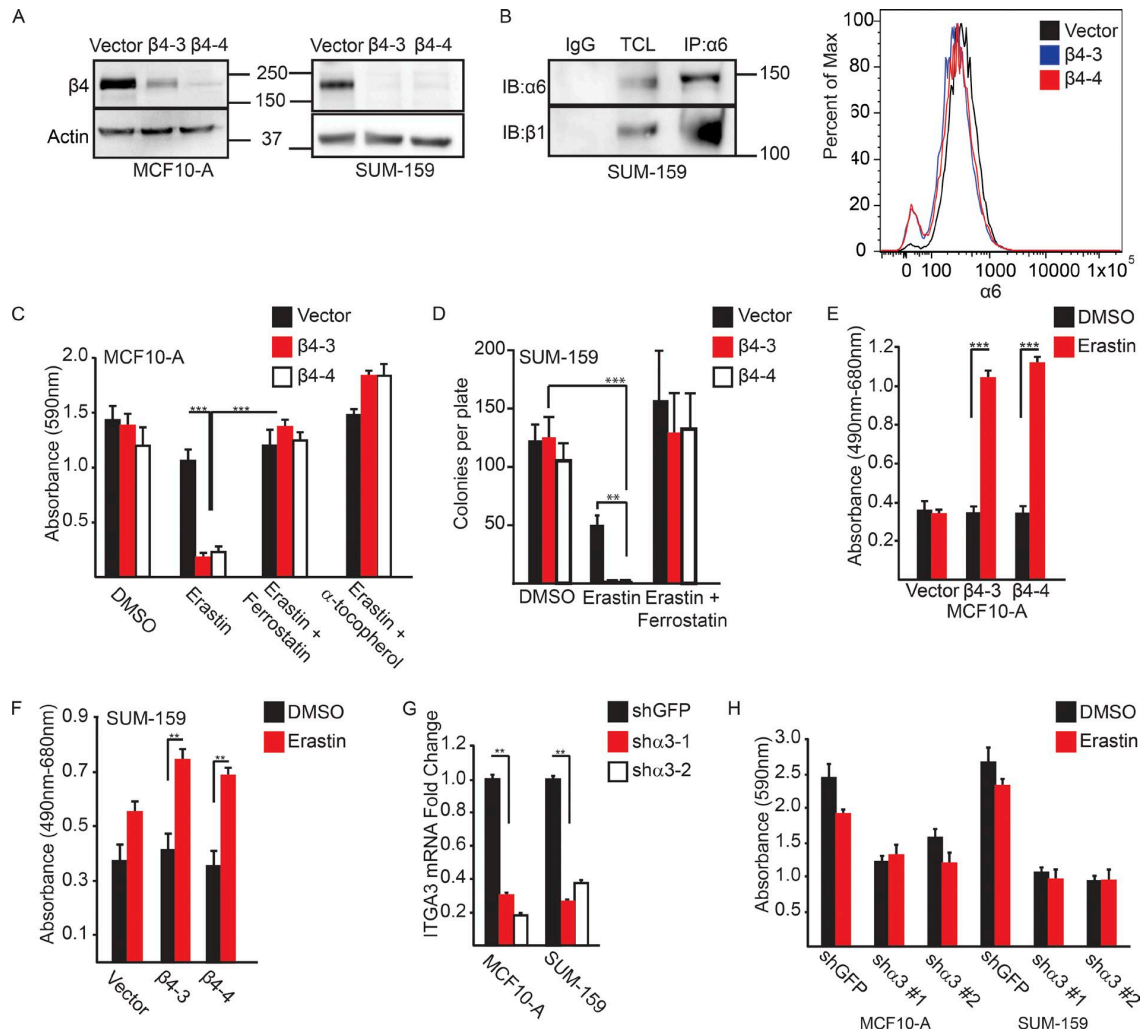
Correspondence to Arthur M. Mercurio: arthur.mercurio@umassmed.edu

Supplemental material can be found at:
http://doi.org/10.1083/jcb.201701136

Figure 1. **The α6β4 integrin promotes evasion of ferroptosis induced by erastin.** (A) The β4-integrin subunit was depleted in MCF10-A and SUM-159 cells by CRISPR/CAS9 using two independent guide RNAs (β4-3 and β4-4). Depletion of β4 expression was verified by immunoblotting. (B) Extracts of β4-depleted cells were immunoprecipitated with an α6 antibody and immunoblotted with a β1 antibody to verify that these cells express α6β1 (left blot). Vector control and β4-depleted cells were assessed for surface expression of the α6-integrin by flow cytometry. (C and D) Control and β4-depleted MCF10-A or SUM-159 cells (5 × 10²) were plated in 60-mm dishes in the presence of either DMSO, 10 µM erastin, erastin and 2 µM ferrostatin-1, or erastin and 500 µM α-tocopherol, and survival was quantified after 7 d by either DMSO extraction of crystal violet-stained cells or colony counting, respectively. (E and F) MCF10-A or SUM-159 vector control and β4-depleted cells were assayed for LDH after 6 h of treatment with either DMSO control or 10 µM erastin. (G) shRNA-mediated depletion of the α3-integrin subunit in MCF10-A and SUM-159 cells was confirmed by qPCR after 7 d of puromycin selection. (H) MCF10-A and SUM-159 α3-depleted cells were plated at clonal density, and survival was quantified as in C and E. All experiments were performed independently three times, and a representative experiment is shown. The bars in graphs represent means ± SD. *, P < 0.05; **, P < 0.01; ***, P < 0.005.

cells) to undergo cell death after treatment with erastin, a ferroptosis inducer (Dixon et al., 2012) as a function of α6β4 expression. For that purpose, we generated a CRISPR/Cas9 deletion of the β4 subunit of the α6β4 heterodimer (Fig. 1 A), leaving the α6β1 heterodimer intact, as assessed by immunoblotting and flow cytometry (Fig. 1 B). We observed that MCF-10A cells that lacked α6β4 were significantly less viable in the presence of erastin compared with control cells, as assessed by colony formation assays (Fig. 1 C). The loss of viability in α6β4-depleted cells in response to erastin was rescued by the addition of ferrostatin-1, a specific inhibitor of ferroptosis (Dixon et al., 2012), or by the addition of lipophilic antioxidant α-tocopherol (Fig. 1 C). Similar results were obtained with SUM-159 cells (Fig. 1 D). Given that ferroptosis is a form

of programmed necrosis (Dixon et al., 2012), we used the lactate dehydrogenase (LDH) assay to assess cytotoxicity in response to erastin. Treatment of α6β4-depleted MCF-10A cells (Fig. 1 E) or SUM-159 cells (Fig. 1 F) with erastin significantly increased extracellular LDH activity, which was not observed with control cells.

An important issue is whether the ability of α6β4 to evade erastin-induced ferroptosis is specific to this integrin. As shown in Fig. 1 B, α6β4-depleted cells expressed the α6β1 integrin, but that integrin was not sufficient to evade ferroptosis under those conditions. We also targeted the α3β1 integrin because it is a laminin receptor expressed by epithelial and carcinoma cells (DiPersio et al., 1997). Expression of the α3 subunit was diminished in both MCF-10A and SUM-159 cells

using shRNAs, and α3 mRNA expression was evaluated by quantitative PCR (qPCR; Fig. 1 G). The α3-depleted cells, in contrast to the β4-depleted cells, were not sensitive to erastin, although they did form significantly fewer colonies than control cells did (Fig. 1 H).

ECM detachment triggers ferroptosis: Evasion by α6β4

The ability of the integrin α6β4 to protect against erastin-induced ferroptosis has important implications for drug targeting. Nonetheless, little is known about pathophysiological stimuli that trigger ferroptosis. Based on previous work indicating that α6β4 can promote cell survival in stress conditions (Bachelder et al., 1999; Zahir et al., 2003), we assessed the susceptibility of α6β4-depleted cells to ferroptosis after detachment from the ECM. We observed that ECM-detached MCF-10A and SUM-159 cells lacking α6β4, but not control cells, exhibited a substantial decrease in viability after 24 h (Fig. 2 A). Ferrostatin-1 treatment of α6β4-depleted cells resulted in a partial rescue of the viability of matrix-detached cells (Fig. 2 A). Similar results were obtained with Hs578t cells, another breast cancer cell line (Fig. 2 B). Treatment with other ferroptosis inhibitors, including liproxstatin-1 (Fig. 2 C; Friedmann Angeli et al., 2014), the iron chelator deferoxamine (DFO), trolox, and α-tocopherol (Dixon et al., 2012), also resulted in a partial rescue of cell death caused by matrix detachment and loss of α6β4 (Fig. 2 D). Detachment of α6β4-depleted cells increased cytotoxicity significantly compared with control cells, as assessed by the LDH assay, and that increase was prevented by ferrostatin-1 (Fig. 2 E).

We also assayed cell viability as a function of time in the presence of ferrostatin-1 using control and α6β4-depleted cells (Fig. 2 F). That analysis revealed that ferroptosis occurs rapidly in the absence of α6β4 (between 4 and 12 h), which is consistent with the LDH data on adherent cells treated with erastin (Fig. 1, E and F). Because anoikis has been studied primarily as a form of apoptosis (Meredith et al., 1993; Frisch and Francis, 1994), we compared the ability of carbobenzoxy-valyl-alanyl-aspartyl-[O-methyl]-fluoromethylketone (Z-VAD-FMK) and ferrostatin-1 to rescue the viability of α6β4-depleted cells after ECM detachment. Each of those inhibitors individually was able to affect a partial rescue, and the combination of both inhibitors rescued viability completely (Fig. 2 G).

To control for the specificity of α6β4 depletion, we engineered a β4 expression construct that could not be targeted by CRISPR–Cas9. Expression of that construct in α6β4-depleted cells protected those cells from the loss of viability caused by ECM detachment (Fig. 3 A). We also assessed the viability of the MCF10-A and SUM-159 α3-depleted cells used in Fig. 1 G in detached conditions and found a moderate decrease in viability that was not rescued with ferrostatin-1 (Fig. 3 B).

We extended our analysis of ferroptosis induced by ECM detachment to human breast tumors. For that purpose, we used patient-derived xenografts (PDXs) of triple-negative breast tumors. After isolation, dissociation, and lineage depletion, tumor cells were sorted based on the level of β4 surface expression into β4[high] and β4[low] populations, taking the top and bottom quartiles, respectively (Fig. 3 C). Those two populations were assessed for viability in detached conditions, either in the presence or absence of ferrostatin-1. Under those conditions, the β4[low] population was significantly less viable than the β4[high] population, and that loss of viability was rescued by ferrostatin-1 (Fig. 3 D).

Src, which is activated by α6β4, protects against ferroptosis

The signaling pathways that enable cells to evade ferroptosis are poorly understood. We focused on the potential role of Src, because several studies have documented the robust activation of Src by α6β4, and examined the functional consequences (Gagnoux-Palacios et al., 2003; Bertotti et al., 2006; Merdek et al., 2007; Dutta and Shaw, 2008; Yang et al., 2010; Sharma et al., 2012; Pavlova et al., 2013; Hoshino et al., 2015). Activation of Src in α6β4-depleted MCF-10A and SUM-159 cells was significantly reduced compared with vector controls, as assessed by Y418 immunoblotting (Fig. 4 A), indicating that α6β4 promotes Src activation in ECM detachment. To evaluate a causal role for Src activation in ferroptosis evasion, control cells were treated with the Src inhibitor PP2 and assayed for viability 24 h after detachment (Fig. 4 B). Strikingly, Src inhibition decreased cell viability significantly, and that loss of viability was rescued by ferrostatin-1 and other ferroptosis inhibitors (Fig. 4 B).

Next, we assessed Src activation in adherent cells in response to erastin based on the assumption that erastin treatment stresses cells and elicits a response to diminish that stress. Indeed, erastin treatment of control MCF-10A and SUM-159 cells significantly increased Src activation compared with α6β4-depleted cells (Fig. 4 C). Moreover, the viability of detached, α6β4-depleted cells was rescued by expression of an inducible, constitutively active Src (Fig. 4 D). These findings support the hypothesis that α6β4 facilitates Src activation in response to stress (ECM detachment or inhibition of the system X_C^- by erastin).

In pursuit of the mechanism by which Src activation protects against ferroptosis, we were intrigued by the recent studies that found the enzyme acyl-CoA synthetase long-chain family member 4 (ACSL4) is required for ferroptosis because it synthesizes polyunsaturated fatty acids that are the primary target of lipid peroxidation (Doll et al., 2017). We quantified *ACSL4* mRNA expression in MCF10-A and SUM-159 control and α6β4-depleted cells in adherent and detached conditions (Fig. 5 A) and found a significant elevation of *ACSL4* mRNA with the loss of α6β4 in both conditions. This elevation of ACSL4 expression was also seen at the protein level in α6β4-depleted cells (Fig. 5 B). Src inhibition increased *ACSL4* expression in control cells (Fig. 5 C), indicating that it has a causal role in regulating this key ferroptotic enzyme. Moreover, reexpression of the β4 subunit in α6β4-depleted cells repressed *ACSL4* (Fig. 5 D), confirming that the repression of *ACSL4* expression is specific to α6β4-mediated signaling. Inhibition of ACSL4 using the thiazolidinedione rosiglitazone (Askari et al., 2007; Doll et al., 2017) increased the viability of detached, α6β4-depleted cells, confirming the key role of ACSL4 in ferroptosis susceptibility (Fig. 5 E). In addition, expression of constitutively active Src suppressed the expression of ACSL4 (Fig. 5 F). These in vitro data were substantiated by comparing β4 and ACSL4 expression in a cohort of patients with breast cancer using cBioportal, where a significant inverse correlation was detected (Fig. 5 G).

The preceding data raise the issue of how α6β4-mediated Src activation represses ACSL4 expression. We focused on STAT3 because it can be activated by Src (Yu et al., 1995) and, more specifically, by the α6β4-Src signaling axis (Guo et al., 2006). Moreover, STAT3 can repress, as well as activate, transcription (Niu et al., 2005). Using the ENCODE database, we identified STAT3 binding in several regions of the *ACSL4*
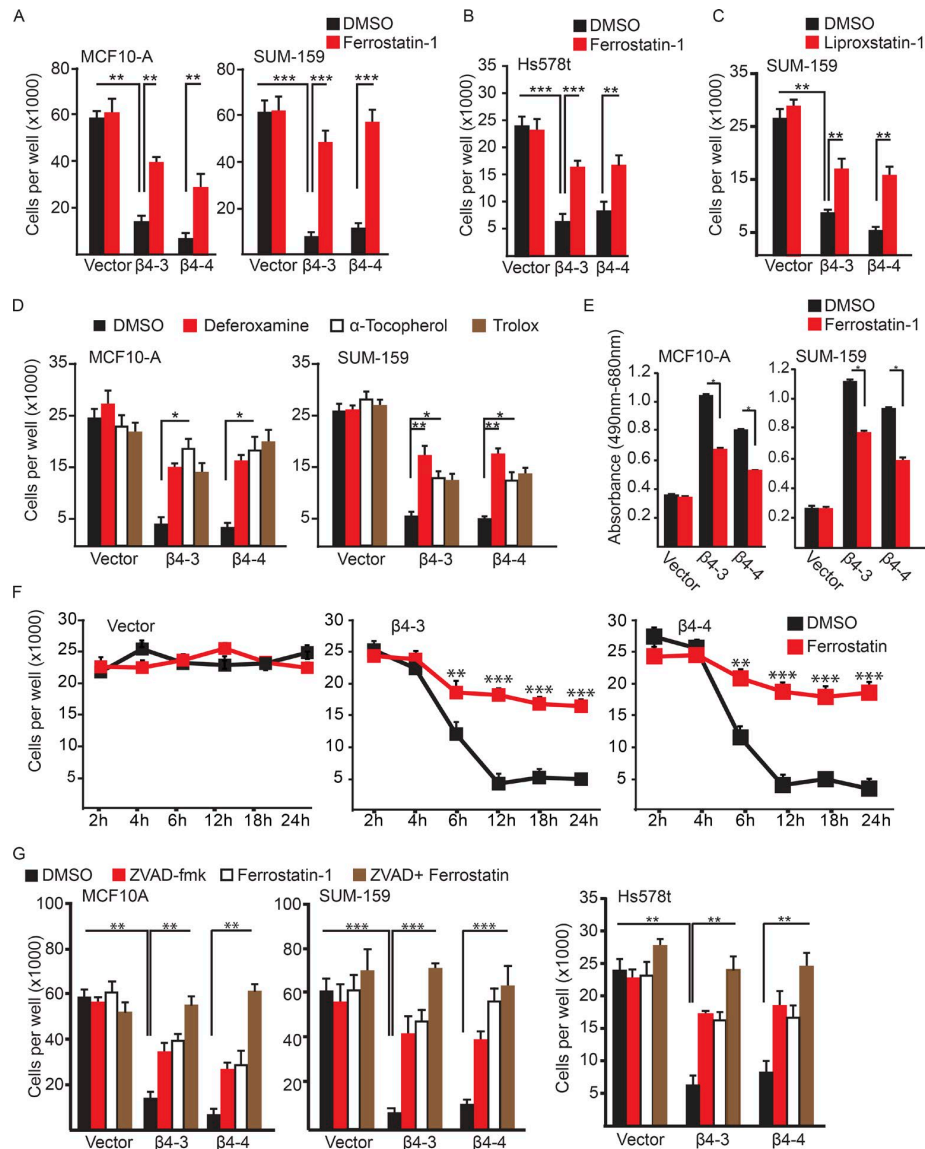
Figure 2. **Matrix-deprived cells are susceptible to ferroptosis in the absence of the α6β4-integrin.** (A) Control and β4-depleted cells were detached for 24 h in the presence of either DMSO or 2 µM ferrostatin-1, and the number of viable cells was quantified. (B) Control and β4-depleted Hs578t cells were detached for 24 h in the presence of either DMSO or 2 µM ferrostatin-1, and the number of viable cells was quantified. (C) Control and β4-depleted SUM-159 cells were detached for 24 h in the presence of either DMSO or 2 µM liproxstatin-1, and the number of viable cells was quantified. (D) Control and β4-depleted MCF-10A and SUM-159 cells were detached for 24 h in the presence of either DMSO, 100 µM DFO, 100 µM α-tocopherol, or 500 µM Trolox, and the number of viable cells was quantified. (E) MCF-10A or SUM-159 vector control and β4-depleted cells were assayed for LDH after 6 h of detachment with either DMSO or 2 µM ferrostatin-1. (F) Vector and β4-depleted cells were incubated for the times indicated with either DMSO or 2 µM ferrostatin-1, and viable cells were quantified. (G) Vector and β4-depleted cells were detached for 24 h in the presence of either DMSO, 2 µM ferrostatin-1, 25 µM Z-VAD-FMK, or ferrostatin-1 and Z-VAD-FMK, and the number of viable cells was quantified. All experiments were performed independently three times and a representative experiment is shown. The bars in graphs represent means ± SD. *, P < 0.05; **, P < 0.01; ***, P < 0.005.

promoter and coding regions of MCF10A cells (Fig. 6 A). We also observed that STAT3 phosphorylation was decreased in α6β4-depleted cells compared with control cells after erastin treatment (Fig. 6, B and C) and ECM detachment (Fig. 6, D and E). In addition, inhibition of STAT3 using 5,15-diphenylpor-phyrin (DPP) increased ACSL4 expression (Fig. 6 F). DPP had no effect on cell viability during the course of that assay (un-published data). Collectively, these data indicate that α6β4-me-diated Src–STAT3 activation represses expression of ACSL4, rendering the cell unable to undergo to ferroptosis.

ECM detachment requires an up-regulation of GPX4 to avoid ferroptosis

One question that arises from these data is why adherent, α6β4-depleted cells require erastin treatment to induce ferro-ptosis, whereas the same cells in ECM-detached conditions undergo ferroptosis spontaneously? As mentioned, ACSL4 is necessary, but not sufficient, for ferroptosis (Doll et al., 2017). Therefore, we sought to identify a regulator of ferroptosis that was altered in detached, but not adherent, conditions. We fo-cused on GPX4 because of its central role in ferroptosis and
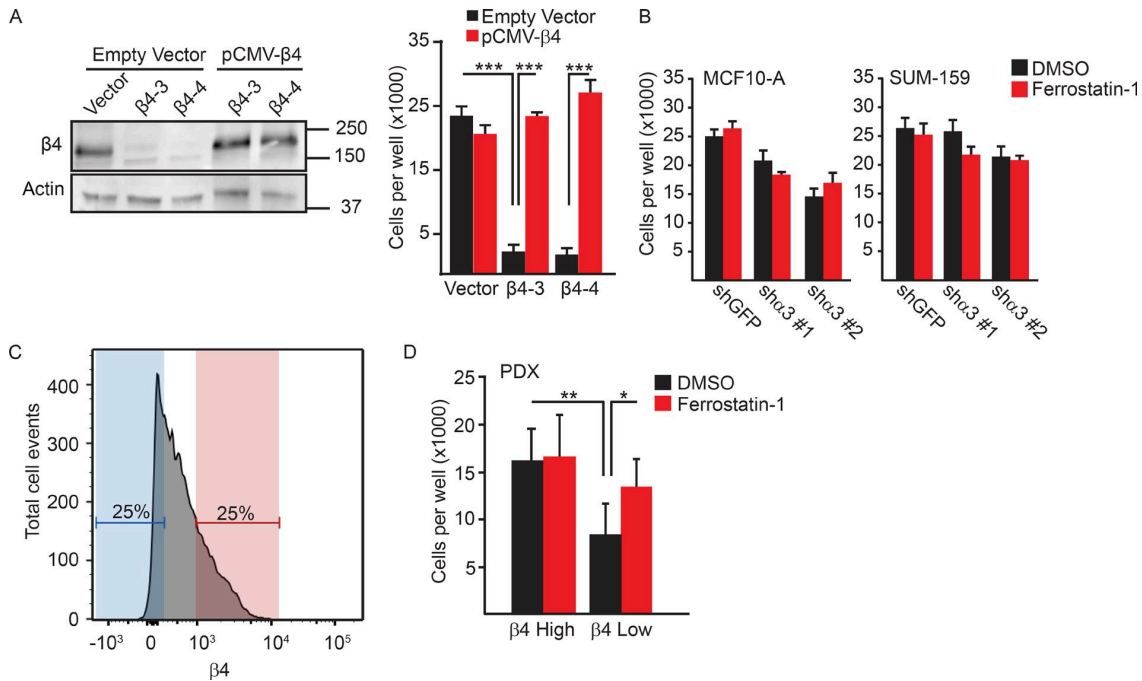
Figure 3. **Evasion of ferroptosis is specific to the α6β4-integrin.** (A) β4-depleted SUM-159 cells were transfected with either a control plasmid (vector) or a β4 expression construct in which the PAM sequences targeted by the guide RNAs were mutated. Rescue of β4 expression was confirmed by immunoblotting and qPCR. Vector control cells, β4-depleted cells, vector control cells transfected with β4 containing PAM mutations, and β4-depleted cells transfected with β4 containing PAM mutations (β4-rescued cells) were detached for 24 h, and the number of viable cells was quantified. (B) MCF10-A and SUM-159 α3-depleted cells were detached and compared with control cells for their viability after 24 h. (C and D) PDXs of triple-negative breast tumors were isolated, dissociated, and lineage-depleted, and the tumor cells were sorted based on the level of β4 surface expression into β4[high] (red) and β4[low] (blue) populations. Those two populations were assessed for viability in detached conditions, either in the presence or absence of ferrostatin-1. All experiments were performed independently three times, and a representative experiment is shown. The bars in graphs represent means ± SD. *, P < 0.05; **, P < 0.01; ***, P < 0.005.

its ability to buffer lipid peroxidation. Moreover, GPX4 is the only glutathione peroxidase that accepts phospholipid hydroperoxides in membranes as oxidizing substrates (Thomas et al., 1990; Roveri et al., 1994; Seiler et al., 2008). There was no significant difference in GPX4 expression in adherent conditions between control and α6β4-depleted cells (Fig. 7 A). However, we observed that ECM detachment caused an increase in GPX4 expression and that cells lacking α6β4 were unable to sustain *GPX4* mRNA expression (Fig. 7 A). That inability to up-regulate GPX4 was also seen at the protein level, and expression levels were rescued with exogenous β4 (Fig. 7 B).

Given that GPX4 buffers lipid peroxidation (Kriska and Girotti, 2005), we quantified lipid peroxidation in ECM-detached cells using the malondialdehyde (MDA) assay and observed that is was significantly greater in α6β4-depleted cells than it was in control cells (Fig. 7 C). In adherent conditions, loss of α6β4 increases lipid peroxidation compared with vector control; however, the loss of ECM contact significantly increases the burden of lipid peroxidation in those α6β4-depleted cells. Accordingly, glutathione peroxidase activity was elevated in detached, vector-controlled MCF10-A and SUM-159 cells compared with α6β4-depleted cells (Fig. 7 D).

To test whether the loss of GPX4 was responsible for the ferroptosis observed in α6β4-depleted cells upon ECM detachment, we expressed exogenous GPX4 in control and α6β4-depleted cells (Fig. 7 E). Exogenous GPX4 expression reduced cell death significantly in ECM-detached MCF10-A and SUM-159 cells lacking α6β4, but it had no effect on the viability of control

cells (Fig. 7 F). Importantly, α6β4-depleted cells that expressed exogenous GPX4 were sensitive to erastin, consistent with the fact that system X_C^-, which is the target of erastin, functions upstream of GPX4 (Yang and Stockwell, 2016; Fig. 7 G).

Discussion

This study advances our knowledge of ferroptosis with respect to physiologic processes that trigger this form of cell death and mechanisms used by cells to resist it. As discussed recently, ferroptosis occurs when a "cell is sabotaged by its own ongoing normal cellular metabolic activity, such as the production of lipid hydroperoxides" and that it can be prevented if these normal activities are inhibited (Dixon, 2017). Our data substantiate that assessment and reveal that physiological (ECM detachment), as well as chemical (erastin), stimuli induce ferroptosis in epithelial and carcinoma cells. We also discovered a novel mechanism used by those cells to prevent such metabolic disruption that involves the α6β4 integrin. The fact that α6β4 expression is characteristic of epithelial and carcinoma cells suggests that those cells have acquired mechanisms to mitigate metabolic stresses that can trigger ferroptosis. Moreover, the ability of α6β4 to evade ferroptosis is not shared by other integrins expressed by those cells, including α6β1 and α3β1, based on our findings.

The key mechanism that we uncovered for the evasion of ferroptosis by α6β4 involves it ability to activate Src in stress
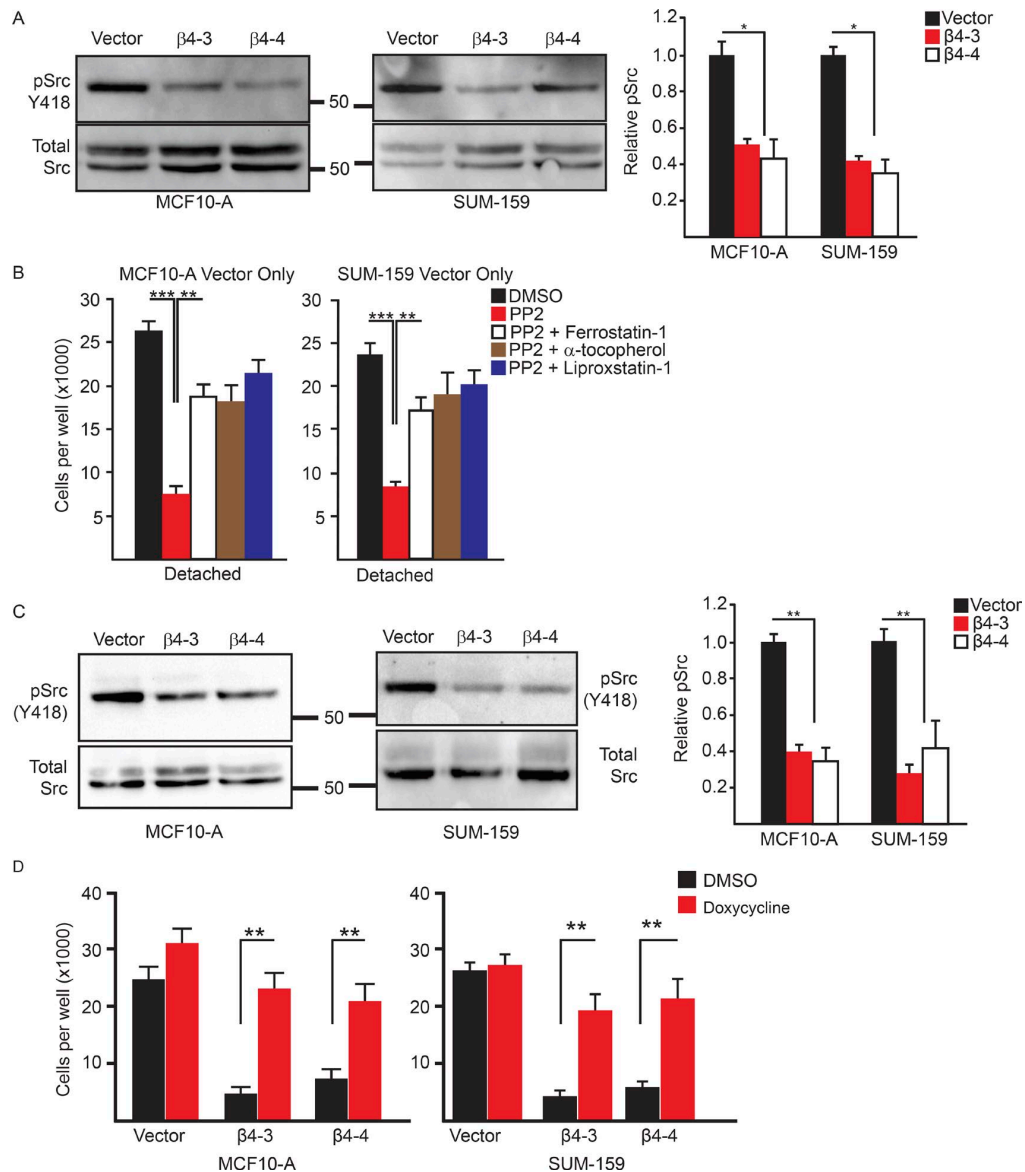
Figure 4. **The integrin α6β4 activates Src to inhibit ferroptosis.** (A) Vector control and β4-depleted cells were assessed for phosphorylated (Y418) Src by immunoblotting 3 h after ECM detachment. Relative phosphorylated Src was quantified by densitometry. (B) Vector control and β4-depleted cells were assessed for viability after 24 h of detachment in the presence of either DMSO, 10 μM PP2, PP2 and 2 μM ferrostatin-1, PP2 and 500 μM α-tocopherol, or PP2 and 2 μM liproxstatin-1. (C) Vector control and β4-depleted cells were assessed for phosphorylated (Y418) Src by immunoblotting after 3 h of incubation with 10 μM erastin. Relative phosphorylated Src was quantified by densitometry. (D) SUM-159 vector control and β4-depleted cells that expressed a doxycycline-inducible, constitutively active Src were incubated for 24 h with 2 μg/ml doxycycline and then assessed for viability after 24 h of detachment. All experiments were performed independently three times, and a representative experiment is shown. The bars in graphs represent means ± SD. *, P < 0.05; **, P < 0.01; ***, P < 0.005.

conditions and the consequent Src-mediated repression of ACSL4. ACSL4 generates a proferroptotic lipid composition in the plasma membrane, which is characterized by increased expression of long polyunsaturated ω6 fatty acids (Doll et al., 2017), and its repression nullifies the ferroptotic response (Doll et al., 2017). The α6β4-Src signaling axis is well established, and it has been implicated in the diverse functions associated with this integrin (Gagnoux-Palacios et al., 2003; Bertotti et al., 2006; Merdek et al., 2007; Dutta and Shaw, 2008; Yang et al., 2010; Sharma et al., 2012; Pavlova et al., 2013; Hoshino et

al., 2015). The ability of Src to evade ferroptosis by repressing ACSL4 via the activation of STAT3, however, is novel and it provides one of the first examples of a major signaling mechanism that has the ability to resist the altered metabolic activity that can trigger this form of cell death. We demonstrate that α6β4-mediated Src activation contributes to ferroptosis resistance, but it is likely that other modes of Src activation result in such resistance, depending on the cellular context. Although not addressed directly, it is likely that α6β4-mediated Src activation in ECM-detached cells is independent of ligand
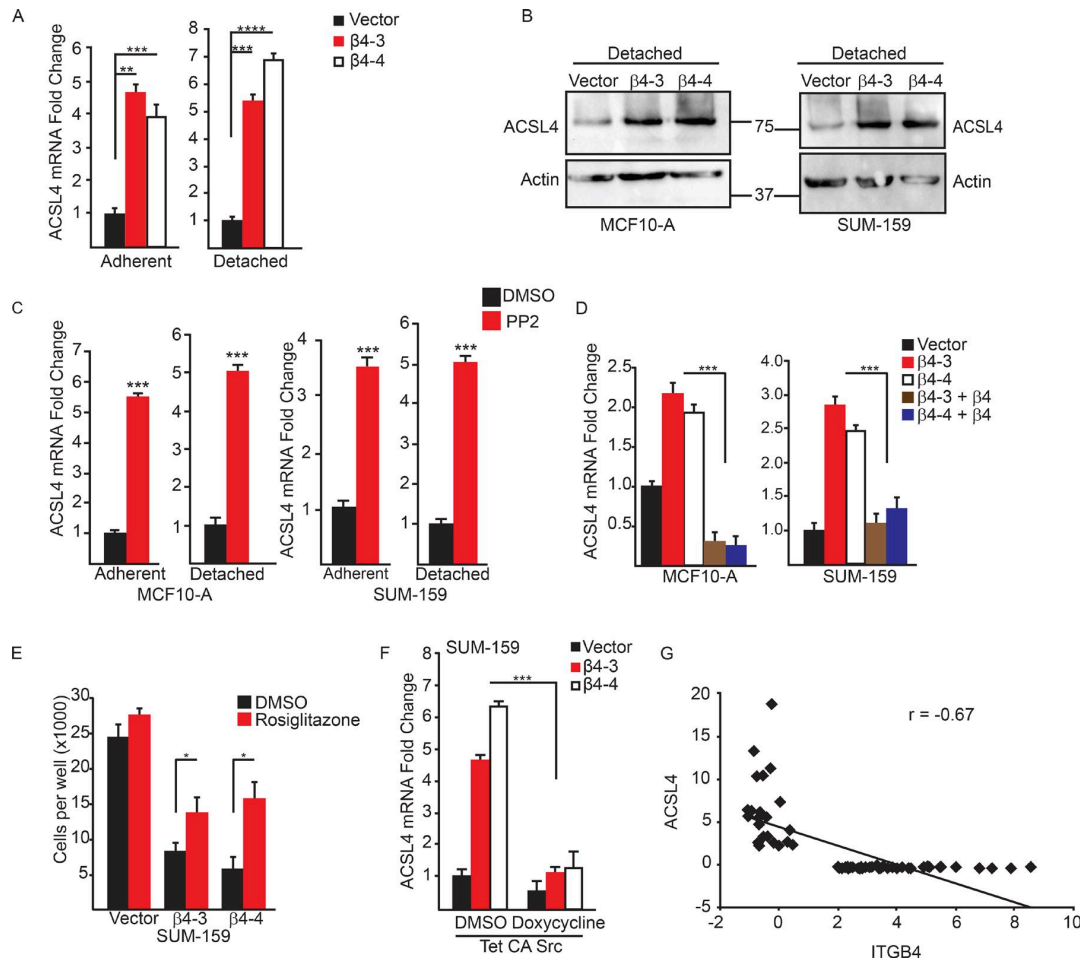
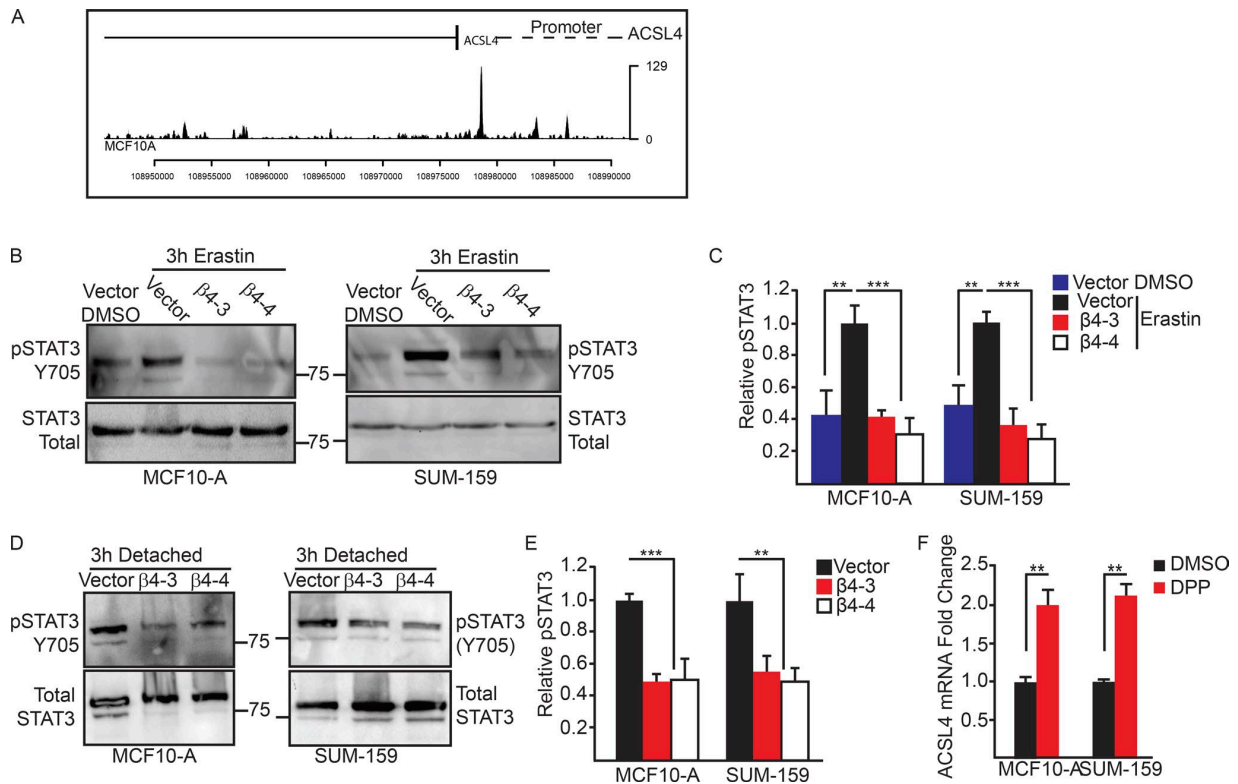Figure 5. **The integrin α6β4 represses ACSL4 to inhibit ferroptosis.** Expression of ACSL4 was assessed by qPCR (A) and immunoblotting (B) in vector control and β4-depleted cells after 2 h of ECM detachment. (C) Expression of ACSL4 was quantified by qPCR in vector control MCF10-A or SUM-159 cells under either adherent or detached conditions after 2 h of treatment with DMSO or 10 μM PP2. (D) Expression of ACSL4 was quantified in adherent vector control, β4-depleted, and β4-rescued cells by qPCR. (E) Vector control and β4-depleted cells were assessed for viability after 24 h of detachment in the presence of either DMSO or the ACSL4 inhibitor 5 μM rosiglitazone. (F) SUM-159 vector control and β4-depleted adherent cells that expressed a doxycycline-inducible, constitutively active Src were incubated for 24 h with 2 μg/ml doxycycline, and the expression of ACSL4 was quantified by qPCR. (G) Expression of ITGB4 and ACSL4 was correlated using a published gene expression database (cBioportal) comprising 70 human breast tumors. The correlation coefficient (*r*) was calculated using Pearson's correlation. Experiments were performed independently three times, and a representative experiment is shown. The bars in graphs represent means ± SD. *, $P < 0.05$; **, $P < 0.01$; ***, $P < 0.005$.

(laminin), based on previous studies that addressed this issue (Pavlova et al., 2013).

Our finding that ECM detachment triggers ferroptosis is significant because little is known about physiologic or pathophysiologic mechanisms that are linked to this cell death process. Moreover, it is widely assumed that cells undergo apoptosis in response to ECM detachment (Meredith et al., 1993; Frisch and Francis, 1994), a phenomenon referred to as anoikis (Frisch and Francis, 1994). Although the discovery of anoikis has been a significant contribution to the field, the relationships among ECM detachment and cell death mechanisms are more complex and anoikis-independent pathways are also involved (Buchheit et al., 2014). There is also evidence that ECM detachment can increase intracellular ROS and cause ROS-dependent cell death (Schafer et al., 2009), although the mechanisms involved are not well understood (Buchheit et al., 2014). Our discovery that ECM detachment can trigger ferro-

ptosis provides one mechanism for these results. As demonstrated here, ECM-detached cells are prone to both ferroptosis and apoptosis in the absence of α6β4. The apoptosis result is consistent with previous studies on this integrin (Bachelder et al., 1999; Zahir et al., 2003). Going forward, it will be important to determine the distinction between these two processes, particularly the point at which a decision is made by a cell to undergo either ferroptosis or apoptosis.

Although GPX4 is emerging as the critical gatekeeper of ferroptosis (Yang et al., 2014; Yang and Stockwell, 2016), biological mechanisms that regulate its expression or activity are poorly understood. In this direction, our findings substantiate the hypothesis that ferroptosis requires both GPX4 inhibition and ACSL4 activity. Adherent cells lacking α6β4 exhibit a significant increase in ACSL4 expression, but they are not prone to ferroptosis because GPX4 expression is sustained and it impedes lipid peroxidation. For that reason, these cells require an

Figure 6. **STAT3 represses transcription of *ACSL4* downstream of the integrin α6β4.** (A) Analysis of MCF10-A cells using the ENCODE database showed binding of STAT3 to the promoter region. The phosphorylation of STAT3 was assessed by immunoblotting in vector control and β4-depleted MCF-10A cells after 3 h of detachment (B) or after incubation with erastin (D) and was also quantified by densitometry (C and E). (F) Expression of *ACSL4* was quantified by qPCR in vector control MCF10-A and SUM-159 adherent cells after 2 h of incubation with the STAT3 inhibitor DPP. Experiments were performed independently three times, and a representative experiment is shown. The bars in graphs represent means ± SD. **, $P < 0.01$; ***, $P < 0.005$.

exogenous inhibitor of GPX4, such as erastin, to undergo ferroptosis. In contrast, ECM detachment is sufficient to trigger ferroptosis in the absence of α6β4 because lipid peroxidation increases as a result of ACSL4 induction and diminished GPX4 expression. Our data indicate that α6β4 contributes to sustaining GPX4 expression in ECM-detached cells, but the mechanism appears to be distinct from α6β4-mediated repression of ACSL4 by Src because Src inhibition does not affect GPX4 expression (unpublished data).

The findings we present have potential implications for breast and other cancers. Although much is known about the mechanisms by which α6β4 contributes to epithelial biology and breast cancer, a cohesive mechanism has not emerged, and the possibility that this integrin protects tumor cells from excessive lipid peroxidation has not been considered. This mechanism is likely to be important for metastasis because this process involves detachment from ECM or the presence of the "foreign" ECM in a distant organ (Cheung and Ewald, 2016). Moreover, we detected a significant inverse correlation between α6β4 and ASCL4 in a large cohort of patients with breast cancer, and we demonstrated that the β4[low] population isolated from PDXs of human breast cancer is much more susceptible to ferroptosis induced by ECM detachment than is the β4[high] population. This latter observation is of particular interest because some chemotherapeutic drugs, as well as more novel therapies, such as the use of nanoparticles to deliver tumor-targeting peptides, function by inducing

ferroptosis (Yang et al., 2014; Kim et al., 2016). Our data suggest that tumor cells with high α6β4 expression could be resistant to such therapies.

Materials and methods

Cell lines and reagents

MCF10-A cells were obtained from the Barbara Ann Karmanos Cancer Institute, and SUM-159 cells were provided by S. Ethier (Medical College of South Carolina, Charleston, SC). Hs578T cells were provided by D. Kim (University of Massachusetts Medical School, Worcester, MA). The pCMV-β4 plasmid was provided by L. Shaw (University of Massachusetts Medical School, Worcester, MA). A Tet-CA-Src-GFP construct was purchased from Addgene (plasmid 83469). All cells were checked quarterly for mycoplasma.

The following antibodies were used: GPX4 (Abcam), actin (Sigma-Aldrich), integrin β4 (505 [Rabinovitz et al., 1999] and 439-9b [Abcam]), α6 (GoH3; MilliporeSigma), and integrin β1 (BD), phospho-Src Y418 (R&D Systems), total Src (Santa Cruz Biotechnology, Inc.), ACSL4 (Santa Cruz Biotechnology, Inc.), phospho-STAT3 Y705 (Cell Signaling Technology), and total STAT3 (Cell Signaling Technology). Other reagents used were: Z-VAD-FMK (SelleckChem), erastin (Sigma-Aldrich), ferrostatin-1 (Sigma-Aldrich), liproxstatin-1 (Sigma-Aldrich), DFO mesylate salt (Sigma-Aldrich), α-tocopherol (Sigma-Aldrich), trolox (Sigma-Aldrich), DPP (Sigma-Aldrich), and rosiglitazone (Tocris Bioscience).
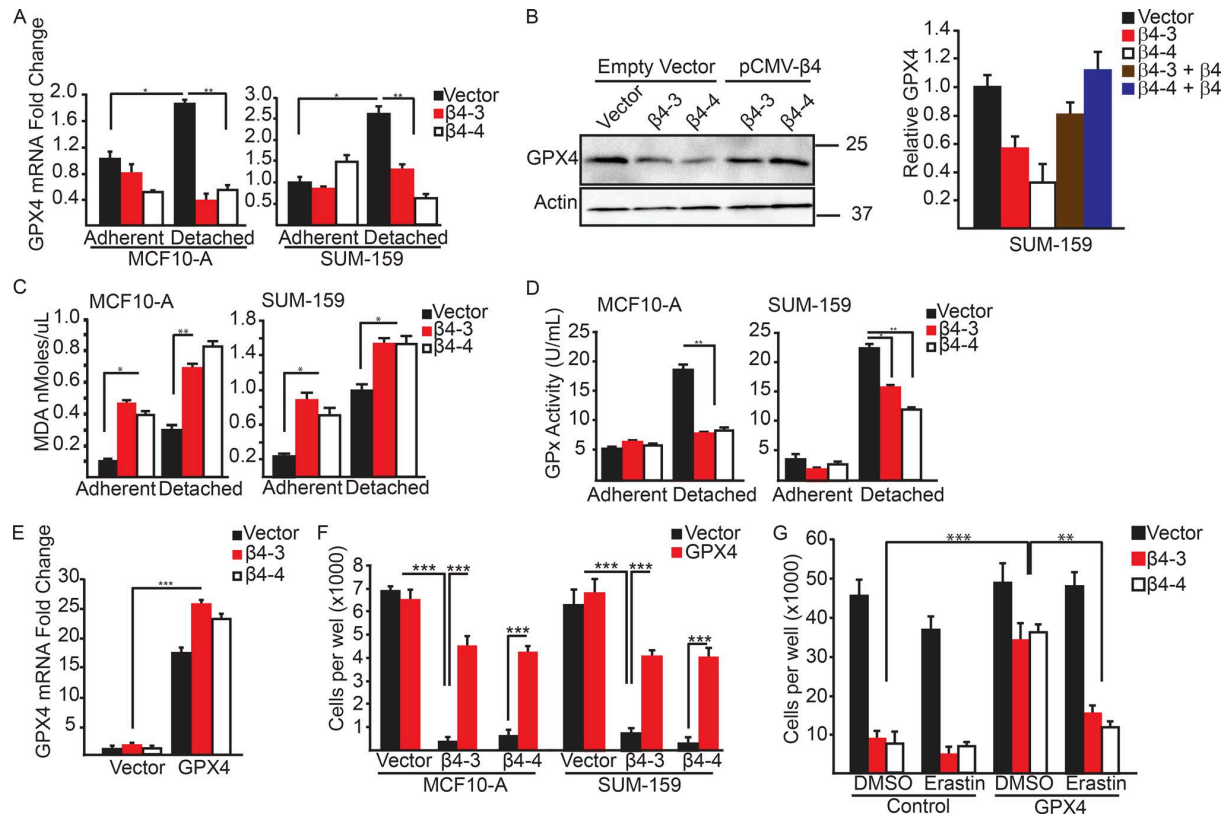
Figure 7. **Matrix-deprived cells exhibit increased lipid peroxidation and an inability to sustain GPX4 expression in the absence of the α6β4-integrin.** (A) GPX4 mRNA expression was quantified by qPCR in control and β4-depleted MCF-10A and SUM-159 cells under adherent or 2-h matrix-deprived conditions. (B) Expression of GPX4 was assessed by immunoblotting in vector control, β4-depleted, and β4-rescued cells after 2 h of detachment. Relative densitometry values are shown. (C) Lipid peroxidation was quantified using the MDA assay in control and β4-depleted, MCF-10A and SUM-159 cells under adherent or 4-h matrix-deprived conditions. (D) GPX enzyme activity was assayed in control and β4-depleted, MCF-10A and SUM-159 cells under adherent or 4-h matrix-deprived conditions. (E) Control and β4-depleted SUM-159 cells were transfected with either a vector control or a GPX4 expression vector. GPX4 mRNA expression was quantified by qPCR. (F) Control and β4-depleted MCF10-A and SUM-159 cells that had been transfected with either a vector control or a GPX4 expression vector were detached for 24 h, and the number of viable cells was quantified. (G) Control and β4-depleted cells that had been transfected with either a vector control or a GPX4 expression vector were detached for 24 h with in the presence of either DMSO or 10 μM erastin, and the number of viable cells was quantified. Experiments were performed independently three times and a representative experiment is shown. The bars in graphs represent means ± SD. *, $P < 0.05$; **, $P < 0.01$; ***, $P < 0.005$.

RNA interference

Lentiviruses containing ITGA3 shRNAs (clone ID TRCN0000057713 or TRCN0000057714; GE Healthcare) or a GFP control (RHS4459) were generated, titrated according to the manufacturer's instructions, and used to transiently infect MCF10-A and SUM-159 vector control and β4-depleted cells, following standard protocols.

PDX tumors

PDX models of triple-negative breast cancer were obtained from the Dana-Farber Cancer Institute and propagated in NSG mice. Tumors were harvested and digested using collagenase at 37°C. Once digested, the cells were filtered using a cell strainer (40 μm), washed twice with PBS, and plated in DMEM/F12 (containing 10% FBS). The next day, cells were stained using a β4 antibody for 1 h and analyzed by flow cytometry. The highest and lowest quartiles of cells expressing β4 were collected and plated immediately for experimentation.

Colony formation assay

MCF10-A and SUM-159 vector control or β4-depleted cells ($5 × 10^2$) were plated on 60-mm dishes. 24 h after plating, cells were incubated in medium containing erastin (10 μM), erastin and ferrostatin-1 (2 μM), or

DMSO control. Media were changed daily with continued exposure. 10 d after the first treatment, plates were washed in PBS, fixed in 4% paraformaldehyde, and stained in crystal violet. Plates were washed clean of excess dye and colonies >50 cells were counted. For some experiments, the crystal violet–stained cells were solubilized with DMSO, and absorbance was read at 590 nm.

Matrix-detachment assays

24-well plates were coated with poly 2-hydroxyethyl methacrylate (polyHEMA; 30 mg/ml; Sigma-Aldrich) and dried overnight. Trypsinized cells were plated ($2.5 × 10^4$ per well) in serum-free medium with the reagents indicated in the figure legends for the times noted. Cells were counted with a hemocytometer using trypan blue exclusion. Total cell number was calculated by multiplying the mean of cells per square by the dilution factor and chamber volume.

Biochemical experiments

For immunoblotting, cells were extracted using radioimmunoprecipitation assay buffer containing protease inhibitors (Boston BioProducts). Extracts were separated by SDS-PAGE and immunoblotted using the antibodies specified in the figure legends. Immunoprecipitation was

performed on precleared lysates by incubation with the primary antibody and, subsequently, protein G sepharose beads (Sigma-Aldrich). Immune complexes were dissociated, and proteins were separated by SDS-PAGE and immunoblotted as described in the figure legends. For qPCR, RNA was isolated from cells with NucleoSpin Gel and the PCR Clean-Up kit (Macherey-Nagel), and cDNAs were produced using the All-In-One cDNA Synthesis SuperMix (BioScript Solutions). qPCR was performed using a SYBR Green master mix (biotool.com). Sequences for primers used are provided in Table S1. The two-tailed Student t test was used to assess statistical significance.

To assess cytotoxicity, the LDH assay (Thermo Fisher Scientific) was used, according to the manufacturer's specifications. In brief, 5,000 cells were cultured in 96-well adherent or polyHEMA-coated plates in serum-free media for 4 h in DMSO, erastin (10 µM), or ferrostatin-1 (2 µM), as indicated. Medium from each well was reacted to form red formazan. Absorbance was read at 490 and 680 nm, and the LDH per well was calculated.

To assay lipid peroxidation, the MDA lipid peroxidation microplate assay (Sigma-Aldrich) was used according to manufacturer's specifications. In brief, cells (10^6) were cultured in serum-free medium on polyHEMA-coated plates for 4 h. Cells were collected, lysed, and reacted with thiobarbituric acid. Fluorescence was read at 532 (excitation) and 590 (emission). Lipid peroxidation levels were normalized to protein concentration. Glutathione peroxidase activity assay (BioVision) was performed according to the manufacturer's specifications. In brief, cells (10^6) were trypsinized and cultured in serum-free medium on polyHEMA-coated plates for 4 h. Cells were lysed and challenged with cumene hydroperoxide to assess the activity of glutathione peroxides. Plates were read at 340 nm 5 min after challenge. Glutathione peroxidase activity was normalized to protein concentration.

Molecular biology experiments

For CRISPR-mediated deletion of the β4 integrin subunit, guide RNAs targeting exon 1 of the β4 sequence were selected using two websites, CRISPR Design (http://crispr.mit.edu) and CRISPRdirect (https://crispr.dbcls.jp). Four guide RNAs were tested, and the two most efficient knockouts were selected and used to control for potential off-target effects. Cells were subcloned by FACS and screened for loss of protein expression by immunoblot. To rescue the β4 deletion, the protospacer-adjacent motif (PAM) sequences targeted by the guide RNAs were mutated using the New England Biolabs, Inc., Q5 site-directed mutagenesis kit in pcDNA3.1-Myc-β4 (16039; Addgene). Mutagenesis primers were designed using the New England BioLabs, Inc., BaseChanger tool. Silent mutations were used to prevent changes in the amino acid sequence (Table S1). To express constitutively active Src, MCF10-A and SUM-159 vector control or β4-depleted cells were incubated with lentiviral-packaged Tet-CA-Src-GFP for 24 h before selection with 2 µg/ml puromycin for 7 d. Src expression was induced by 24-h incubation with 2 µg/ml doxycycline. To express GPX4, a plasmid construct for GPX4 was purchased from OriGene (RC208065). Cells were transfected with 10 µg DNA using Lipofectamine 2000 (Thermo Fisher Scientific) and incubated for 48 h before use.

ENCODE database analysis

The signal of the STAT3 chromatin immunoprecipitation sequencing on the human MCF10A cell line (a stably expressed Er–Src fusion protein treated with 0.01% ethanol) was downloaded from the ENCODE project (https://www.encodeproject.org/experiments/ENCSR000DOZ /; National Human Genome Research Institute). The track was plotted with the Bioconductor trackViewer (version 1.12.0) package.

Statistical analysis

The bars in graphs represent means ± SD. All experiments were repeated at least three times. The p-value was calculated using Student's t test and a p-value <0.05 was considered significant.

Online supplemental material

Table S1 lists the primers used for qPCR and mutagenesis analyses.

References

Askari, B., J.E. Kanter, A.M. Sherrid, D.L. Golej, A.T. Bender, J. Liu, W.A. Hsueh, J.A. Beavo, R.A. Coleman, and K.E. Bornfeldt. 2007. Rosiglitazone inhibits acyl-CoA synthetase activity and fatty acid partitioning to diacylglycerol and triacylglycerol via a peroxisome proliferator-activated receptor-gamma-independent mechanism in human arterial smooth muscle cells and macrophages. *Diabetes.* 56:1143–1152. https://doi.org/10.2337/db06-0267

Bachelder, R.E., M.J. Ribick, A. Marchetti, R. Falcioni, S. Soddu, K.R. Davis, and A.M. Mercurio. 1999. p53 inhibits α6β4 integrin survival signaling by promoting the caspase 3-dependent cleavage of AKT/PKB. *J. Cell Biol.* 147:1063–1072. https://doi.org/10.1083/jcb.147.5.1063

Bertotti, A., P.M. Comoglio, and L. Trusolino. 2006. β4 integrin activates a Shp2-Src signaling pathway that sustains HGF-induced anchorage-independent growth. *J. Cell Biol.* 175:993–1003. https://doi.org/10.1083 /jcb.200605114

Buchheit, C.L., K.J. Weigel, and Z.T. Schafer. 2014. Cancer cell survival during detachment from the ECM: multiple barriers to tumour progression. *Nat. Rev. Cancer.* 14:632–641. https://doi.org/10.1038/nrc3789

Cheung, K.J., and A.J. Ewald. 2016. A collective route to metastasis: Seeding by tumor cell clusters. *Science.* 352:167–169. https://doi.org/10.1126/ science.aaf6546

DiPersio, C.M., K.M. Hodivala-Dilke, R. Jaenisch, J.A. Kreidberg, and R.O. Hynes. 1997. α3β1 Integrin is required for normal development of the epidermal basement membrane. *J. Cell Biol.* 137:729–742. https://doi .org/10.1083/jcb.137.3.729

Dixon, S.J. 2017. Ferroptosis: bug or feature? *Immunol. Rev.* 277:150–157. https ://doi.org/10.1111/imr.12533

Dixon, S.J., K.M. Lemberg, M.R. Lamprecht, R. Skouta, E.M. Zaitsev, C.E. Gleason, D.N. Patel, A.J. Bauer, A.M. Cantley, W.S. Yang, et al. 2012. Ferroptosis: an iron-dependent form of nonapoptotic cell death. *Cell.* 149:1060–1072. https://doi.org/10.1016/j.cell.2012.03.042

Doll, S., B. Proneth, Y.Y. Tyurina, E. Panzilius, S. Kobayashi, I. Ingold, M. Irmler, J. Beckers, M. Aichler, A. Walch, et al. 2017. ACSL4 dictates ferroptosis sensitivity by shaping cellular lipid composition. *Nat. Chem. Biol.* 13:91–98. https://doi.org/10.1038/nchembio.2239

Dutta, U., and L.M. Shaw. 2008. A key tyrosine (Y1494) in the β4 integrin regulates multiple signaling pathways important for tumor development

and progression. *Cancer Res.* 68:8779–8787. https://doi.org/10.1158/0008-5472.CAN-08-2125

Friedmann Angeli, J.P., M. Schneider, B. Proneth, Y.Y. Tyurina, V.A. Tyurin, V.J. Hammond, N. Herbach, M. Aichler, A. Walch, E. Eggenhofer, et al. 2014. Inactivation of the ferroptosis regulator Gpx4 triggers acute renal failure in mice. *Nat. Cell Biol.* 16:1180–1191. https://doi.org/10.1038/ncb3064

Frisch, S.M., and H. Francis. 1994. Disruption of epithelial cell-matrix interactions induces apoptosis. *J. Cell Biol.* 124:619–626. https://doi.org/10.1083/jcb.124.4.619

Gagnoux-Palacios, L., M. Dans, W. van't Hof, A. Mariotti, A. Pepe, G. Meneguzzi, M.D. Resh, and F.G. Giancotti. 2003. Compartmentalization of integrin α6β4 signaling in lipid rafts. *J. Cell Biol.* 162:1189–1196. https://doi.org/10.1083/jcb.200305006

Giancotti, F.G. 2007. Targeting integrin β4 for cancer and anti-angiogenic therapy. *Trends Pharmacol. Sci.* 28:506–511. https://doi.org/10.1016/j.tips.2007.08.004

Guo, W., Y. Pylayeva, A. Pepe, T. Yoshioka, W.J. Muller, G. Inghirami, and F.G. Giancotti. 2006. β 4 integrin amplifies ErbB2 signaling to promote mammary tumorigenesis. *Cell.* 126:489–502. https://doi.org/10.1016/j.cell.2006.05.047

Hanahan, D., and R.A. Weinberg. 2011. Hallmarks of cancer: the next generation. *Cell.* 144:646–674. https://doi.org/10.1016/j.cell.2011.02.013

Hoshino, A., B. Costa-Silva, T.L. Shen, G. Rodrigues, A. Hashimoto, M. Tesic Mark, H. Molina, S. Kohsaka, A. Di Giannatale, S. Ceder, et al. 2015. Tumour exosome integrins determine organotropic metastasis. *Nature.* 527:329–335. https://doi.org/10.1038/nature15756

Jiang, L., N. Kon, T. Li, S.J. Wang, T. Su, H. Hibshoosh, R. Baer, and W. Gu. 2015. Ferroptosis as a p53-mediated activity during tumour suppression. *Nature.* 520:57–62. https://doi.org/10.1038/nature14344

Kim, S.E., L. Zhang, K. Ma, M. Riegman, F. Chen, I. Ingold, M. Conrad, M.Z. Turker, M. Gao, X. Jiang, et al. 2016. Ultrasmall nanoparticles induce ferroptosis in nutrient-deprived cancer cells and suppress tumour growth. *Nat. Nanotechnol.* 11:977–985. https://doi.org/10.1038/nnano.2016.164

Kriska, T., and A.W. Girotti. 2005. A thin layer chromatographic method for determining the enzymatic activity of peroxidases catalyzing the two-electron reduction of lipid hydroperoxides. *J. Chromatogr. B Analyt. Technol. Biomed. Life Sci.* 827:58–64. https://doi.org/10.1016/j.jchromb.2005.03.045

Lipscomb, E.A., and A.M. Mercurio. 2005. Mobilization and activation of a signaling competent alpha6beta4integrin underlies its contribution to carcinoma progression. *Cancer Metastasis Rev.* 24:413–423. https://doi.org/10.1007/s10555-005-5133-4

Merdek, K.D., X. Yang, C.A. Taglienti, L.M. Shaw, and A.M. Mercurio. 2007. Intrinsic signaling functions of the β4 integrin intracellular domain. *J. Biol. Chem.* 282:30322–30330. https://doi.org/10.1074/jbc.M703156200

Meredith, J.E. Jr., B. Fazeli, and M.A. Schwartz. 1993. The extracellular matrix as a cell survival factor. *Mol. Biol. Cell.* 4:953–961. https://doi.org/10.1091/mbc.4.9.953

Niu, G., K.L. Wright, Y. Ma, G.M. Wright, M. Huang, R. Irby, J. Briggs, J. Karras, W.D. Cress, D. Pardoll, et al. 2005. Role of Stat3 in regulating p53 expression and function. *Mol. Cell. Biol.* 25:7432–7440. https://doi.org/10.1128/MCB.25.17.7432-7440.2005

Pavlova, N.N., C. Pallasch, A.E. Elia, C.J. Braun, T.F. Westbrook, M. Hemann, and S.J. Elledge. 2013. A role for PVRL4-driven cell-cell interactions in tumorigenesis. *eLife.* 2:e00358. https://doi.org/10.7554/eLife.00358

Rabinovitz, I., A. Toker, and A.M. Mercurio. 1999. Protein kinase C-dependent mobilization of the α6β4 integrin from hemidesmosomes and its association with actin-rich cell protrusions drive the chemotactic migration of carcinoma cells. *J. Cell Biol.* 146:1147–1160. https://doi.org/10.1083/jcb.146.5.1147

Roveri, A., M. Maiorino, C. Nisii, and F. Ursini. 1994. Purification and characterization of phospholipid hydroperoxide glutathione peroxidase from rat testis mitochondrial membranes. *Biochim. Biophys. Acta.* 1208:211–221. https://doi.org/10.1016/0167-4838(94)90106-6

Safa, A.R. 2016. Resistance to Cell Death and Its Modulation in Cancer Stem Cells. *Crit. Rev. Oncog.* 21:203–219. https://doi.org/10.1615/CritRevOncog.2016016976

Schafer, Z.T., A.R. Grassian, L. Song, Z. Jiang, Z. Gerhart-Hines, H.Y. Irie, S. Gao, P. Puigserver, and J.S. Brugge. 2009. Antioxidant and oncogene rescue of metabolic defects caused by loss of matrix attachment. *Nature.* 461:109–113. https://doi.org/10.1038/nature08268

Seiler, A., M. Schneider, H. Förster, S. Roth, E.K. Wirth, C. Culmsee, N. Plesnila, E. Kremmer, O. Rådmark, W. Wurst, et al. 2008. Glutathione peroxidase 4 senses and translates oxidative stress into 12/15-lipoxygenase dependent- and AIF-mediated cell death. *Cell Metab.* 8:237–248. https://doi.org/10.1016/j.cmet.2008.07.005

Sharma, C., I. Rabinovitz, and M.E. Hemler. 2012. Palmitoylation by DHHC3 is critical for the function, expression, and stability of integrin α6β4. *Cell. Mol. Life Sci.* 69:2233–2244. https://doi.org/10.1007/s00018-012-0924-6

Thomas, J.P., P.G. Geiger, M. Maiorino, F. Ursini, and A.W. Girotti. 1990. Enzymatic reduction of phospholipid and cholesterol hydroperoxides in artificial bilayers and lipoproteins. *Biochim. Biophys. Acta.* 1045:252–260. https://doi.org/10.1016/0005-2760(90)90128-K

Yang, W.S., and B.R. Stockwell. 2016. Ferroptosis: Death by Lipid Peroxidation. *Trends Cell Biol.* 26:165–176. https://doi.org/10.1016/j.tcb.2015.10.014

Yang, W.S., R. SriRamaratnam, M.E. Welsch, K. Shimada, R. Skouta, V.S. Viswanathan, J.H. Cheah, P.A. Clemons, A.F. Shamji, C.B. Clish, et al. 2014. Regulation of ferroptotic cancer cell death by GPX4. *Cell.* 156:317–331. https://doi.org/10.1016/j.cell.2013.12.010

Yang, W.S., K.J. Kim, M.M. Gaschler, M. Patel, M.S. Shchepinov, and B.R. Stockwell. 2016. Peroxidation of polyunsaturated fatty acids by lipoxygenases drives ferroptosis. *Proc. Natl. Acad. Sci. USA.* 113:E4966–E4975. https://doi.org/10.1073/pnas.1603244113

Yang, X., U. Dutta, and L.M. Shaw. 2010. SHP2 mediates the localized activation of Fyn downstream of the α6β4 integrin to promote carcinoma invasion. *Mol. Cell. Biol.* 30:5306–5317. https://doi.org/10.1128/MCB.00326-10

Yu, C.L., D.J. Meyer, G.S. Campbell, A.C. Larner, C. Carter-Su, J. Schwartz, and R. Jove. 1995. Enhanced DNA-binding activity of a Stat3-related protein in cells transformed by the Src oncoprotein. *Science.* 269:81–83. https://doi.org/10.1126/science.7541555

Zahir, N., J.N. Lakins, A. Russell, W. Ming, C. Chatterjee, G.I. Rozenberg, M.P. Marinkovich, and V.M. Weaver. 2003. Autocrine laminin-5 ligates α6β4 integrin and activates RAC and NFκB to mediate anchorage-independent survival of mammary tumors. *J. Cell Biol.* 163:1397–1407. https://doi.org/10.1083/jcb.200302023

Cell clustering mediated by the adhesion protein PVRL4 is necessary for α6β4 integrin–promoted ferroptosis resistance in matrix-detached cells

Caitlin W. Brown[1], John J. Amante, and Arthur M. Mercurio[2]

From the Department of Molecular, Cell, and Cancer Biology, University of Massachusetts Medical School, Worcester, Massachusetts 01605

Edited by Alex Toker

Ferroptosis is an iron-dependent form of programmed cell death characterized by the accumulation of lipid-targeting reactive oxygen species that kill cells by damaging their plasma membrane. The lipid repair enzyme GSH peroxidase 4 (GPX4) protects against this oxidative damage and enables cells to resist ferroptosis. Recent work has revealed that matrix-detached carcinoma cells can be susceptible to ferroptosis and that they can evade this fate through the signaling properties of the α6β4 integrin, which sustains GPX4 expression. Although these findings on ferroptosis are provocative, they differ from those in previous studies indicating that matrix-detached cells are prone to apoptosis via a process referred to as anoikis. In an effort to reconcile these discrepant findings, here we observed that matrix-detached epithelial and carcinoma cells cluster spontaneously via a mechanism that involves the cell adhesion protein PVRL4 (also known as Nectin-4). We found that this clustering process allows these cells to survive by stimulating a PVRL4/α6β4/Src signaling axis that sustains GPX4 expression and buffers against lipid peroxidation. In the absence of α6β4, PVRL4-mediated clustering induced an increase in lipid peroxidation that was sufficient for triggering ferroptosis. When the clustering was inhibited, single cells did not exhibit a significant increase in lipid peroxidation in the absence of α6β4, and they were more susceptible to apoptosis than to ferroptosis. These results indicate that ferroptosis induction depends on cell clustering in matrix-detached cells that lack α6β4 and imply that the fate of matrix-detached cells can be determined by the state of their cell–cell interactions.

Ferroptosis is defined as an iron-dependent form of programmed cell death that is characterized by the accumulation of intracellular soluble and lipid reactive oxygen species (ROS)[3] that damage the plasma membrane by peroxidation of polyunsaturated fatty acids (1). At a mechanistic level, ferroptosis is triggered by the loss of activity of the lipid repair enzyme GSH

peroxidase 4 (GPX4), which catalyzes the reduction of lipids and other peroxides and is a target of several ferroptosis inducers (2). The antiporter system X_C^-, which imports cystine into the cell in exchange for glutamate, also has a critical role in protecting against ferroptosis because cysteine, the monomeric form of cystine, is a building block for the antioxidant GSH, which is a co-factor for GPX4 (3, 4). Molecules that inhibit system X_C^-, such as erastin, trigger ferroptosis and have proven to be useful for studying this process in detail (4, 5).

Rapid progress is being made in unraveling the biochemical nature of ferroptosis and determining its role in specific biological and pathological processes. A central theme that is emerging from these studies is the essential role of GPX4 in enabling cells to resist ferroptosis, a role that is particularly important for more aggressive tumor cells (6). Less is known, however, about the cell biological context of the mechanisms used to either promote or evade ferroptosis. Recently, we discovered that ferroptosis is a component of cell death induced by the detachment of epithelial and carcinoma cells from the matrix (7). We also observed that the α6β4 integrin has the ability to confer ferroptosis resistance under these conditions. In other terms, matrix-detached cells undergo ferroptosis but only in the absence of α6β4. The mechanism underlying this phenomenon involves the ability of α6β4 to sustain GPX4 expression and activity in matrix-detached cells and buffer the increase in lipid peroxidation that occurs in these cells, which can trigger ferroptosis (7).

Our findings on ferroptosis are provocative, but they differ from prior studies concluding that matrix-detached cells are prone to apoptosis, a process referred to as anoikis, unless survival mechanisms are enabled (8, 9). In an effort to reconcile these discrepant findings, we observed that matrix-detached epithelial and carcinoma cells cluster spontaneously by a mechanism that involves PVRL4 (also known as Nectin-4). If this clustering is inhibited, then single cells are more susceptible to apoptosis in the absence of α6β4. Based on these observations, we explored the possibility of a functional connection between cell clustering and ferroptosis. Indeed, the data we report reveal that ferroptosis depends on cell clustering in matrix-detached cells that lack α6β4.

Results

Matrix-detached cells cluster spontaneously by a mechanism that is independent of α6β4

Our interest in understanding the distinction between ferroptosis and apoptosis in matrix-detached carcinoma cells was
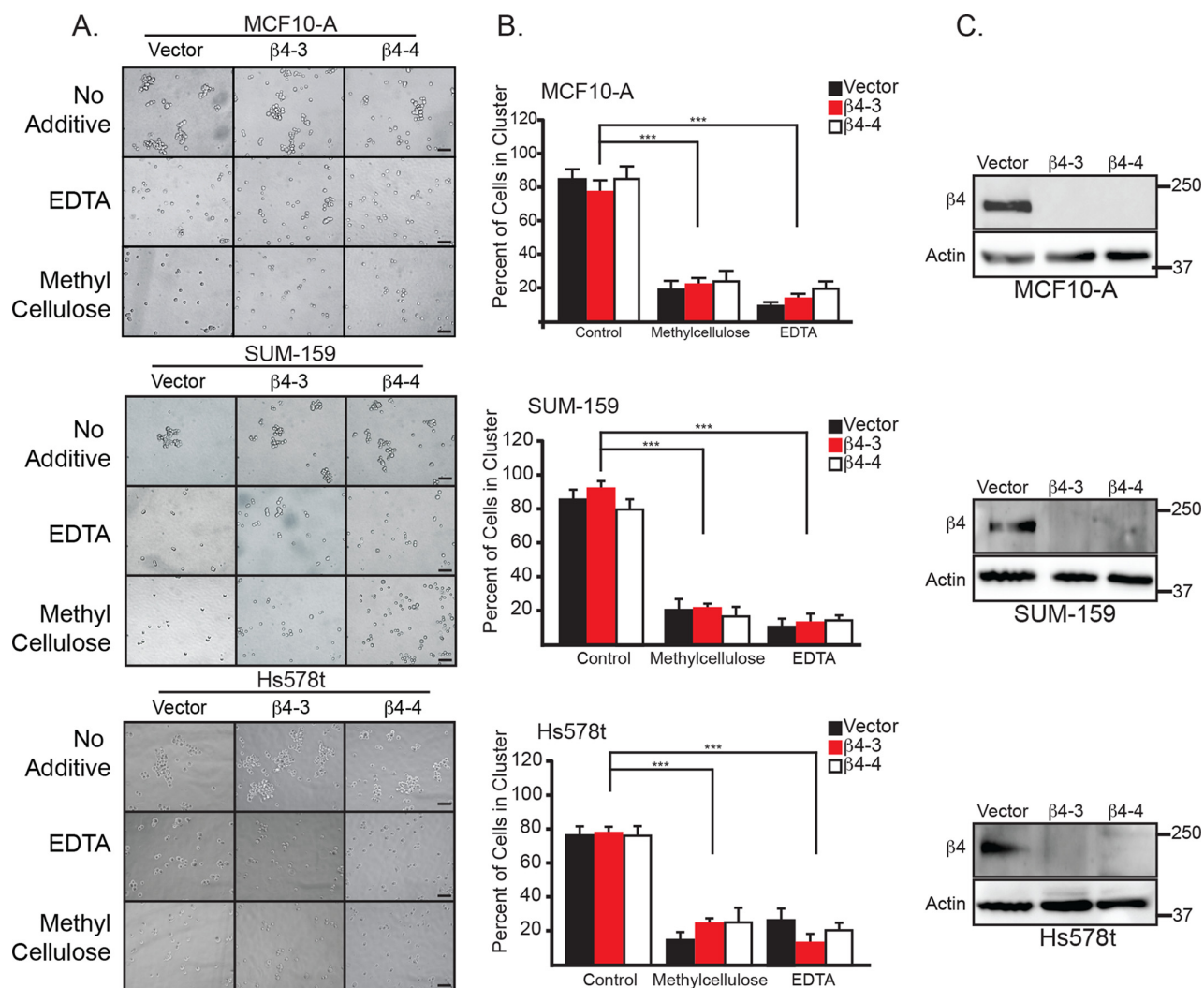
[3] The abbreviations used are: ROS, reactive oxygen species; Z-VAD-fmk, benzyloxycarbonyl-VAD-fluoromethyl ketone; MDA, malondialdehyde; Ab, antibody; pen/strep, penicillin/streptomycin; qPCR, quantitative PCR.

Figure 1. Breast epithelial and carcinoma cells preferentially cluster upon matrix detachment. *A*, MCF10-A, SUM-159, and Hs578t cells (vector and β4-depleted) were detached and allowed to cluster spontaneously or treated with either 2 mM EDTA or 0. 5% methylcellulose to generate single-cell suspensions. Photomicrographs were taken 2 h post-detachment. *Scale bars* = 10 microns. *B*, quantification of MCF10-A, SUM-159, and Hs578t clusters was performed by counting the total number of single and clustered cells, total number of clusters (defined as ≥ 3 cells). Six independent photos of each cell line and each condition were quantified. ***, *p* < 0.005. *C*, the β4 integrin subunit was depleted in Hs578t cells by CRISPR/Cas9 using two independent guide RNAs (β4-3 and β4-4). Depletion of β4 expression was verified by immunoblotting.

piqued by the observation that immortalized mammary epithelial cells (MCF10-A) and breast carcinoma cells (SUM-159 and Hs578t) cluster spontaneously upon detachment (Fig. 1, *A* and *B*). These clusters could be dissociated into single cells with either 0.5% methylcellulose or 2 mM EDTA (Fig. 1, *A* and *B*). Interestingly, we did not observe significant differences in cluster number upon depletion of α6β4 using CRISPR/Cas9 to knock down the β4 subunit using two guide RNAs that target different regions of the first exon of ITGB4 (referred to as β4-3 and β4-4) (Fig. 1, *B* and *C*), indicating that this integrin does not contribute to clustering.

Clustering of matrix-detached cells influences the relative levels of ferroptosis and apoptosis in the absence of α6β4

The observations described above prompted us to assess the role of cell clustering in ferroptosis that is triggered by the loss

of α6β4. For this purpose, we assayed cell viability 24 h after matrix detachment as a function of α6β4 expression in clustered cells or single cells (MCF10-A, SUM-159, and Hs578t) that had been generated using either methylcellulose or EDTA. These cells, which express α6β4, remained viable 24 h after matrix detachment regardless of their clustering status (Fig. 2, *A*–*C*). In response to loss of α6β4 by CRISPR/Cas9-mediated knockdown of the β4 subunit, however, a dramatic decrease in viability was seen under all conditions (Fig. 2, *A*–*C*), confirming the importance of the α6β4 integrin in maintaining survival in response to stress. It is important to note that CRISPR-mediated depletion of the β4 subunit in these cells does affect expression of the α6 integrin subunit, and they express the α6β1 integrin (7). Specificity is also evidenced by our previous finding that expression of the β4 construct that cannot be targeted by these CRISPRs in β4-depleted cells rescued their
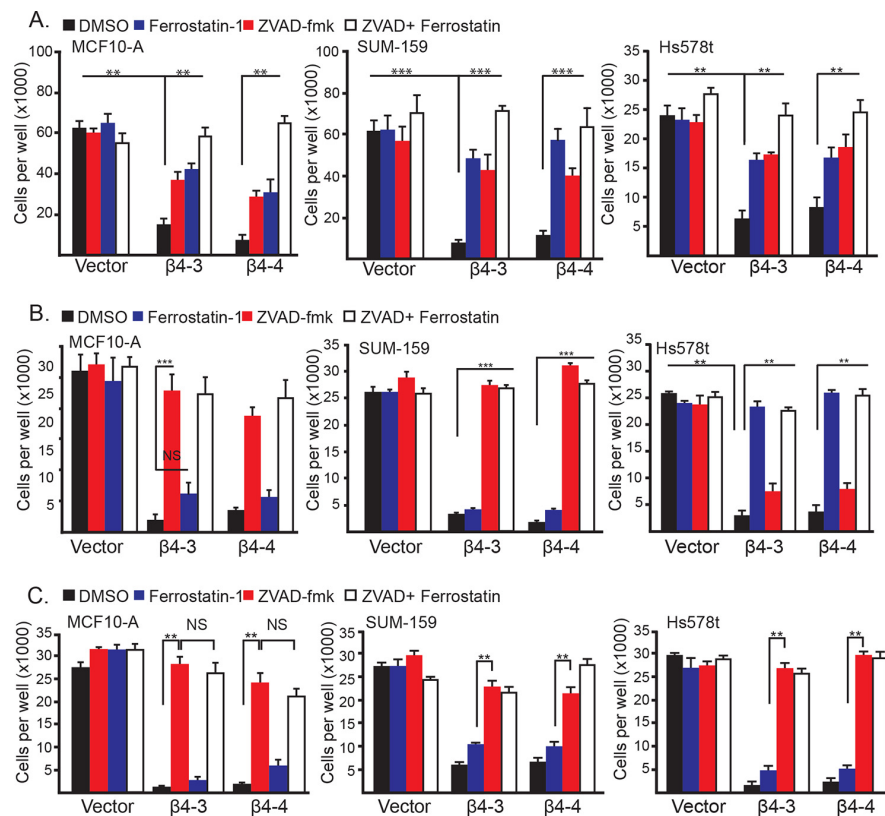
Figure 2. Clustering of matrix-detached cells influences the relative levels of ferroptosis and apoptosis in the absence of $\alpha6\beta4$. *A*, control and $\beta4$-depleted cells were detached for 24 h in the presence of either DMSO, ferrostatin-1 (2 μM), Z-VAD-fmk (25 μM), or ferrostatin-1 and Z-VAD-fmk, and the number of viable cells was quantified. *B*, control and $\beta4$-depleted cells were detached for 24 h with 2 mM EDTA in the presence of either DMSO, ferrostatin-1 (2 μM), Z-VAD-fmk (25 μM), or ferrostatin-1 and Z-VAD-fmk, and the number of viable cells was quantified. *C*, control and $\beta4$-depleted cells were detached for 24 h with 0.5% methylcellulose in the presence of either DMSO, ferrostatin-1 (2 μM), Z-VAD-fmk (25 μM), or ferrostatin-1 and Z-VAD-fmk, and the number of viable cells was quantified. *NS*, not significant. **, $p < 0.01$, ***, $p < 0.005$.

viability under matrix-detached conditions (7). Moreover, the $\alpha3\beta1$ integrin does not promote ferroptosis resistance in these cells (7).

To determine whether the nature of cell death differed between clustered and single detached cells in the absence of $\alpha6\beta4$, we compared the ability of ferrostatin-1, Z-VAD-fmk, or both inhibitors to rescue the viability of detached, $\alpha6\beta4$-depleted cells in the presence or absence of either methylcellulose or EDTA. In the absence of methylcellulose or EDTA, either inhibitor alone yielded a partial rescue of viability, and the use of both inhibitors resulted in a complete rescue (Fig. 2*A*), indicating that ferroptosis and apoptosis contribute to the death of these cells. Interestingly, though, ferrostatin-1 was unable to rescue viability in the presence of methylcellulose or EDTA (single cells), but Z-VAD-fmk did rescue viability almost completely (Fig. 2, *B* and *C*). These results indicate that cell clustering predisposes cells to ferroptosis in the absence of $\alpha6\beta4$ and that disruption of these clusters results in apoptosis. Moreover, the finding that $\alpha6\beta4$-depleted cells are prone to both ferroptosis and apoptosis in the absence of EDTA and methylcellulose probably reflects the fact that this population is comprised of a mixture of clustered and single cells (Fig. 1*A*).

Lipid peroxidation is significantly higher in clustered, detached cells compared with single cells in the absence of $\alpha6\beta4$

To understand why clustered but not single cells are prone to ferroptosis in the absence of $\alpha6\beta4$, we quantified lipid peroxidation, which is the root cause of ferroptosis, using the malondialdehyde (MDA) assay. Indeed, depletion of $\alpha6\beta4$ resulted in a marked increase in lipid peroxidation in clustered but not single cells (Fig. 3*A*). This finding suggests that the clustering of detached cells has the potential to increase lipid peroxidation to levels that are sufficient to trigger ferroptosis and that $\alpha6\beta4$ mitigates these effects on clustered cells. The observation that detached single cells do not exhibit this increase in lipid peroxidation is consistent with our finding that these cells are not susceptible to ferroptosis.

The above results suggest that $\alpha6\beta4$ function differs between detached clustered and single cells and that this integrin facilitates a mechanism to evade ferroptosis in detached, clustered cells. Based on our previous work (7), we focused on the ability of $\alpha6\beta4$ to induce GPX4 expression and activity in these distinct populations. We observed that GPX4 mRNA (Fig. 3*B*) and protein (Fig. 3*C*) expression increased significantly upon matrix detachment of clustered cells (2 h), but this increase was less
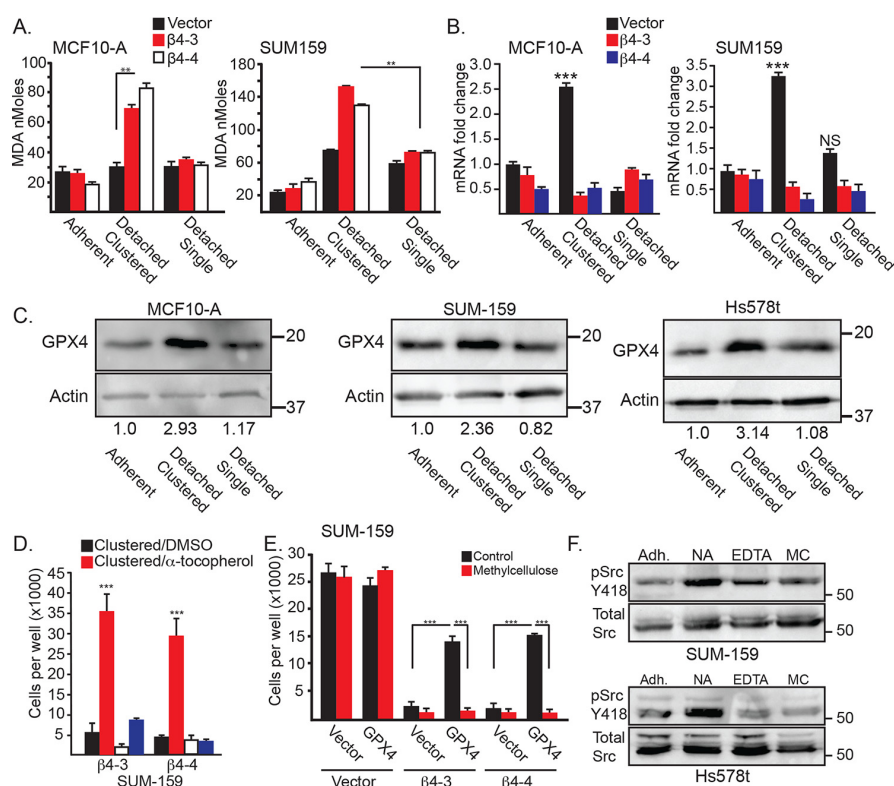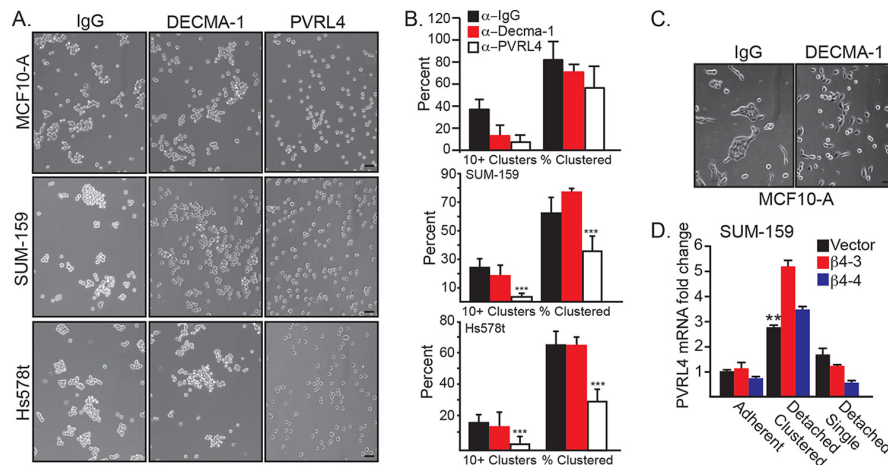
Figure 3. Clustering of matrix-detached cells influences lipid peroxidation, GPX4 expression, and Src activity. *A,* lipid peroxidation was quantified using the MDA assay in control and β4-depleted MCF10-A and SUM-159 cells under either adherent, detached clustered (no additive), or detached single (0.5% methylcellulose) conditions for 4 h. Similar results were obtained using 2 mM EDTA. *B,* GPX4 mRNA expression was quantified by qPCR in control and β4-depleted MCF10-A and SUM-159 cells under either adherent, detached clustered (no additive) or detached single (0.5% methylcellulose) conditions for 2 h. *C,* GPX4 protein expression was assessed by immunoblotting in control MCF10-A, SUM-159, and Hs578t cells under detached clustered (no additive) or detached single (0.5% methylcellulose) conditions for 4 h. Immunoblots were quantified by densitometry, and the ratio of the intensity of the GPX4/actin bands relative to adherent cells is shown under the blots. *D,* SUM-159 β4-depleted cells were detached for 24 h with either no additive (clustered) or 2 mM EDTA (single) in the presence of either DMSO or 500 mM α-tocopherol, and the number of viable cells was quantified. *E,* control and β4-depleted cells SUM-159 cells that had been transfected with either a vector control or a GPX4 expression vector were detached for 24 h with no additive (*Control*) or 0.5% methylcellulose, and the number of viable cells was quantified. *F,* SUM-159 and Hs578t control cells were assessed for phosphorylated (Tyr-418) Src by immunoblotting under adherent conditions (*Adh*) as well as following 2 h of matrix detachment with no additive (*NA*), 2 mM EDTA (*EDTA*), or 0.5% methylcellulose (*MC*). *NS,* not significant. **, $p < 0.01$, ***, $p < 0.005$.

evident in single cells. The increase in GPX4 expression depends on α6β4, consistent with our previous results (7). Moreover, the viability of the clustered, α6β4-depleted cells was rescued by either the lipophilic antioxidant α-tocopherol (Fig. 3*D*) or exogenous expression of GPX4 (Fig. 3*E*). In contrast, neither α-tocopherol nor GPX4 re-expression in α6β4-depleted, single cells rescued viability. These data infer that α6β4 signaling differs between clustered and single, matrix-detached cells. Given that the induction of GPX4 expression upon matrix detachment depends on α6β4/Src signaling (7), we assessed Src activation in detached clustered and single cells as a function of α6β4 expression. Matrix detachment caused an increase in activated Src in clustered cells, as assayed by Tyr-418 immunoblotting, that was dependent on α6β4 expression and was not detected in either EDTA- or methylcellulose-treated cells (Fig. 3*F*).

PVRL4 mediates clustering of matrix-detached cells and ferroptosis resistance

An important issue that arose from our data concerns the mechanism by which matrix-detached cells cluster and the contribution of this mechanism to ferroptosis resistance. The possibility that this clustering is mediated by E-cadherin is negated by the fact that two of the cell lines we studied (SUM-159 and Hs578t) have a mesenchymal phenotype and express little, if any, E-cadherin. We confirmed this assumption by treating matrix-detached cells with a function-blocking E-cadherin Ab (DECMA-1) and observed no effect on clustering (Fig. 4*A*). Interestingly, however, DECMA-1 had no effect on the percentage of MCF10-A cells in clusters, although it did cause a significant decrease in the number of large (10+ cells) clusters (Fig. 4*B*). In contrast, treatment of adherent MCF10-A cells with DECMA-1 disrupted cell–cell adhesion (Fig. 4*C*). For this reason, we focused on the cell surface receptor PVRL4 (also referred to as nectin-4) because it has been shown to mediate the clustering of matrix-detached carcinoma cells by interacting in *trans* with PVRL1 (10). Importantly, PVRL4 also maintains the survival of these cells by interacting with α6β4 in *cis* and enabling Src activation (10). These seminal studies, however, did not consider a potential role for PVRL4 in ferroptosis resistance. For this reason, we initially examined the ability of a function-blocking PVRL4 Ab to disrupt the clustering of

Figure 4. PVRL4 mediates clustering upon matrix detachment. *A*, MCF10-A, SUM-159, and Hs578t vector control cells were detached and allowed to aggregate in the presence of 4 μg/ml of either IgG, DECMA-1, or a PVRL4-blocking Ab. Photomicrographs were taken 2 h post-detachment. *Scale bars* = 10 μm. *B*, quantification of MCF10-A, SUM-159, and Hs578t clusters was performed by counting the total number of single and clustered cells, the total number of clusters (defined as ≥ 3 cells), and the number of large clusters (defined as ≥ 10 cells). **, $p < 0.01$, ***, $p < 0.005$. *C*, MCF10-A cells were detached and allowed to readhere in the presence of either IgG or DECMA-1. Photomicrographs were taken at 24 h. *Scale bar* = 10 μm. *D*, SUM-159 control and β4-depleted cells under adherent, detached clustered, or detached single cell conditions were assessed for expression of PVRL4 mRNA by qPCR.

matrix-detached cells and found that this Ab was as effective as either EDTA or methylcellulose in disrupting clusters into single cells (Fig. 4*A*). Depletion of β4 did not significantly affect PVRL4 expression in β4-depleted cells (Fig. 4*D*).

The above finding prompted us to assess the contribution of PVRL4 to the cell death that occurs upon matrix detachment. Matrix-detached cells that express α6β4 exhibited no significant loss of viability in response to treatment with the PVRL4 function-blocking antibody compared with the IgG control (Fig. 5*A*), supporting our conclusion that this integrin promotes the survival of clustered and single, matrix-detached cells. As we reported previously (7), matrix-detached cells that lack α6β4 exhibit a dramatic loss of viability that is rescued by ferrostatin-1. In marked contrast, α6β4-depleted cells treated with the PVRL4 function-blocking antibody exhibited a significant loss of viability that was rescued by Z-VAD-fmk and not ferrostatin-1 (Fig. 5*B*). This result indicates that disruption of PVRL4-mediated clustering of α6β4-depleted cells renders them sensitive to apoptosis as opposed to ferroptosis and that PVRL4 is necessary to execute ferroptosis in this population of cells.
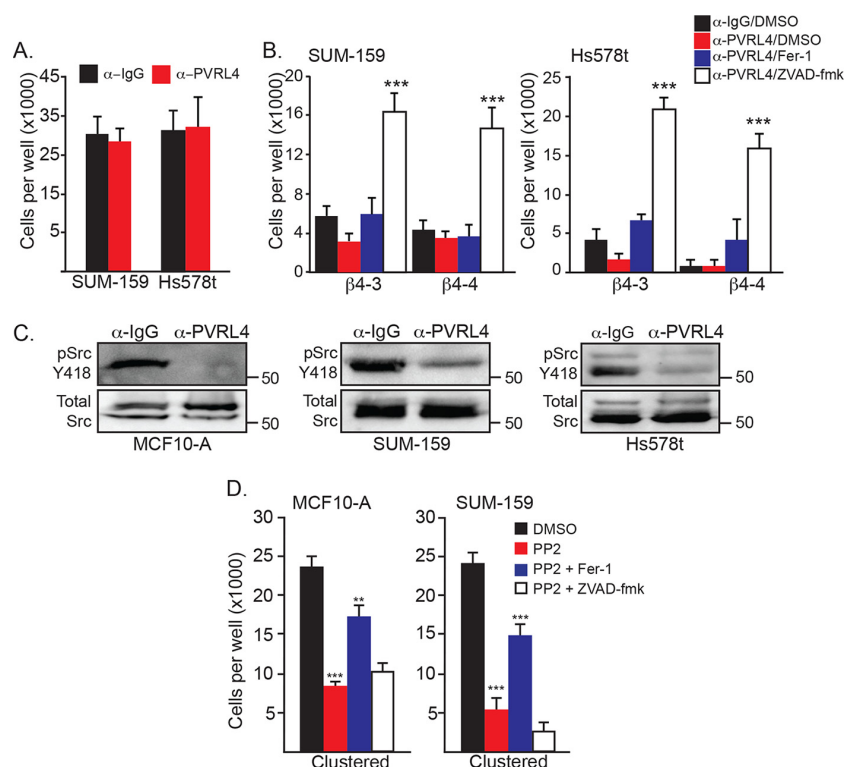
Given that α6β4-mediated Src signaling maintains the survival of matrix-detached cells (7), we examined the impact of the PVRL4 function-blocking antibody on Src activation in matrix-detached cells. Indeed, disruption of cell clustering by this antibody resulted in a significant decrease in Src activation compared with control cells, as assessed by phospho-Src (Tyr-418) immunoblotting (Fig. 5*C*). A causal role for Src activation in ferroptosis resistance is indicated by the observation that Src inhibition using PP2 decreased the viability of clustered, matrix-detached cells significantly and that this loss of viability was rescued by ferrostatin-1 but not Z-VAD-fmk. (Fig. 5*D*). Together, these results indicate that PVRL4-mediated clustering is necessary for α6β4-mediated Src activation.

Discussion

The results of this study reveal an intimate relationship between the clustering of matrix-detached carcinoma cells and ferroptosis. We conclude from our data that matrix-detached carcinoma cells cluster spontaneously and that this clustering triggers an increase in lipid peroxidation that is sufficient to induce ferroptosis. Ferroptosis can be evaded under these conditions when these cells express the α6β4 integrin, which functions to buffer lipid peroxidation by sustaining GPX4 expression. In marked contrast, dissociation of clustered, detached cells into single cells results in apoptosis in the absence of α6β4. An important and novel inference from these data is that the fate of matrix-detached cells can be determined by the state of their cell–cell interactions.

Our findings build upon the seminal study by Elledge and co-workers (10) that identified PVRL4 in a gain-of-function screen for genes that promote the survival of matrix-detached carcinoma cells. Not only did they implicate PVRL4 in the clustering of matrix-detached carcinoma cells and anoikis resistance, they also demonstrated that PVRL4 enables α6β4-mediated Src activation and the importance of this pathway in the survival of these detached cells. Our work substantiates these findings and extends them to ferroptosis resistance. Indeed, we demonstrate that the PVRL4/α6β4/Src axis allows matrix-detached cells to resist ferroptosis by sustaining GPX4 expression and minimizing lipid peroxidation, establishing a novel role for PVRL4 in ferroptosis resistance mechanisms. Interestingly, however, we also show that PVRL4 can promote ferroptosis in the absence of α6β4 by mediating cell clustering and contributing, either directly or indirectly, to increased lipid peroxidation. In other terms, this observation implies that the process of cell clustering mediated by PVRL4 stimulates an increase in lipid peroxidation by a mechanism to be determined and that this scenario does not occur in single cells, which do not engage PVRL4-mediated adhesion.

Figure 5. PVRL4-mediated cell clustering is necessary for $\alpha6\beta4$-dependent Src activation. *A*, SUM-159 and Hs578t control cells were detached for 24 h in the presence of either IgG or a PVRL4 Ab, and the number of viable cells was quantified. *B*, SUM-159 and Hs578t $\beta4$-depleted cells were detached for 24 h in the presence of either IgG and DMSO, PVRL4 Ab, PVRL4 Ab and ferrostatin-1 (2 μM), or PVRL4 and Z-VAD-fmk (25 μM), and the number of viable cells was quantified. *C*, MCF10-A, SUM-159 and Hs578t control cells were detached for 2 h in the presence of either IgG or a PVRL4-blocking Ab, and phosphorylation of Src (Tyr-418) was assessed by immunoblotting. *D*, cells (MCF10-A and SUM-159) were assessed for viability after 24 h of detachment (clustered conditions) in the presence of either DMSO, PP2 (10 μM), or PP2 in combination with either ferrostatin-1 (2 μM) or Z-VAD-fmk (25 μM). **, $p < 0.01$, ***, $p < 0.005$.

Previous studies have noted the role of cell "aggregation" in promoting apoptosis resistance in matrix-detached squamous carcinoma and ErbB2-expressing MCF10-A mammary epithelial cells (11, 12). These studies focused on cells that expressed E-cadherin, and they implicated E-cadherin as the mediator of cell aggregation and apoptosis resistance. For this reason, our finding that PVRL4 mediates the clustering of matrix-detached MCF10-A cells is intriguing and raises the need to investigate the relationship between E-cadherin- and PVRL4-mediated cell–cell adhesion. Our primary interest, however, is survival mechanisms used by aggressive carcinoma cells, which often exhibit a mesenchymal phenotype and express little, if any, E-cadherin (13). In fact, the carcinoma cell lines used in our study are mesenchymal when grown as adherent cells but retain the ability to engage in cell–cell adhesion upon matrix detachment, a scenario that mimics the transition from aggressive primary carcinomas to circulating tumor cells, which tend to cluster (14).

Although studies of the nature of cell death triggered by matrix detachment have focused largely on apoptosis, it is becoming apparent that other modes of cell death can occur that involve elevated ROS levels (15, 16). Our findings establish ferroptosis as one such ROS-mediated form of cell death. They also provide insight into the cell biological parameters that influence ferroptosis by revealing how the clustering of matrix-detached carcinoma cells can promote ferroptosis as opposed to apoptosis. On a broader level, the role of ferroptosis in eliminating matrix-detached carcinoma cells is timely and significant based on the recent realization that aggressive carcinoma cells with a mesenchymal phenotype are highly sensitive to ferroptosis unless they enable mechanisms that sustain GPX4 expression (6). Based on our data, PVRL4/$\alpha6\beta4$/Src signaling in the context of cell clustering could be one such mechanism.

Experimental procedures

Cell lines and reagents

MCF10-A cells were obtained from the Barbara Ann Karmanos Cancer Institute, and SUM-159 cells were provided by Dr. Stephen Ethier (Medical College of South Carolina). Hs578T cells were provided by Dr. Dohoon Kim (UMass Medical School). MCF10-A cells were maintained in Dulbecco's modified Eagle's medium/F-12 (Gibco) with 5% horse serum, 1% pen/strep (Gibco), 20 ng/ml epidermal growth factor (Peprotech), 0.5 mg/ml hydrocortisone (Gibco), 100 ng/ml cholera toxin (Sigma), and 10 μg/ml insulin (Sigma). SUM-159 cells were maintained in F-12 (Gibco) medium with 5% fetal bovine serum (Hyclone), 1% pen/strep, 0.5 mg/ml hydrocortisone, and 10 μg/ml insulin. Hs578t cells were maintained in Dulbecco's modified Eagle's medium high-glucose (Gibco) with 10% fetal bovine serum, 1% pen/strep, and 10 μg/ml insulin. All cells were checked quarterly for mycoplasma and authenticated

using the University of Arizona Genetic Core. The following antibodies were used: GPX4 (Abcam, ab125066), actin (Sigma-Aldrich), integrin β4 (505; Ref. 18), phospho-Src Y418 (R&D Systems, MAB2685), total Src (Santa Cruz Biotechnology, sc-8056), DECMA-1 (Abcam, ab11512), PVRL4 (R&D Systems, 17402; Cell Signaling Technology, 17402). Other reagents used were as follows: Z-VAD-fmk (SelleckChem), ferrostatin-1 (Sigma-Aldrich), α-tocopherol (Sigma-Aldrich), and PP2 (SelleckChem).

Matrix detachment assays

Twenty-four-well plates were coated with 800 μl of poly-HEMA (30 mg/ml, Sigma-Aldrich) and dried overnight at room temperature. Cells were trypsinized, and complete medium was used to quench the trypsin. Cells were counted, and the remaining suspension was diluted to 2.5×10^4 cells/100 μl and plated (100 μl/well) in cell-line specific serum-free medium with the reagents indicated in the figure legends for the times noted. Four wells were plated per condition as technical replicates. Cells were counted with a hemocytometer using trypan blue exclusion. Total cell number was calculated by multiplying average cells per square by dilution factor and chamber volume.

Biochemical experiments

For all experiments, three wells were plated per condition for each independent experiment as technical replicates, and at least three independent experiments were performed. For immunoblotting, cells collected in to prechilled tubes and spun down before washing twice in ice-cold PBS. Protein was extracted using radioimmune precipitation assay buffer containing protease and phosphatase inhibitors (Boston Bioproducts, Worcester, MA) by lysing cells for 15 min on ice, followed by centrifugation at maximum speed for 15 min at 4 °C. Supernatant was collected, and protein concentration was quantified using Bradford reagent (Bio-Rad). Samples (25 μg of protein) were separated by SDS-PAGE and immunoblotted using the Abs specified in the figure legends. For qPCR, RNA was isolated from cells using the NucleoSpin Gel and PCR Clean-Up kit (Macherey-Nagel). Briefly, cells were collected and lysed immediately following centrifugation, and RNA was isolated following the manufacturer's specifications. RNA concentrations were determined by Nanodrop, and complementary DNA (1 μg/sample) was produced using All-In-One cDNA Synthesis SuperMix (BioScript). qPCR was performed using Cyber Green Master Mix (BioTool). The sequences for primers used are as follows: 18S, 5′-AACCCGTTGAACCCCATT-3′ (forward) and 5′-CCATCCAATCG GTAGTAGCG-3′ (reverse), derived from NT_167214.1; GPX4, 5′-GAGGCAAGACCGAAGTAA-ACTAC-3′ (forward) and 5′-CCGAACTGGTTACACGG-GAA-3′ (reverse), derived from NC_000019.10.

To assay lipid peroxidation, the MDA lipid peroxidation microplate assay (Sigma-Aldrich) was used according to the manufacturer's specifications. Briefly, cells (1×10^6) were cultured in cell-line specific, serum-free medium on polyhydroxy-ethylmethacrylate (polyHEMA)– coated plates for 4 h. Three wells were plated per condition for each independent experiment as technical replicates. Cells were collected, lysed, and reacted with thiobarbituric acid for 1 h at 95 °C. An aliquot of lysate (5 μl) was saved for protein concentration determina-

tion using the Bradford assay prior to reaction with thiobarbituric acid. Fluorescence was read at 532 (excitation)/590 (emission). Lipid peroxidation levels were normalized to protein concentration.

Molecular biology experiments

For CRISPR-mediated deletion of the β4 integrin subunit, guide RNAs (sgRNA) targeting exon 1 of the β4 sequence were selected using CRISPR Design (http://crispr.mit.edu)[4] and CRISPRdirect (https://crispr.dbcls.jp; 17).[4] Four guide RNAs were tested, and the two most efficient knockouts were selected. The guide RNA sequences used were as follows: B4-3, 5′-CACCGTTGTCCAGATCATCGGACA-3′ and 5′-AAAC-TGTCCGATGATCTGG ACAAC-3′; B4-4, 5′-CACCGAAA-TCCAATAGTGTAGTCGC-3′ and 5′-AAACGCGACTACA-CTAT TGGATTTC-3′. Cells were subcloned by FACS and screened for loss of protein expression by immunoblotting. New CRISPR-depleted cells were generated every 3 months to control for potential secondary effects caused by long-term gene depletion. To express GPX4, a plasmid construct for GPX4 was purchased from Origene (RC208065). Cells were transfected with 10 μg of DNA using Lipofectamine 2000 (Thermo Fisher) and incubated for 48 h prior to use.

Statistical analysis

The error bars in graphs represent mean $\pm$ S.D. All experiments were repeated at least three times. The p values were calculated using ANOVA, and a p value of less than 0.05 was considered significant.

References

1. Stockwell, B. R., Friedmann Angeli, J. P., Bayir, H., Bush, A. I., Conrad, M., Dixon, S. J., Fulda, S., Gascón, S., Hatzios, S. K., Kagan, V. E., Noel, K., Jiang, X., Linkermann, A., Murphy, M. E., Overholtzer, M., *et al.* (2017) Ferroptosis: a regulated cell death nexus linking metabolism, redox biology, and disease. *Cell* **171,** 273–285 CrossRef Medline
2. Yang, W. S., SriRamaratnam, R., Welsch, M. E., Shimada, K., Skouta, R., Viswanathan, V. S., Cheah, J. H., Clemons, P. A., Shamji, A. F., Clish, C. B., Brown, L. M., Girotti, A. W., Cornish, V. W., Schreiber, S. L., and Stockwell, B. R. (2014) Regulation of ferroptotic cancer cell death by GPX4. *Cell* **156,** 317–331 CrossRef Medline
3. Dixon, S. J., Patel, D. N., Welsch, M., Skouta, R., Lee, E. D., Hayano, M., Thomas, A. G., Gleason, C. E., Tatonetti, N. P., Slusher, B. S., and Stockwell, B. R. (2014) Pharmacological inhibition of cystine–glutamate exchange induces endoplasmic reticulum stress and ferroptosis. *eLife* **3,** e02523 CrossRef Medline
4. Yang, W. S., and Stockwell, B. R. (2016) Ferroptosis: death by lipid peroxidation. *Trends Cell Biol.* **26,** 165–176 CrossRef Medline
5. Dixon, S. J., Lemberg, K. M., Lamprecht, M. R., Skouta, R., Zaitsev, E. M., Gleason, C. E., Patel, D. N., Bauer, A. J., Cantley, A. M., Yang, W. S.,

---

[4] Please note that the JBC is not responsible for the long-term archiving and maintenance of this site or any other third party– hosted site.

Morrison, B., 3rd, and Stockwell, B. R. (2012) Ferroptosis: an iron-dependent form of nonapoptotic cell death. *Cell* **149,** 1060–1072 CrossRef Medline

6. Viswanathan, V. S., Ryan, M. J., Dhruv, H. D., Gill, S., Eichhoff, O. M., Seashore-Ludlow, B., Kaffenberger, S. D., Eaton, J. K., Shimada, K., Aguirre, A. J., Viswanathan, S. R., Chattopadhyay, S., Tamayo, P., Yang, W. S., Rees, M. G., *et al.* (2017) Dependency of a therapy-resistant state of cancer cells on a lipid peroxidase pathway. *Nature* **547,** 453–457 CrossRef Medline

7. Brown, C. W., Amante, J. J., Goel, H. L., and Mercurio, A. M. (2017) The α6β4 integrin promotes resistance to ferroptosis. *J. Cell Biol.* **216,** 4287–4297 CrossRef Medline

8. Meredith, J. E., Jr., Fazeli, B., and Schwartz, M. A. (1993) The extracellular matrix as a cell survival factor. *Mol. Biol. Cell* **4,** 953–961 CrossRef Medline

9. Frisch, S. M., and Francis, H. (1994) Disruption of epithelial cell-matrix interactions induces apoptosis. *J. Cell Biol.* **124,** 619–626 CrossRef Medline

10. Pavlova, N. N., Pallasch, C., Elia, A. E., Braun, C. J., Westbrook, T. F., Hemann, M., and Elledge, S. J. (2013) A role for PVRL4-driven cell-cell interactions in tumorigenesis. *eLife* **2,** e00358 Medline

11. Shen, X., and Kramer, R. H. (2004) Adhesion-mediated squamous cell carcinoma survival through ligand-independent activation of epidermal growth factor receptor. *Am. J. Pathol.* **165,** 1315–1329 CrossRef Medline

12. Rayavarapu, R. R., Heiden, B., Pagani, N., Shaw, M. M., Shuff, S., Zhang, S., and Schafer, Z. T. (2015) The role of multicellular aggregation in the survival of ErbB2-positive breast cancer cells during extracellular matrix detachment. *J. Biol. Chem.* **290,** 8722–8733 CrossRef Medline

13. Neve, R. M., Chin, K., Fridlyand, J., Yeh, J., Baehner, F. L., Fevr, T., Clark, L., Bayani, N., Coppe, J. P., Tong, F., Speed, T., Spellman, P. T., DeVries, S., Lapuk, A., Wang, N. J., *et al.* (2006) A collection of breast cancer cell lines for the study of functionally distinct cancer subtypes. *Cancer Cell* **10,** 515–527 CrossRef Medline

14. Aceto, N., Bardia, A., Miyamoto, D. T., Donaldson, M. C., Wittner, B. S., Spencer, J. A., Yu, M., Pely, A., Engstrom, A., Zhu, H., Brannigan, B. W., Kapur, R., Stott, S. L., Shioda, T., Ramaswamy, S., *et al.* (2014) Circulating tumor cell clusters are oligoclonal precursors of breast cancer metastasis. *Cell* **158,** 1110–1122 CrossRef Medline

15. Schafer, Z. T., Grassian, A. R., Song, L., Jiang, Z., Gerhart-Hines, Z., Irie, H. Y., Gao, S., Puigserver, P., and Brugge, J. S. (2009) Antioxidant and oncogene rescue of metabolic defects caused by loss of matrix attachment. *Nature* **461,** 109–113 CrossRef Medline

16. Hawk, M. A., Gorsuch, C. L., Fagan, P., Lee, C., Kim, S. E., Hamann, J. C., Mason, J. A., Weigel, K. J., Tsegaye, M. A., Shen, L., Shuff, S., Zuo, J., Hu, S., Jiang, L., Chapman, S., *et al.* (2018) RIPK1-mediated induction of mitophagy compromises the viability of extracellular-matrix-detached cells. *Nat. Cell Biol.* **20,** 272–284 CrossRef Medline

17. Naito, Y., Hino, K., Bono, H., and Ui-Tei, K. (2015) CRISPRdirect: software for designing CRISPR/Cas guide RNA with reduced off-target sites. *Bioinformatics* **31,** 1120–1123 CrossRef Medline

18. Rabinovitz, I., Toker, A., and Mercurio, A. M. (1999) Protein kinase C-dependent mobilization of the α6β4 integrin from hemidesmosomes and its association with actin-rich cell protrusions drive the chemotactic migration of carcinoma cells. *J. Cell Biol.* **146,** 1147–1160 CrossRef Medline

SASBMB

Cell clustering mediated by the adhesion protein PVRL4 is necessary for α6β4 integrin–promoted ferroptosis resistance in matrix-detached cells

Caitlin W. Brown, John J. Amante and Arthur M. Mercurio

Access the most updated version of this article at doi: 10.1074/jbc.RA118.003017

Alerts:
- When this article is cited
- When a correction for this article is posted

Click here to choose from all of JBC's e-mail alerts

This article cites 18 references, 7 of which can be accessed free at
http://www.jbc.org/content/293/33/12741.full.html#ref-list-1

Prominin2 Drives Ferroptosis Resistance by Stimulating Iron Export

Graphical Abstract

Highlights

- Pro-ferroptotic stimuli induce expression of the pentaspanin protein Prominin2

- Prominin2 facilitates ferroptosis resistance in epithelial and carcinoma cells

- Prominin2 promotes formation of ferritin-containing multivesicular bodies and exosomes

- Exosomal transport of ferritin out of the cell inhibits ferroptosis
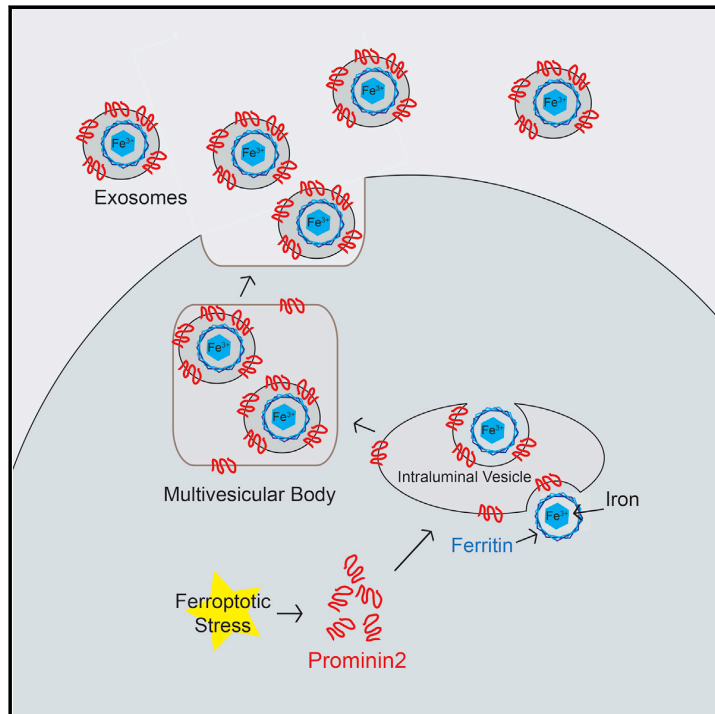
Authors

Caitlin W. Brown, John J. Amante, Peter Chhoy, ..., Christina E. Baer, Scott J. Dixon, Arthur M. Mercurio

Correspondence

arthur.mercurio@umassmed.edu

In Brief

Cells differ in their capacity to resist ferroptosis but mechanisms that contribute to resistance are not well understood. Brown et al. demonstrate that resistant cells are characterized by their ability to induce expression of Prominin2, which stimulates the formation of ferritin-containing multivesicular bodies/exosomes that transport iron out of the cell.

CellPress

Developmental Cell

Article

CellPress

Prominin2 Drives Ferroptosis Resistance by Stimulating Iron Export

Caitlin W. Brown,[1] John J. Amante,[1] Peter Chhoy,[1] Ameer L. Elaimy,[1] Haibo Liu,[1] Lihua Julie Zhu,[1] Christina E. Baer,[2,3] Scott J. Dixon,[4] and Arthur M. Mercurio[1,5,*]
[1]Department of Molecular, Cell and Cancer Biology, University of Massachusetts Medical School, Worcester, MA 01605, USA
[2]Department of Microbiology and Physiological Systems, University of Massachusetts Medical School, Worcester, MA 01605, USA
[3]Sanderson Center for Optical Examination, University of Massachusetts Medical School, Worcester, MA 01605, USA
[4]Department of Biology, Stanford University, Stanford, CA, USA
[5]Lead Contact
*Correspondence: arthur.mercurio@umassmed.edu
https://doi.org/10.1016/j.devcel.2019.10.007

SUMMARY

Ferroptosis, regulated cell death characterized by the iron-dependent accumulation of lethal lipid reactive oxygen species, contributes to tissue homeostasis and numerous pathologies, and it may be exploited for therapy. Cells differ in their sensitivity to ferroptosis, however, and a key challenge is to understand mechanisms that contribute to resistance. Using RNA-seq to identify genes that contribute to ferroptosis resistance, we discovered that pro-ferroptotic stimuli, including inhibition of the lipid hydroperoxidase GPX4 and detachment from the extracellular matrix, induce expression of prominin2, a pentaspanin protein implicated in regulation of lipid dynamics. Prominin2 facilitates ferroptosis resistance in mammary epithelial and breast carcinoma cells. Mechanistically, prominin2 promotes the formation of ferritin-containing multivesicular bodies (MVBs) and exosomes that transport iron out of the cell, inhibiting ferroptosis. These findings reveal that ferroptosis resistance can be driven by a prominin2-MVB-exosome-ferritin pathway and have broad implications for iron homeostasis, intracellular trafficking, and cancer.

INTRODUCTION

Ferroptosis is a regulated form of non-apoptotic cell death characterized by the iron-dependent accumulation of lethal lipid reactive oxygen species (ROS) (Dixon et al., 2012; Yang et al., 2016; Yang and Stockwell, 2016). This process can contribute to pathological cell death in brain, kidney, heart, and other tissues (Do Van et al., 2016; Fang et al., 2019; Friedmann Angeli et al., 2014; Hangauer et al., 2017; Hirschhorn and Stockwell, 2019). There is also an interest in understanding the role of ferroptosis in cancer and potentially exploiting this mechanism therapeutically (Dixon and Stockwell, 2019). Interestingly, fer-

roptosis sensitivity varies substantially among cancer cells from distinct tissue lineages that express certain tumor suppressors or have acquired unique cell drug-tolerant or de-differentiated cell states (Hangauer et al., 2017; Jiang et al., 2015; Tsoi et al., 2018; Viswanathan et al., 2017; Yang et al., 2014; Zhang et al., 2019). At the molecular level, mechanisms that can account for the observed variation in ferroptosis sensitivity between cells remain largely elusive.

Ferroptosis can be initiated by a number of stimuli that disrupt intracellular glutathione-mediated antioxidant systems or directly overload the cell with iron (Stockwell et al., 2017). For example, it is possible to induce ferroptosis by depriving cells of the thiol-containing amino acid cystine (the disulfide of cysteine), a key glutathione precursor, or by directly inhibiting the reduced glutathione (GSH)-dependent phospholipid hydroperoxide glutathione peroxidase 4 (GPX4) (Dixon et al., 2012; Yang et al., 2014). GPX4 catalyzes the reduction of reactive lipid hydroperoxides to non-reactive lipid alcohols. This reaction is essential to prevent a buildup of lipid hydroperoxides, which can participate in Fenton chemistry reactions when free iron is present that lead to the generation of toxic lipid alkoxy radicals and subsequently other reactive lipid breakdown products (Dixon and Stockwell, 2019). The execution of ferroptosis, therefore, relies on the combined presence of oxidizable lipids (e.g., polyunsaturated phospholipids) and free iron, which, in the absence of sufficient GPX4-mediated lipid peroxide detoxification, result in oxidative destruction of the plasma membrane and other internal organelle membranes (Agmon et al., 2018; Magtanong et al., 2019). Physiological stress such as detachment of cells from the extracellular matrix can increase ROS and is sufficient to trigger ferroptosis if GPX4 activity is inhibited (Brown et al., 2017).

Iron is essential for cell growth, but it can also promote toxic ROS formation, as occurs during ferroptosis (Torti et al., 2018). How intracellular iron homeostasis contributes to ferroptosis sensitivity is only partially understood. Iron can be taken into cells via the transferrin and transferrin receptor system, and genetic silencing of the transferrin receptor partially inhibits ferroptosis (Gao et al., 2016; Yang and Stockwell, 2008). NCOA4-mediated, lysosomal-dependent degradation of the iron storage protein ferritin contributes to the pool of free intracellular iron and

CellPress

thereby promotes ferroptosis; genetic depletion of *NCOA4* or chemical inhibition of lysosomal acidification both attenuate ferroptosis (Gao et al., 2016; Hou et al., 2016; Torii et al., 2016). Furthermore, manipulation of ferroportin-mediated iron export can alter ferroptosis sensitivity, with reduced ferroportin expression leading to less iron export and increased ferroptosis sensitivity (Geng et al., 2018; Ma et al., 2016). Thus, the modulation of intracellular free iron levels by the cellular iron homeostatic network emerges as a key regulator of ferroptosis sensitivity. Interestingly, intracellular free iron levels can vary between cancer cells and cancer cell states (e.g., in metastatic versus non-metastatic cells), which might be expected to contribute to differences in ferroptosis sensitivity (Geng et al., 2018). There is also some evidence that iron levels may be dynamically regulated within the cell in response to ferroptosis-inducing conditions, suggesting that uncharacterized regulatory mechanisms may alter intracellular iron, possibly in an attempt to negatively regulate the onset of ferroptosis (Ma et al., 2016).

In this study, we used an unbiased approach to investigate how mammary epithelial and breast carcinoma cells survive in response to pharmacological and physiological ferroptotic stress. We observed that cells can resist the onset of ferroptosis by dynamically upregulating an unprecedented iron export pathway involving multivesicular body (MVB)/exosome trafficking of ferritin and iron out of the cell. This process limits the intracellular accumulation of free iron and inhibits the onset of ferroptosis. By contrast, inactivation of this program, either normally or following chemical or genetic inhibition of key steps of this process, substantially increases ferroptosis sensitivity. These findings pinpoint a mechanism that leads to variation in ferroptosis sensitivity and suggest that dynamic MVB/exosome-mediated iron export may be a homeostatic mechanism acting to restrict the initiation of ferroptosis, thereby preventing cell death under conditions of sub-lethal stress exposure.

RESULTS

Prominin2 Is Induced by Ferroptotic Stress and Promotes Resistance to Ferroptotic Cell Death

To gain insight into mechanisms that promote ferroptosis resistance, we exploited our recent finding that detachment of certain cells from the extracellular matrix (ECM) is a pro-ferroptotic stress (Brown et al., 2017, 2018). We reasoned that cells that can survive under detached conditions may do so by upregulating a protective gene expression program that prevents cell death. To identify such genes, we compared mRNA expression in adherent and ECM-detached MCF10A immortalized breast epithelial cells by RNA-sequencing (GSE115059). *PROM2*, which encodes the pentaspanin protein prominin2, captured our attention because its expression was significantly increased in ECM-detached cells compared to adherent cells. Also, it is thought to have a role in lipid dynamics and membrane organization, processes that could be relevant for ferroptosis resistance (Doll et al., 2017; Florek et al., 2007; Jászai et al., 2010; Singh et al., 2013). We confirmed that prominin2 was rapidly upregulated in MCF10A cells in response to ECM detachment at the protein and mRNA level (Figures 1A and 1B). Increased PROM2 was also observed in detached versus adherent Hs578t breast cancer cells (Figure 1B). Silencing of prominin2

expression in both MCF10A and Hs578t cells resulted in a significant loss of viability in ECM-detached conditions (Figures 1B and 1C). Cell viability under these conditions was rescued by co-treatment with a specific inhibitor of ferroptosis, ferrostatin-1 (Dixon et al., 2012), but not the pan-caspase inhibitor ZVAD-fmk (Figure 1C). These data indicate that failure to upregulate *PROM2* upon ECM detachment can result in the induction of ferroptosis.

We next investigated whether pharmacological inhibition of GPX4 altered prominin2 expression and impacted ferroptosis in adherent cells. MCF10A and Hs578t cells were treated with RSL3, a covalent GPX4 inhibitor (Yang et al., 2014), for 2 h resulting in increased prominin2 mRNA and protein expression in both cell lines (Figures 1D and 1E). This effect was not a generic response to ROS stress because culturing with H_2O_2 did not increase prominin2 expression (Figure S1A). Moreover, expression of a related family member, prominin1 (CD133), was not altered significantly by RSL3, substantiating the specificity of the ferroptotic effect for prominin2 (Figure S1A). Unlike MCF10A and Hs578t cells, RSL3 did not induce prominin2 in MDA-MB-231 cells, another breast cancer cell line (Figures 1D and 1E). We observed that the induction of prominin2 expression correlated with resistance to ferroptosis induced by GPX4 inhibition. MCF10A and Hs578t cells were resistant to RSL3-induced cell death at concentrations up to 2.5 μM, while MDA-MB-231 cells were killed by RSL3 concentrations as low as 0.5 μM (Figure 1F).

Given the above results, we assessed whether prominin2 was necessary for resistance to ferroptosis. For this purpose, we silenced prominin2 expression in MCF10A and Hs578t cells (Figure S1B) and examined the sensitivity of these cells to ferroptosis compared to control cells. Here, we tested the covalent GPX4 inhibitors RSL3 and ML210 (Weïwer et al., 2012), the indirect GPX4 inhibitor FIN56 (Shimada et al., 2016), and the GSH-depleting agent erastin, which reduces GPX4 activity indirectly by preventing the synthesis of its key cofactor (Dixon et al., 2012). Control MCF10A cells were more resistant to these compounds than Hs578t cells (Figures 2A and 2B). Nonetheless, a significant increase in sensitivity to all four compounds was observed in prominin2 knockdown cells compared to control cells for both cell lines (Figures 2A, 2B, S2A, and S2B). Loss of cell viability in prominin2-depleted cells was completely rescued by ferrostatin-1, indicating that the greater sensitivity of prominin2-silenced cells was not caused by the induction of an alternative mode of cell death (Figure 2C). Given the results obtained with genetic silencing, we next tested whether overexpression of prominin2 was sufficient to inhibit ferroptosis. Indeed, in MDA-MB-231 cells, exogenous prominin2 expression was sufficient to inhibit cell death in response to RSL3, ML210, FIN56, and erastin (Figures 2D, S2C, and S2D). Thus, prominin2 expression promotes resistance to ferroptosis. Subsequent experiments were performed using RSL3 as a prototypic GPX4 inhibitor.

Prominin2 Promotes the Formation of Multivesicular Bodies and Exosomes

To gain insight into how prominin2 may promote ferroptosis resistance, we assessed its subcellular localization following GPX4 inhibition. Immunofluorescence microscopy revealed that prominin2 localizes in discrete cytoplasmic puncta in
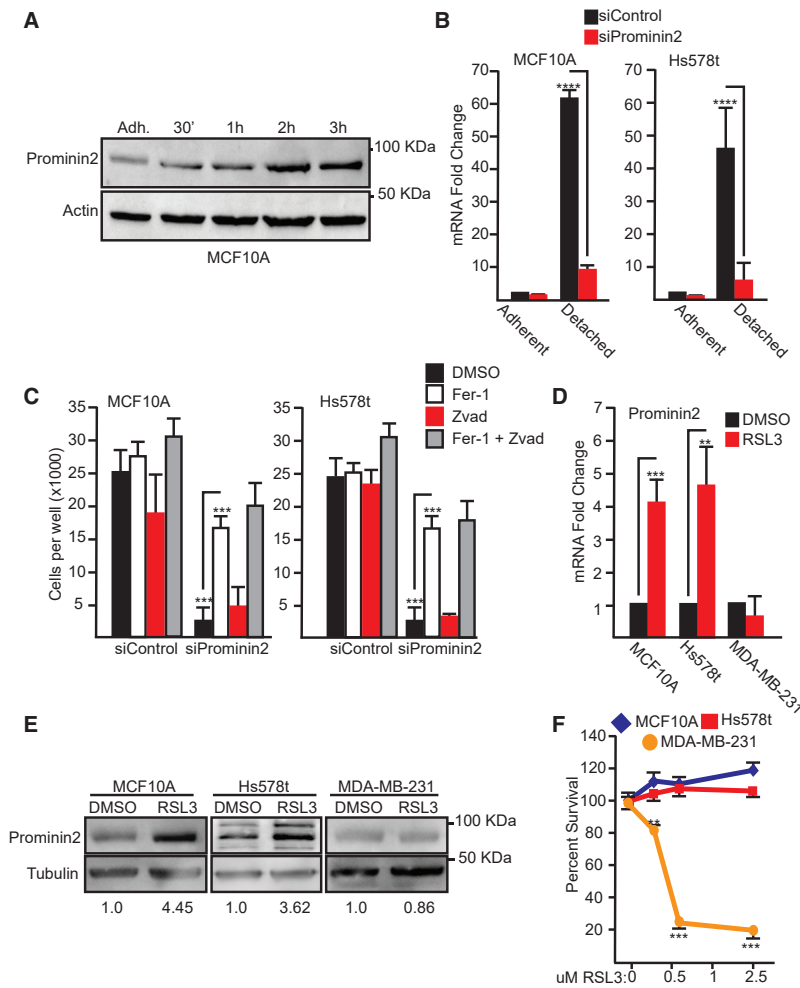
Figure 1. Prominin2 Is a Ferroptosis Stress Response Protein

(A) MCF10A cells were detached from ECM for 30 min, 1 h, 2 h, or 3 h. Extracts from these cells were immunoblotted for prominin2 and actin. Immunoblot is representative of three independent experiments.

(B) MCF10A and Hs578t cells were transfected with either control siRNA or prominin2 siRNA for 48 h and then maintained under adherent or ECM-detached conditions for 2 h. PROM2 mRNA expression was quantified by qPCR. Shown is representative experiment of three independent replicates.

(C) siControl or siProminin2-treated MCF10A and Hs578t cells were maintained in ECM detached conditions for 24 h in the presence of either DMSO, ferrostatin-1 (2 μM), ZVAD-fmk (25 μM), or ferrostatin-1 and ZVAD-fmk and the number of viable cells was quantified. Shown is representative experiment of three independent replicates.

(D) Adherent MCF10A, Hs578t, and MDA-MB-231 cells were treated with either DMSO or RSL3 for 2 h and PROM2 mRNA expression was quantified by qPCR. Shown is representative experiment of three independent replicates.

(E) Extracts from the cells in (D) were immunoblotted with antibodies specific for prominin2 and tubulin. The densitometric analysis of these immunoblots (normalized to 1.0 for each cell line) obtained from analysis of three independent experiments is shown below the blots.

(F) Adherent MCF10A, Hs578t, and MDA-MB-231 cells were treated with DMSO or RSL3 24 h and the percent of surviving cells was quantified. Absorbance was normalized to DMSO control. Shown is representative experiment of three independent replicates.

response to GPX4 inhibition by RSL3 (Figures 3A and S3A). As determined using organelle-specific markers, these puncta did not co-localize with early endosomes (Rab5A), peroxisomes (catalase), caveolae (phospho-Caveolin-1), autophagosomes (LC3), or mitochondria (Mitotracker) (Figure S3B). By contrast, a striking co-localization was observed between prominin2 and TSG101, a marker of multivesicular bodies (MVBs) (Razi and Futter, 2006) (Figures 3A and S3A). MVBs are late endosomes containing cargo within their lumen bound in intraluminal vesicles (ILVs) (Felder et al., 1990; Gruenberg and Maxfield, 1995). The cargo can be sorted for degradation in lysosomes or released into the extracellular space as exosomes (Futter et al., 1996; Hart and Young, 1991). The co-localization of prominin2 and TSG101 was evident as early as 30 min following the inhibition of GPX4, and this co-localization was most prominent in the perinuclear region (Figures 3B and S4A). At later times (1.5–2 h), this co-localization was evident throughout the cytoplasm. We also observed that prominin2 exhibited some co-localization with the lysosomal marker LAMP1 (Cella et al., 1996) (Figure S3C), which is expected given that some MVBs are trafficked to lysosomes (Futter et al., 1996; Razi and Futter, 2006). However, we

discounted a role for lysosomes in ferroptosis resistance under these conditions based on the observation that NH_4Cl treatment, which inhibits lysosome function (Hart and Young, 1991), had no effect on the survival of either control or prominin2-depleted cells following GPX4 inhibition (Figure S3D).

The above results prompted us to assess whether prominin2 promotes MVB formation in response to GPX4 inhibition. RSL3-treated MCF10A and Hs578t cells contained more TSG101-positive structures than vehicle control-treated cells, indicating that GPX4 inhibition induces MVB formation (Figures 3A, 3B, and S4A). Prominin2 localization to MVBs in RSL3-treated MCF10A and Hs578t cells was confirmed by co-localization with Alix and CD9 (Figures S4B and S4C). We then evaluated whether the formation of these structures is dependent on prominin2 using transmission electron microscopy (TEM). Indeed, RSL3-treated MCF10A cells contained significantly more MVBs per cell than control cells, an effect that was not observed in prominin2-silenced cells (Figure 3C). Notably, this RSL3-stimulated increase in MVBs was rapid (within 2 h). Immunofluorescence microscopy also revealed a reduction in TSG101-positive puncta in prominin2-depleted MCF10A and Hs578t cells
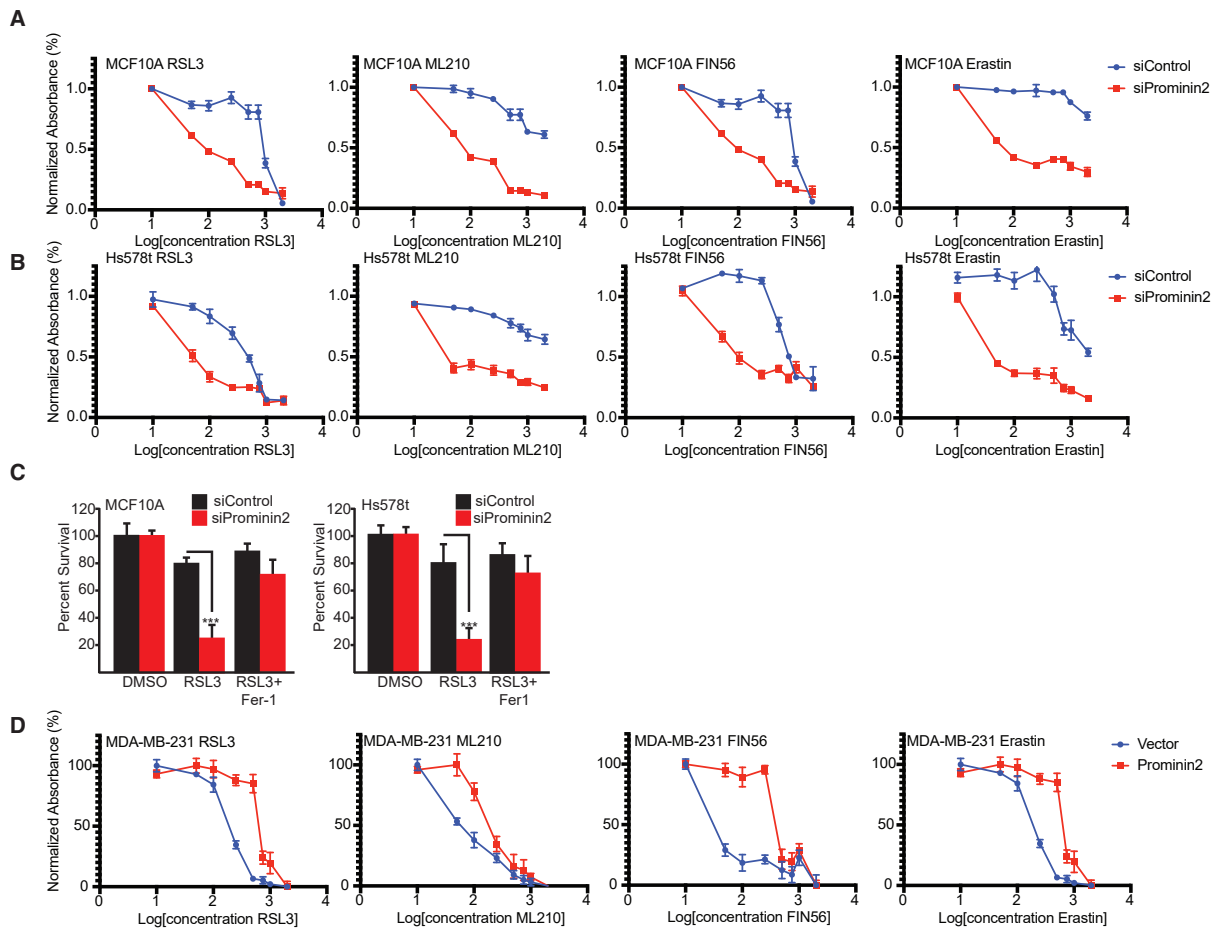
Figure 2. Prominin2 Increases Resistance to Ferroptosis

(A) Prominin2 expression was diminished in adherent MCF10A cells for 48 h using siRNA prior to treatment with RSL3, ML210, FIN56, or erastin for 24 h. The percent of surviving cells was quantified and compared to cells transfected with an siRNA control. Absorbance was normalized to DMSO control. Shown is representative experiment of three independent replicates. See Supplemental Information for the IC$_{50}$ values for these conditions.

(B) Prominin2 expression was diminished in adherent Hs578t cells for 48 h using siRNA prior to treatment with RSL3, ML210, FIN56, or erastin for 24 h. The percent of surviving cells was quantified and compared to cells transfected with an siRNA control. Absorbance was normalized to DMSO control. Shown is representative experiment of three independent replicates. See Supplemental Information for the IC$_{50}$ values for these conditions.

(C) Prominin2 expression was diminished in adherent MCF10A and Hs578t cells for 48 h using siRNA. Cells were treated with either DMSO, RSL3 (5 μM), or RSL3 and ferrostatin-1 (2 μM) for 24 h and the percent of surviving cells was quantified. Shown is representative experiment of three independent replicates. (D) MDA-MB-231 cells were transfected with either a prominin2 expression construct or a vector control prior to treatment with either DMSO or RSL3 for 2 hrs. The percent of surviving cells was quantified. Absorbance was normalized to DMSO control. Shown is a representative experiment of three independent replicates.

compared to control cells (Figures 3D, 3E, S5A, and S5B). Conversely, exogenous prominin2 expression in MDA-MB-231 cells increased the number of TSG101-positive structures and, as noted above, reduced ferroptosis sensitivity (Figures 3F and S5C). Consistent with a causal role for MVBs in ferroptosis resistance, diminishing TSG101 expression increased the sensitivity of MCF10A and Hs578t cells to RSL3-induced cell death (Figures 4A, 4B, and S6A), and this death was rescued with ferrostatin-1 (Figure 4C). These data indicate that GPX4 inhibition stimulates prominin2 expression and prominin2-dependent MVB formation, which promote ferroptosis resistance.

MVBs can fuse with the plasma membrane and release ILVs as exosomes (Harding et al., 1984; Pan et al., 1985). Indeed, we observed distinct ILVs in MVBs consistent with the size of exosomes (~80 nm) (Raposo and Stoorvogel, 2013) in RSL3-treated cells (Figure 3C). To assess the impact of GPX4 inhibition on exosome formation, exosomes were harvested by ultracentrifugation from control (DMSO) and RSL3-treated MCF10A and Hs578t cells. The presence of an exosome fraction was confirmed by TEM (Figure S6B). GPX4 inhibition increased exosome formation as evidenced by the fact that a significant amount of protein was present in the exosome preparation of RSL3-treated cells (Figure 4D). In contrast, exosomal protein in control cells was not detected in this experiment (data not shown). Analysis of these exosomes by immunoblotting revealed that they contained prominin2, CD63, and TSG101 providing
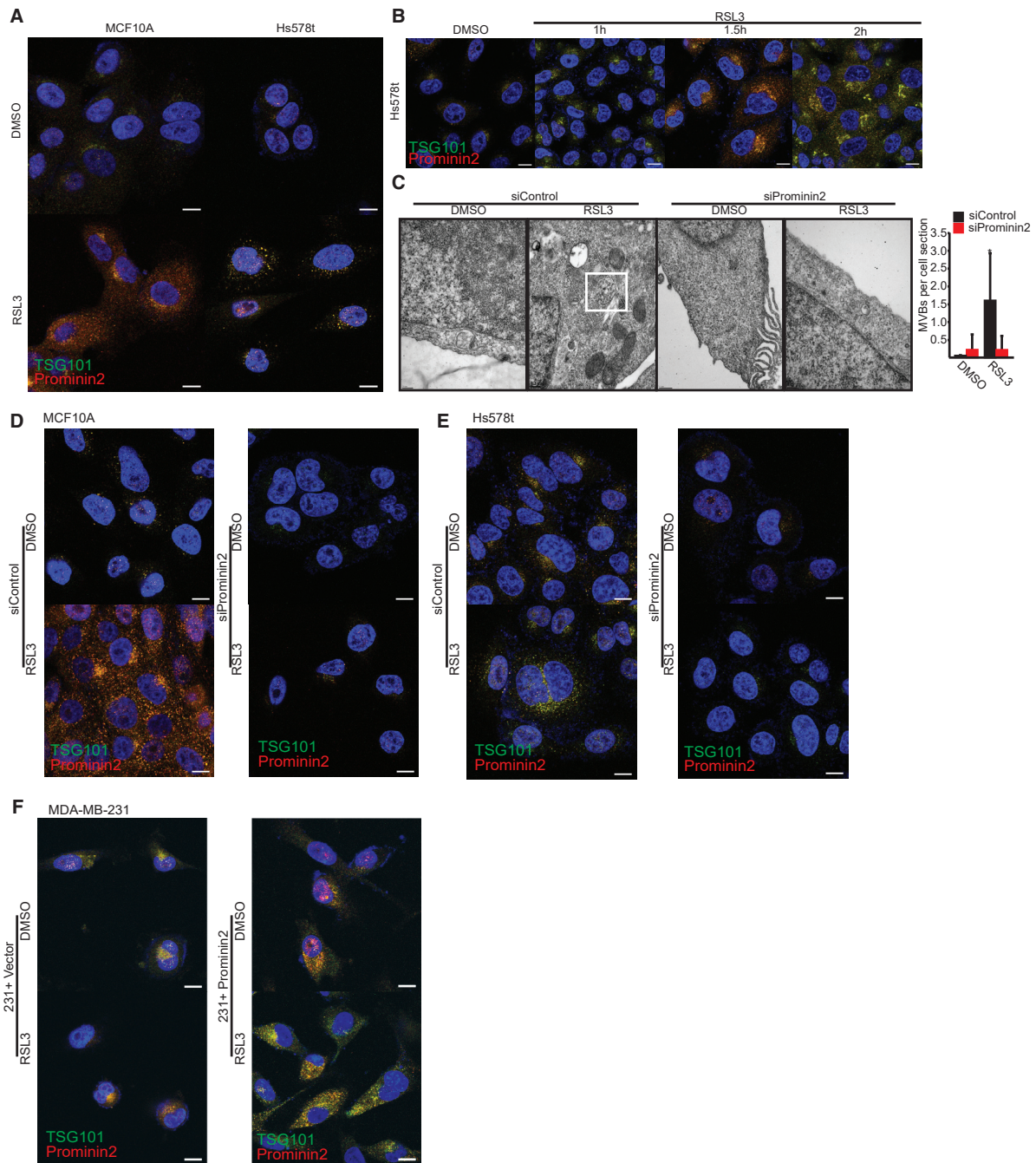
Figure 3. Prominin2 Promotes the Formation of MVBs in Response to GPX4 Inhibition

(A) Adherent MCF10A and Hs578t cells were treated with either DMSO or RSL3 for 2 h and immunostained using Abs specific for TSG101 (green) and prominin2 (red). Scale bar, 10 μm. For all immunofluorescence images, merged images are shown in the main figures and single channel images are provided in Supplemental Information. Also, for all experiments, image acquisition settings were the same for DMSO and RSL3-treated cells. Shown is a representative image of three independent replicates.

(B) Adherent Hs578t cells were treated with either DMSO or RSL3 for either 1, 1.5, or 2 h and immunostained using Abs specific for TSG101 (green) and prominin2 (red). Scale bar, 10 μm. Shown is a representative image of three independent replicates.

(legend continued on next page)

evidence that they were generated by prominin2-dependent MVB formation (Figure 4D). Importantly, they did not contain GM130, a Golgi marker, indicating that their isolation was not contaminated with other cell membranes. To test whether exosome release was essential for resistance to GPX4 inhibition, we used the sphingomyelinase inhibitor GW4869 and found that inhibition of exosome release increased the sensitivity of control MCF10A and Hs578t cells to RSL3, but it did not significantly impact the viability of prominin2-depleted cells (Figure 4E).

Ferroptosis Resistance Is Facilitated by MVB/Exosome Iron Transport

Our results indicated that prominin2-mediated MVB and exosome formation promote ferroptosis resistance. We hypothesized that this resistance mechanism involved MVBs and exosome-mediated export of a factor that would otherwise promote ferroptosis. Given that the iron storage protein ferritin can be secreted from cells in exosomes (Truman-Rosentsvit et al., 2018), we reasoned that MVB/exosome-mediated ferritin export inhibits ferroptosis. In support of this hypothesis, we observed that ferritin co-localized with prominin2 in RSL3-treated MCF10A and Hs578t cells, but not in vehicle control (DMSO)-treated cells (Figure 5A). We also identified ferritin protein in exosomes harvested from these cells (Figure 5B). These exosomes contained iron as detected by inductively coupled plasma mass spectrometry (ICP-MS) (3,400 ng per exosome collection), further supporting our hypothesis. MDA-MB-231 cells do not increase ferritin expression following GPX4 inhibition. However, the expression of exogenous prominin2 induced a more punctate pattern of ferritin localization in RSL3-treated compared to control cells (Figure 5C). An alternative explanation for our findings was that prominin2 enhanced the membrane localization of the iron exporter ferroportin, which has been shown to play a role in ferroptosis sensitivity (Geng et al., 2018). However this did not appear to be the case because prominin2 did not co-localize with ferroportin (SLC40A1) (Figure S6C).

A causal role for ferritin in ferroptosis resistance is supported by the finding that knock down of both the ferritin heavy chain (FTH1) and light chain (FTL) increased cell death triggered by GPX4 inhibition in both MCF10A and Hs578t cells (Figures 5D, 5E, and S6D). Importantly, this death was rescued by either ferrostatin-1 or the iron chelator deferoxamine (DFO), providing evidence for its ferroptotic nature (Figure 5F).

Our data suggested that GPX4 inhibition stimulates the formation of MVBs containing ferritin and that these structures transport iron out of the cell. To test this hypothesis, we quantified the free iron concentration in control and RSL3-treated

MCF10A and Hs578t cells and observed no significant difference between these two groups (Figure 6A). However, when either prominin2 or both FTH1 and FTL were silenced, we observed an increase in the concentration of free iron following RSL3 treatment (Figures 6A, 6B, and S6D). Additional evidence for prominin2 regulation of iron levels was obtained by quantifying free iron in control and prominin2-expressing MDA-MB-231 cells in response to GPX4 inhibition. Prominin2 expression in these cells prevented the increase in iron in response to RSL3 that was observed in control cells (Figure 6C). Also, disabling the MVB pathway by decreasing expression of TSG101 significantly increased the concentration of free intracellular iron following GPX4 inhibition (Figure 6D). These results indicate that blocking MVB/exosome-mediated ferritin export results in an accumulation of intracellular iron upon GPX4 inhibition.

ECM-Detached Cells Resist Ferroptosis by Prominin2-Mediated MVB/Exosome Formation

Based on the observation that ECM-detachment is a ferroptotic stress that induces prominin2 expression (Figure 1B), we investigated whether prominin2 promotes MVB formation and iron transport in ECM-detached cells. Indeed, cell death in ECM-detached, prominin2-depleted MCF10A and Hs578t cells was rescued by the iron chelator deferoxamine, consistent with a defect in iron export promoting cell death (Figure 7A). Also, ECM detachment increased the concentration of free iron in prominin2-depleted compared to control cells, an effect that was most noticeable 2 h post-detachment, which is coincident with the onset of ferroptosis (Figure 7B). Similar to RSL3-treated adherent cells, ECM detachment increased the frequency of MVBs based on TEM analysis, and this increase was dependent on prominin2 (Figure 7C). Exosome release is indicated by the fusion of an MVB with the plasma membrane (Figure 7C). Co-localization of prominin2 and TSG101 was also evident in ECM-detached MCF10A and Hs578t cells (Figure 7D), similar to the co-localization seen in adherent, RSL3-treated cells (Figure 3A). These results indicate that physiological ferroptotic stress can be evaded by the prominin2/MVB iron export pathway.

DISCUSSION

We have uncovered a cell biological mechanism of ferroptosis resistance that has broad implications for understanding how cells respond to pro-ferroptotic conditions. The critical component of this mechanism is the pentaspanin protein prominin2, whose expression can be increased by pharmacological and physiological triggers of ferroptosis. The induction of prominin2

(C) MCF10A cells were transfected with either control siRNA or prominin2 siRNA for 48 h and then treated with either DMSO or RSL3 for 1.5 h. These cells were fixed and processed for TEM. The frequency of MVBs (white box) per section was quantified (right graph). Shown is representative image of five total cells quantified per group.

(D) MCF10A cells and were transfected with either control siRNA or prominin2 siRNA for 48 h and then treated with either DMSO or RSL3 for 2 h. These cells were then immunostained using Abs specific for TSG101 (green) and prominin2 (red). Scale bar, 10 μm. Shown is a representative image of three independent replicates.

(E) Hs578t cells were transfected with either control siRNA or prominin2 siRNA for 48 h and then treated with either DMSO or RSL3 for 2 h. These cells were then immunostained using Abs specific for TSG101 (green) and prominin2 (red). Scale bar, 10 μm. Shown is a representative image of three independent replicates.

(F) MDA-MB-231 cells were transfected with either a prominin2 expression construct or a vector control prior to treatment with either DMSO or RSL3 for 2 h. These cells were then immunostained using antibodies specific for TSG101 (green) and prominin2 (red). Scale bar, 10 μm. Shown is a representative image of three independent replicates.
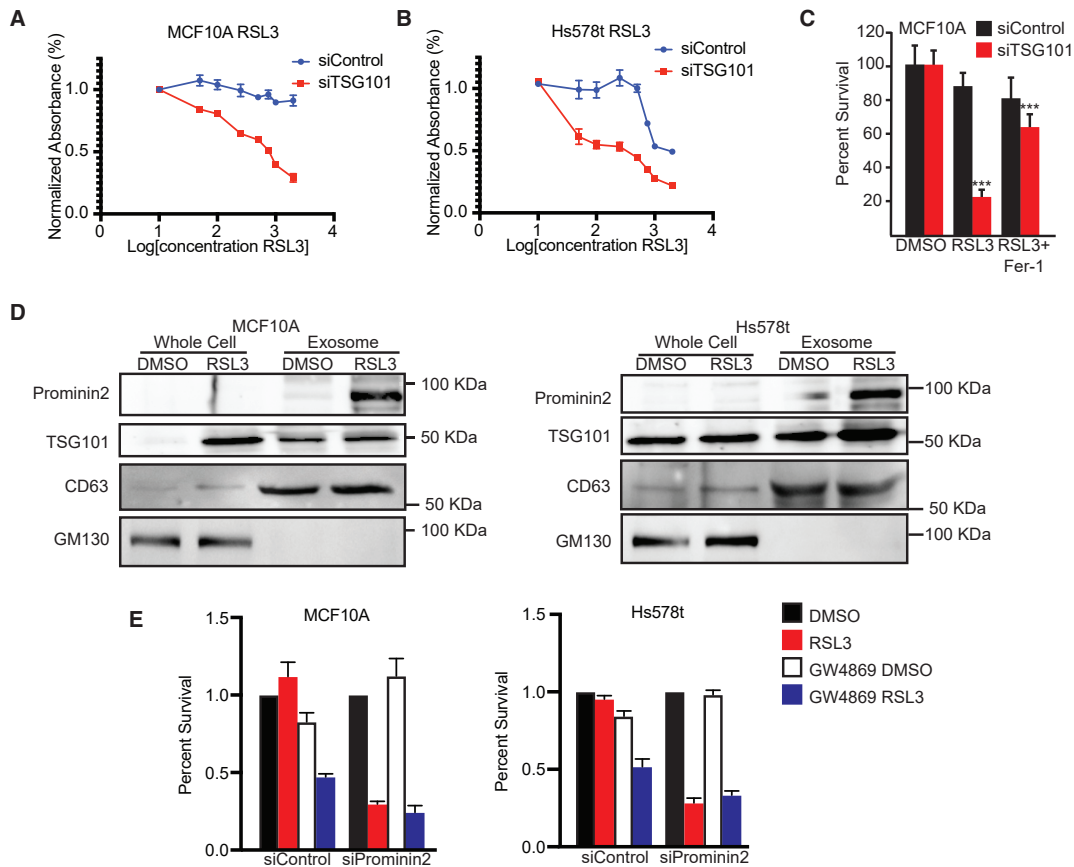
Figure 4. Multivesicular Body Formation Is Required for Evasion of Ferroptosis

(A) TSG101 expression was diminished in adherent MCF10A cells for 48 h using siRNA prior to treatment with DMSO or RSL3 for 24 h. The percent of surviving cells was quantified and compared to cells transfected with an siRNA control. Absorbance was normalized to DMSO control. Shown is a representative experiment of three independent replicates.

(B) TSG101 expression was diminished in adherent Hs578t cells for 48 h using siRNA prior to treatment with DMSO or RSL3 for 24 h. The percent of surviving cells was quantified and compared to cells transfected with an siRNA control. Absorbance was normalized to DMSO control. Shown is a representative experiment of three independent replicates.

(C) TSG101 expression was diminished in adherent MCF10A cells for 48 h using siRNA prior to treatment with DMSO, RSL3, or RSL3 and ferrostatin-1 for 24 h. The percent of surviving cells was quantified and compared to cells transfected with an siRNA control. Absorbance was normalized to DMSO control. Shown is a representative experiment of three independent replicates.

(D) Exosomes were isolated from cell culture medium of MCF10A and Hs578t cells treated for 24 h with 1 μM RSL3 by ultracentrifugation. The exosome pellets were lysed and protein concentration was assessed. Exosomes from RSL3-treated MCF10A and Hs578t cells were immunoblotted for TSG101, prominin2, GM130, and CD63. See Supplemental Information for TEM of exosomes. Shown is a representative immunoblot of three independent collections.

(E) Prominin2 expression was diminished in MCF10A and Hs578t cells for 48 h using siRNA prior to treatment with either DMSO, RSL3 (5 μM), or RSL3 and the exosome inhibitor GW4869 (20 μM) for 24 h and the percent of surviving cells was quantified. Shown is representative experiment of three independent replicates.

expression in response to ferroptotic stress promotes the formation of MVBs and exosomes that function to transport iron out of the cell and, consequently, impede ferroptosis. The existence of this mechanism suggests that cells have evolved a regulated means to evade ferroptosis that involves limiting the intracellular concentration of this potentially toxic metal in times of stress. Cells that cannot induce prominin2 and export ferritin are therefore highly sensitive to the induction of ferroptosis.

Our finding that prominin2 is at the nexus of a ferroptosis resistance mechanism heightens interest in this protein. While little is known about prominin2, there is evidence that it can localize to

microvilli, cilium, and other protrusions from the apical and basolateral membranes in epithelial cells (Florek et al., 2007; Jászai et al., 2010; Singh et al., 2013) and by binding cholesterol, regulate lipid microdomains (Florek et al., 2007). In contrast to these studies, however, we observed that prominin2 is not localized on the plasma membrane but rather intracellularly in MVBs. Mechanistically, how prominin2 stimulates MVB formation is an important topic for future investigation. One possibility is that prominin2 regulates cholesterol levels in late endosomes, a process that appears to be critical for MVB formation (Kobuna et al., 2010).
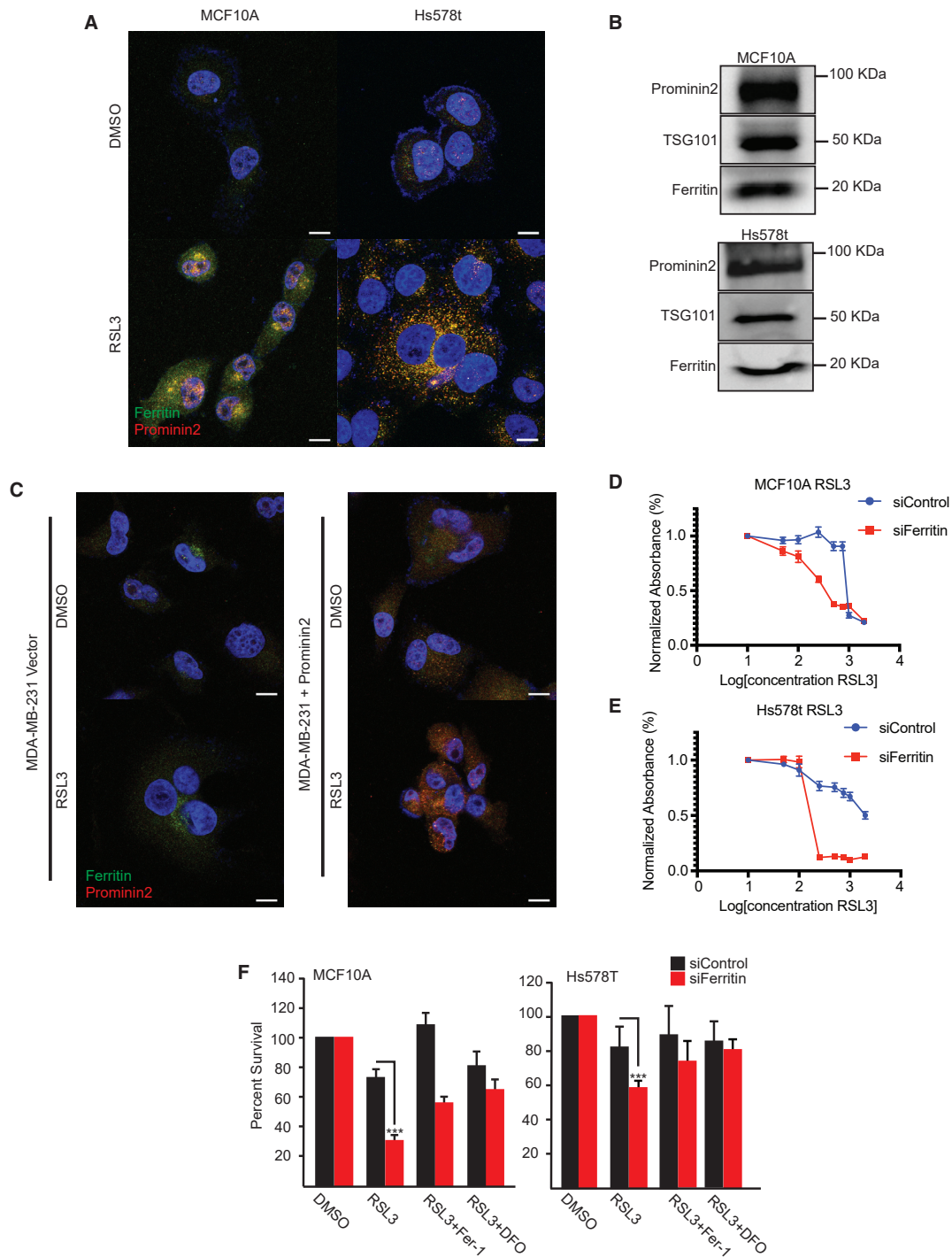
Figure 5. Prominin2 and Ferritin Contribute to the Regulation of Free Iron

(A) Adherent MCF10A and Hs578t cells were treated with either DMSO or RSL3 for 2 h and immunostained using Abs specific for ferritin (green) and prominin2 (red). Scale bar, 10 μm. Images are representative of three independent experiments with similar results.

(B) Exosomes purified from RSL3-treated MCF10A cells as described in Figure 3F were immunoblotted for ferritin.
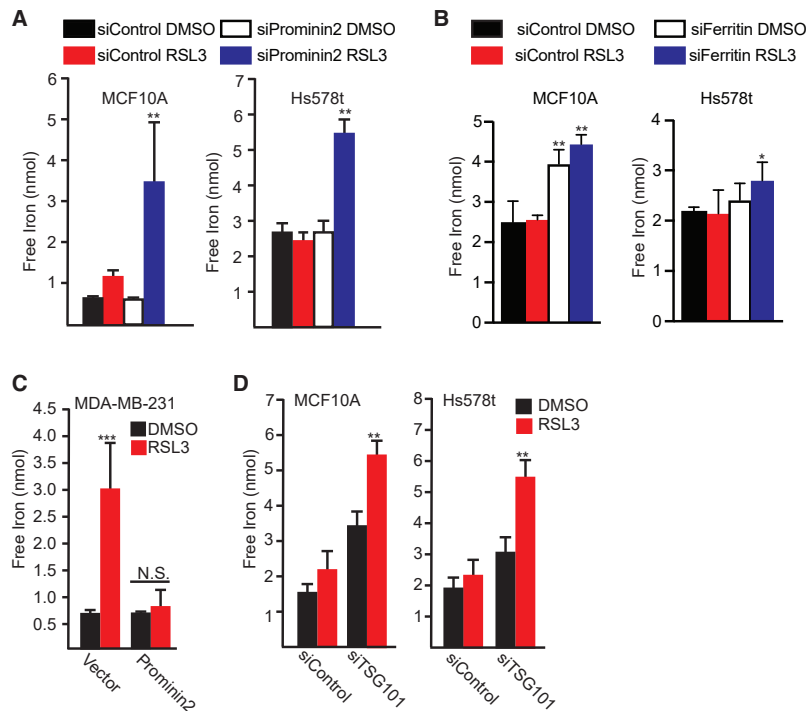
Figure 6. GPX4 Inhibition Alters Free Iron Concentration

(A) Adherent MCF10A and Hs578t cells were transfected with either control siRNA or prominin2 siRNA for 48 h and then treated with 5 μM RSL3 for 2 h. Total free iron was quantified and reported in nM. Shown is a representative experiment of three independent replicates.

(B) Adherent MCF10A and Hs578t cells were transfected with either control siRNA or ferritin heavy chain siRNA for 48 h and then treated with RSL3 for 2 h. Total free iron was quantified and reported in nM. Shown is a representative experiment of three independent replicates.

(C) Adherent MDA-MB-231 cells were transfected with either a prominin2 expression construct or a vector control prior to treatment with either DMSO or RSL3 for 2 h. Total free iron was quantified and reported as nMoles. Shown is a representative experiment of three independent replicates.

(D) Adherent MCF10A and Hs578t cells were transfected with either control siRNA or TSG101 siRNA for 48 h and then treated with either DMSO or RSL3 for 2 h. Total free iron was quantified and reported as nanomoles. Shown is a representative experiment of three independent replicates.

Free iron is essential for the execution of ferroptosis (Dixon et al., 2012, 2014), and an increase in iron import combined with reduced ferritin storage capacity is a characteristic of erastin-sensitive cells (Torti et al., 2018; Yang and Stockwell, 2008). The concept that intracellular iron levels and ferroptosis sensitivity may be modulated on short (<2 h) timescales through the export of ferritin from the cell via an MVB/exosome pathway had not been considered previously. Speculatively, reducing ferroptosis sensitivity may be a physiological role for the process of MVB-mediated ferritin export observed previously (Truman-Rosentsvit et al., 2018). Our results imply that cytosolic iron increases in response to GPX4 inhibition or ECM detachment, but that this iron can be captured, incorporated into MVBs, and exported from the cell in exosomes if prominin2 expression is sufficient. It could be argued that the uptake of the released, ferritin-containing exosomes by neighboring cells diminishes the overall decrease in intracellular iron. However, our finding that exosomes accumulate detectably in the medium suggests that the rate of exosome release from cells far exceeds their rate of uptake. In this direction, it is possible that a cell with partially oxidized membranes as a result of GPX4 inhibition is defective in exosome uptake.

This mechanism of prominin2-mediated ferroptosis resistance has potential implications for efforts that seek to induce ferroptosis as a mode of anti-cancer therapy. For example, inhibiting GPX4 activity can selectively kill certain tumor cells via ferroptosis (Viswanathan et al., 2017; Yang et al., 2014). Given that cells can acquire resistance to GPX4 inhibition by inducing prominin2, strategies that simultaneously block prominin2 expression or function may enhance sensitivity to GPX4 inhibitors. Indeed, analysis of the Broad Institute Cancer Therapeutics Response Portal resource indicates that high levels of prominin2 expression are significantly correlated with resistance to the GPX4 inhibitor ML210 across hundreds of cancer cells lines (https://portals.broadinstitute.org/ctrp/?featureName=PROM2). Given that prominin2 expression is correlated with poor clinical outcomes in several cancers (Saha et al., 2019), prominin2-mediated MVB formation and iron export may also be relevant to the emerging role of ferroptosis in tumor suppression (Jiang et al., 2015).

(C) MDA-MB-231 cells were transfected with either a prominin2 expression construct or a vector control prior to treatment with either DMSO or RSL3 for 2 h. These cells were then immunostained using antibodies specific for ferritin heavy chain (green) and prominin2 (red). Scale bar, 10 μm. Shown are representative images of three independent experiments.

(D) MCF10A cells were transfected with either control siRNA or ferritin heavy chain siRNA for 48 h and then treated with increasing concentrations of RSL3 for 24 h, and the percent of surviving cells was quantified. Shown is representative experiment of three independent replicates.

(E) Hs578t cells were transfected with either control siRNA or ferritin heavy chain siRNA for 48 h and then treated with increasing concentrations of RSL3 for 24 h, and the percent of surviving cells was quantified. Shown is representative experiment of three independent replicates.

(F) MCF10A and Hs578t cells were transfected with either control siRNA or ferritin siRNA for 48 h and then treated with increasing concentrations of either DMSO, RSL3 and ferrostatin-1, or RSL3 and deferoxamine (DFO) for 24 h. The percent of surviving cells was then quantified. Shown is a representative experiment of three independent replicates.

CellPress
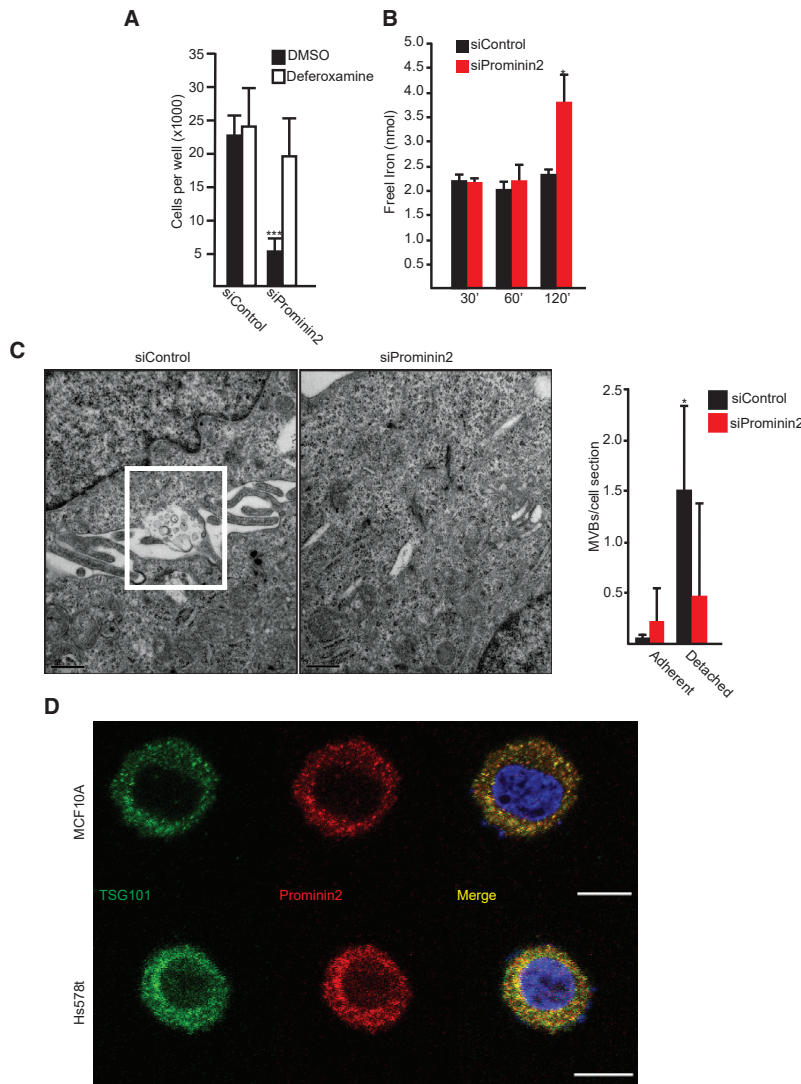
Figure 7. Detachment from the Extracellular Matrix Induces Prominin2-Dependent MVB Formation to Rescue Ferroptosis

(A) Control and prominin2-depleted MCF10A cells were maintained in ECM-detached conditions for 24 h in the presence of either DMSO or deferoxamine and the number of viable cells was quantified. Shown is a representative experiment of three independent replicates.

(B) Control and prominin2-depleted MCF10A cells were maintained in ECM-detached conditions for the indicated times and total free iron was quantified. Shown is a representative experiment of three independent replicates.

(C) Control and prominin2-depleted MCF10A cells were maintained in ECM-detached conditions for 2 h and processed for TEM. The frequency of MVBs (white box) per section was quantified (right graph). Shown is a representative image of five total cells quantified per group.

(D) MCF10A and Hs578t cells were maintained in ECM-detached conditions for 2 h, fixed, and immunostained for TSG101 (green) and prominin2 (red). Scale bar, 10 μm. Shown are representative images of three independent experiments.

STAR★METHODS

Detailed methods are provided in the online version of this paper and include the following:

- KEY RESOURCES TABLE
- LEAD CONTACT AND MATERIALS AVAILABILITY
- EXPERIMENTAL MODEL AND SUBJECT DETAILS
- METHODS DETAILS
  - Cell-Based Assays
  - Biochemical Experiments
  - Molecular Biology Experiments
  - Immunofluorescence Microscopy
  - Exosome Isolation
  - Transmission Electron Microscopy
- QUANTIFICATION AND STATISTICAL ANALYSIS
- DATA AND CODE AVAILABILITY

SUPPLEMENTAL INFORMATION

Supplemental Information can be found online at https://doi.org/10.1016/j.devcel.2019.10.007.

AUTHOR CONTRIBUTIONS

C.W.B. and A.M.M. conceived the study, designed experiments, and wrote the manuscript. C.W.B. performed most of the experiments. J.J.A., P.C., and A.L.E. contributed to specific experiments. L.J.Z. performed bioinformatic

analysis of RNA-sequencing data. C.E.B. assisted with immunofluorescence imaging. S.J.D. provided critical input into the study and manuscript.

DECLARATION OF INTERESTS

The authors declare no competing interests.

REFERENCES

Agmon, E., Solon, J., Bassereau, P., and Stockwell, B.R. (2018). Modeling the effects of lipid peroxidation during ferroptosis on membrane properties. Sci. Rep. 8, 5155.

Brown, C.W., Amante, J.J., Goel, H.L., and Mercurio, A.M. (2017). The α6β4 integrin promotes resistance to ferroptosis. J. Cell Biol. 216, 4287–4297.

Brown, C.W., Amante, J.J., and Mercurio, A.M. (2018). Cell clustering mediated by the adhesion protein PVRL4 is necessary for α6β4 integrin-promoted ferroptosis resistance in matrix-detached cells. J. Biol. Chem. 293, 12741–12748.

Cella, N., Cornejo-Uribe, R.R., Montes, G.S., Hynes, N.E., and Chammas, R. (1996). The lysosomal-associated membrane protein LAMP-1 is a novel differentiation marker for HC11 mouse mammary epithelial cells. Differentiation 61, 113–120.

Dixon, S.J., Lemberg, K.M., Lamprecht, M.R., Skouta, R., Zaitsev, E.M., Gleason, C.E., Patel, D.N., Bauer, A.J., Cantley, A.M., Yang, W.S., et al. (2012). Ferroptosis: an iron-dependent form of nonapoptotic cell death. Cell 149, 1060–1072.

Dixon, S.J., Patel, D.N., Welsch, M., Skouta, R., Lee, E.D., Hayano, M., Thomas, A.G., Gleason, C.E., Tatonetti, N.P., Slusher, B.S., et al. (2014). Pharmacological inhibition of cystine–glutamate exchange induces endoplasmic reticulum stress and ferroptosis. Elife 3, e02523.

Dixon, S.J., and Stockwell, B.R. (2019). The hallmarks of ferroptosis. Annu. Rev. Cancer Biol. 3, 35–54.

Do Van, B., Gouel, F., Jonneaux, A., Timmerman, K., Gelé, P., Pétrault, M., Bastide, M., Laloux, C., Moreau, C., Bordet, R., et al. (2016). Ferroptosis, a newly characterized form of cell death in Parkinson's disease that is regulated by PKC. Neurobiol. Dis. 94, 169–178.

Doll, S., Proneth, B., Tyurina, Y.Y., Panzilius, E., Kobayashi, S., Ingold, I., Irmler, M., Beckers, J., Aichler, M., Walch, A., et al. (2017). ACSL4 dictates ferroptosis sensitivity by shaping cellular lipid composition. Nat. Chem. Biol 13, 91–98.

Fang, X., Wang, H., Han, D., Xie, E., Yang, X., Wei, J., Gu, S., Gao, F., Zhu, N., Yin, X., et al. (2019). Ferroptosis as a target for protection against cardiomyopathy. Proc. Natl. Acad. Sci. USA 116, 2672–2680.

Felder, S., Miller, K., Moehren, G., Ullrich, A., Schlessinger, J., and Hopkins, C.R. (1990). Kinase activity controls the sorting of the epidermal growth factor receptor within the multivesicular body. Cell 61, 623–634.

Florek, M., Bauer, N., Janich, P., Wilsch-Braeuninger, M., Fargeas, C.A., Marzesco, A.M., Ehninger, G., Thiele, C., Huttner, W.B., and Corbeil, D. (2007). Prominin-2 is a cholesterol-binding protein associated with apical and basolateral plasmalemmal protrusions in polarized epithelial cells and released into urine. Cell Tissue Res. 328, 31–47.

Friedmann Angeli, J.P., Schneider, M., Proneth, B., Tyurina, Y.Y., Tyurin, V.A., Hammond, V.J., Herbach, N., Aichler, M., Walch, A., Eggenhofer, E., et al. (2014). Inactivation of the ferroptosis regulator Gpx4 triggers acute renal failure in mice. Nat. Cell Biol. 16, 1180–1191.

Futter, C.E., Pearse, A., Hewlett, L.J., and Hopkins, C.R. (1996). Multivesicular endosomes containing internalized EGF-EGF receptor complexes mature and then fuse directly with lysosomes. J. Cell Biol. 132, 1011–1023.

Gao, M., Monian, P., Pan, Q., Zhang, W., Xiang, J., and Jiang, X. (2016). Ferroptosis is an autophagic cell death process. Cell Res. 26, 1021–1032.

Geng, N., Shi, B.J., Li, S.L., Zhong, Z.Y., Li, Y.C., Xua, W.L., Zhou, H., and Cai, J.H. (2018). Knockdown of ferroportin accelerates erastin-induced ferroptosis in neuroblastoma cells. Eur. Rev. Med. Pharmacol. Sci. 22, 3826–3836.

Gruenberg, J., and Maxfield, F.R. (1995). Membrane transport in the endocytic pathway. Curr. Opin. Cell Biol. 7, 552–563.

Hangauer, M.J., Viswanathan, V.S., Ryan, M.J., Bole, D., Matov, A., Galeas, J., Dhruv, H.D., Berens, M.E., Schreiber, S.L., McCormick, F., and McManus, M.T. (2017). Drug-tolerant persister cancer cells are vulnerable to GPX4 inhibition. Nature 551, 247–250.

Harding, C., Heuser, J., and Stahl, P. (1984). Endocytosis and intracellular processing of transferrin and colloidal gold-transferrin in rat reticulocytes: demonstration of a pathway for receptor shedding. Eur. J. Cell Biol. 35, 256–263.

Hart, P.D., and Young, M.R. (1991). Ammonium chloride, an inhibitor of phagosome-lysosome fusion in macrophages, concurrently induces phagosome-endosome fusion, and opens a novel pathway: studies of a pathogenic mycobacterium and a nonpathogenic yeast. J. Exp. Med. 174, 881–889.

Hirschhorn, T., and Stockwell, B.R. (2019). The development of the concept of ferroptosis. Free Radic. Biol. Med. 133, 130–143.

Hou, W., Xie, Y., Song, X., Sun, X., Lotze, M.T., Zeh, H.J., 3rd, Kang, R., and Tang, D. (2016). Autophagy promotes ferroptosis by degradation of ferritin. Autophagy 12, 1425–1428.

Jászai, J., Farkas, L.M., Fargeas, C.A., Janich, P., Haase, M., Huttner, W.B., and Corbeil, D. (2010). Prominin-2 is a novel marker of distal tubules and collecting ducts of the human and murine kidney. Histochem. Cell Biol. 133, 527–539.

Jiang, L., Kon, N., Li, T., Wang, S.J., Su, T., Hibshoosh, H., Baer, R., and Gu, W. (2015). Ferroptosis as a p53-mediated activity during tumour suppression. Nature 520, 57–62.

Kobuna, H., Inoue, T., Shibata, M., Gengyo-Ando, K., Yamamoto, A., Mitani, S., and Arai, H. (2010). Multivesicular body formation requires OSBP-related proteins and cholesterol. PLoS Genet. 6, e1001055.

Ma, S., Henson, E.S., Chen, Y., and Gibson, S.B. (2016). Ferroptosis is induced following siramesine and lapatinib treatment of breast cancer cells. Cell Death Dis. 7, e2307.

Magtanong, L., Ko, P.J., To, M., Cao, J.Y., Forcina, G.C., Tarangelo, A., Ward, C.C., Cho, K., Patti, G.J., Nomura, D.K., et al. (2019). Exogenous monounsaturated fatty acids promote a Ferroptosis-resistant cell state. Cell Chem. Biol. 26, 420–432.

Pan, B.T., Teng, K., Wu, C., Adam, M., and Johnstone, R.M. (1985). Electron microscopic evidence for externalization of the transferrin receptor in vesicular form in sheep reticulocytes. J. Cell Biol. 101, 942–948.

Raposo, G., and Stoorvogel, W. (2013). Extracellular vesicles: exosomes, microvesicles, and friends. J. Cell Biol. 200, 373–383.

Razi, M., and Futter, C. (2006). Distinct roles for Tsg101 and Hrs in multivesicular body formation and inward vesiculation. Mol. Biol. Cell 8, 3469–3483.

Saha, S.K., Islam, S.M.R., Kwak, K.S., Rahman, M.S., and Cho, S.G. (2019). PROM1 and PROM2 expression differentially modulates clinical prognosis of cancer: a multiomics analysis. Cancer Gene Ther. https://doi.org/10.1038/s41417-019-0109-7.

Shimada, K., Skouta, R., Kaplan, A., Yang, W.S., Hayano, M., Dixon, S.J., Brown, L.M., Valenzuela, C.A., Wolpaw, A.J., and Stockwell, B.R. (2016). Global survey of cell death mechanisms reveals metabolic regulation of ferroptosis. Nat. Chem. Biol. 12, 497–503.

Singh, R.D., Schroeder, A.S., Scheffer, L., Holicky, E.L., Wheatley, C.L., Marks, D.L., and Pagano, R.E. (2013). Prominin-2 expression increases protrusions, decreases caveolae and inhibits Cdc42 dependent fluid phase endocytosis. Biochem. Biophys. Res. Commun. 434, 466–472.

Stockwell, B.R., Friedmann Angeli, J.P., Bayir, H., Bush, A.I., Conrad, M., Dixon, S.J., Fulda, S., Gascón, S., Hatzios, S.K., Kagan, V.E., et al. (2017). Ferroptosis: a regulated cell death nexus linking metabolism, redox biology, and disease. Cell 171, 273–285.

Torii, S., Shintoku, R., Kubota, C., Yaegashi, M., Torii, R., Sasaki, M., Suzuki, T., Mori, M., Yoshimoto, Y., Takeuchi, T., et al. (2016). An essential role for functional lysosomes in ferroptosis of cancer cells. Biochem. J. 473, 769–777.

Torti, S.V., Manz, D.H., Paul, B.T., Blanchette-Farra, N., and Torti, F.M. (2018). Iron and Cancer. Annu. Rev. Nutr. 21, 97–125.

Truman-Rosentsvit, M., Spektor, B.D.L., Cohen, L.A., Belizowsky-Moshe, S., Lifshitz, L., Ma, J., Li, W., Kesselman, E., Abutbul-Ionita, I., et al. (2018). Ferritin is secreted via two distinct non-classical vesicular pathways. Blood 131, 342–352.

Tsoi, J., Robert, L., Paraiso, K., Galvan, C., Sheu, K.M., Lay, J., Wong, D.J.L., Atefi, M., Shirazi, R., Wang, X., et al. (2018). Multi-stage differentiation defines melanoma subtypes with differential vulnerability to drug-induced iron-dependent oxidative stress. Cancer Cell 33, 890–904.

Viswanathan, V.S., Ryan, M.J., Dhruv, H.D., Gill, S., Eichhoff, O.M., Seashore-Ludlow, B., Kaffenberger, S.D., Eaton, J.K., Shimada, K., Aguirre, A.J., et al. (2017). Dependency of a therapy-resistant state of cancer cells on a lipid peroxidase pathway. Nature 547, 453–457.

Weïwer, M., Bittker, J.A., Lewis, T.A., Shimada, K., Yang, W.S., MacPherson, L., Dandapani, S., Palmer, M., Stockwell, B.R., and Schreiber, S.L. (2012). Development of small-molecule probes that selectively kill cells induced to express mutant RAS. Bioorg. Med. Chem. Lett. 22, 1822–1826.

Yang, W.S., Kim, K.J., Gaschler, M.M., Patel, M., Shchepinov, M.S., and Stockwell, B.R. (2016). Peroxidation of polyunsaturated fatty acids by lipoxygenases drives ferroptosis. Proc. Natl. Acad. Sci. USA 113, E4966–E4975.

Yang, W.S., SriRamaratnam, R., Welsch, M.E., Shimada, K., Skouta, R., Viswanathan, V.S., Cheah, J.H., Clemons, P.A., Shamji, A.F., Clish, C.B., et al. (2014). Regulation of ferroptotic cancer cell death by GPX4. Cell 156, 317–331.

Yang, W.S., and Stockwell, B.R. (2008). Synthetic lethal screening identifies compounds activating iron-dependent, nonapoptotic cell death in oncogenic-RAS-harboring cancer cells. Chem. Biol. 15, 234–245.

Yang, W.S., and Stockwell, B.R. (2016). Ferroptosis: death by lipid peroxidation. Trends Cell Biol. 26, 165–176.

Zhang, Y., Tan, H., Daniels, J.D., Zandkarimi, F., Liu, H., Brown, L.M., Uchida, K., O'Connor, O.A., and Stockwell, B.R. (2019). Imidazole ketone erastin induces ferroptosis and slows tumor growth in a mouse lymphoma model. Cell Chem. Biol. 26, 623–633.

CellPress

STAR★METHODS

KEY RESOURCES TABLE

REAGENT or RESOURCE	SOURCE	IDENTIFIER
Antibodies		
Prominin2, Rabbit Polyclonal	Abcam	Cat#ab74977; Lot GR182311-23
Tubulin, Mouse Monoclonal	Sigma-Aldrich	Cat#T5168; Lot 038M4813V; RRID: AB_477579
TSG101, Mouse Monoclonal	Genetex	Cat#GTX70255; Clone: 4A10; Lot 43353; RRID: AB_373239
Ferritin Heavy Chain (FTH1), Rabbit Monoclonal	Thermo Fisher	Cat#701934; Lot 2010234; RRID: AB_2633038
Ferritin Light Chain (FTL), Rabbit Polyclonal	Abcam	Cat#ab69090; RRID: AB_1523609
Catalase, Mouse Monoclonal	Abcam	Cat#ab110292; Lot GR107615-C; RRID: AB_10859065
Phospho-Caveolin1, Mouse Monoclonal	Santa Cruz Biotechnology	Cat#sc-373837; RRID: AB_10988387
Rab5A, Rabbit Polyclonal	Santa Cruz Biotechnology	Cat#sc-46692; Clone D-11; Lot D0518; RRID: AB_628191
LC3, Mouse Monoclonal	MBL International	Cat#M152-3; RRID: AB_1279144
LAMP1, Mouse Monoclonal	R&D Systems	Cat#MAB4800; RRID: AB_10719137
Alexa Fluor® 488 Goat Anti-Mouse	BioLegend	Cat#405319; RRID: AB_2563044
Alexa Fluor® 555 Donkey Anti-Rabbit	BioLegend	Cat#406412; RRID: AB_2563181
ALIX, Mouse Monoclonal	Abcam	Cat#ab117600; RRID: AB_10899268
NCOA4, Mouse Monoclonal	Sigma-Aldrich	Cat#SAB1404569-100UG; RRID: AB_10759525
Ferroportin/SLC40A1, Mouse Monoclonal	Novus Biologicals	Cat# NBP2-45357SS; RRID: AB_1215496
CD63, Rabbit Monoclonal	Abcam	Cat#ab217345; RRID: AB_2754982
Chemicals, Peptides, and Recombinant Proteins		
MitoTracker	Thermo Fisher	Cat#M7512
RSL3	SelleckChem	Cat#S8155
FIN56	SelleckChem	Cat#S8254
ML210	Sigma-Aldrich	Cat#SML0521
Erastin	SelleckChem	Cat#S7242
Ferrostatin-1	Sigma-Aldrich	Cat#SML0583
ZVAD-FMK	SelleckChem	Cat#S7023
GW4869	Sigma-Aldrich	Cat#D1692
Deferoxamine (DFO)	Sigma-Aldrich	Cat#D9533
Lipofectamine 3000	Thermo Fisher	Cat#L3000008
0.1% Triton	JT Baker	Cat#X198-05
Bovine Serum Albumin	MilliporeSigma	Cat#A7906
4% Paraformaldehyde	Boston Bioproducts	Cat#BM-155
RIPA Lysis Buffer	Boston Bioproducts	Cat#BP-115
Vectashield Antifade with DAPI	Vector Labs	Cat#H-1200
Crystal Violet	Fisher Scientific	Cat#C581
DMSO	Fisher Scientific	Cat#BP231
G418	Gibco	Cat#10131035
60-mm Low Attachment Plates	S-Bio	Cat#MS-9035xz
Ammonium Chloride	MilliporeSigma	Cat#A-0171

(Continued on next page)

Continued

REAGENT or RESOURCE	SOURCE	IDENTIFIER
Critical Commercial Assays		
Iron Assay	Abcam	Cat#ab83366
Bradford Assay	Bio-Rad	Cat#5000006
Deposited Data		
MCF10A RNAseq	GEO	GSE115059
Experimental Models: Cell Lines		
Human Normal Mammary Epithelial, MCF10A	Barbara Ann Karmanos Cancer Institute	N/A
Human Triple Negative Breast Carcinoma, Hs578T	Laboratory of Dr. Dohoon Kim (University of Massachusetts Medical School)	N/A
Human Triple Negative Breast Carcinoma, MDA-MB-231	ATCC	Cat# HTB-26
Experimental Models: Organisms/Strains		
Escherichia coli Competent Cells	Promega	Cat#L2005
Oligonucleotides		
Custom *18s*	Forward 5′-AACCCGTTGAACCCCATT-3′, Reverse 5′-CCATCCAATCGGTAGTAGCG-3′	N/A
Custom *Prom2*	Forward 5′- GCTCAGGAACCCAAACCTGT-3′, Reverse 5′- GGCAGGCCATACATCCTTCT-3′	N/A
Custom *Prom1*	Forward 5′- AGTCGGAAACTGGCAGATAGC-3′, Reverse 5′- GGTAGTGTTGTACTGGGCCAAT-3′	N/A
Prom2 siRNA	Santa Cruz Biotechnology	Cat#sc-94521
TSG101 siRNA	Santa Cruz Biotechnology	Cat#sc-36752
FTL siRNA	Santa Cruz Biotechnology	Cat#sc-40577
FTH1 siRNA	Santa Cruz Biotechnology	Cat#sc-40575
Recombinant DNA		
pRP[Exp]-EGFP/Neo-CMV>hPROM2 [NM_001165978.2]	Vectorbuilder	N/A
Exosome Cyto-Tracer, PCT-CD63-GFP	System Biosciences	Cat#CYTO120-VA-1
Software and Algorithms		
GraphPad Prism	GraphPad Software	https://www.graphpad.com/scientific-software/prism/
Other		
DMEM High Glucose Media	Gibco	Cat#11965118
DMEM/F:12 Media	Gibco	Cat#11320082
8 Well Chamber Slides	Mattek	Cat#CCS-8
Cholera Toxin	MilliporeSigma	Cat#C8052
EGF	Peprotech	Cat#AF-100-15
Hydrocortisone	MilliporeSigma	Cat#H4001
Insulin	MilliporeSigma	Cat#I5500
0.5 % Trypsin-EDTA (10x)	Gibco	Cat#15400-54

LEAD CONTACT AND MATERIALS AVAILABILITY

Further information and requests for resources and reagents should be directed to and will be fulfilled by the Lead Contact, Arthur Mercurio (arthur.mercurio@umassmed.edu).

EXPERIMENTAL MODEL AND SUBJECT DETAILS

MCF10A cells were obtained from the Barbara Ann Karmanos Cancer Institute. Hs578T cells were provided by Dr. Dohoon Kim (UMASS Medical School). MDA-MB-231 cells were obtained from the American Type Culture Collection. All cells were checked quarterly for mycoplasma and authenticated using the University of Arizona Genetics Core.

METHODS DETAILS

Cell-Based Assays

Assays to assess survival in response to matrix detachment were performed as described (Brown et al., 2017). To assay survival in response to GPX4 inhibition, adherent cells in 96 well plates (1.0×10^4 per well) were treated with either DMSO, RSL3, ML210, FIN56 or erastin for 24 hrs with and without ferrostatin-1 or DFO. Subsequently, cells were fixed in 4% paraformaldehyde, stained with crystal violet and read on a microplate reader at absorbance 595. Absorbances were normalized to DMSO.

Biochemical Experiments

Immunoblotting and qPCR were performed as described (Brown et al., 2017). Sequences for primers used were as follows: 18s Forward 5′-AACCCGTTGAACCCCATT-3′, Reverse 5′-CCATCCAATCGGTAGTAGCG-3′, PROM2 Forward 5′- GCTCAGGAACC CAAACCTGT-3′, Reverse 5′- GGCAGGCCATACATCCTTCT-3′, PROM1 Forward 5′- AGTCGGAAACTGGCAGATAGC-3′, Reverse 5′- GGTAGTGTTGTACTGGGCCAAT-3′.

Total free iron was quantified using the Iron Assay Kit per manufacturer's specifications. Briefly, adherent cells in 10 cm plates (1.0×10^6/well) were treated with either DMSO or RSL3 for 2 hrs, lysed and supernatant was reduced using the provided iron reducer before the mixture was reacted with an iron probe. Plates were read at 595 nm and total iron concentration was obtained using an iron standard curve.

Molecular Biology Experiments

siRNA-mediated silencing of gene expression was performed with Lipofectamine 3000 per the manufacturer's guidelines using control, prominin2, *TSG101*, or *FTH1* siRNAs. To express prominin2 in MDA-MB-231 cells, a pCMV-prominin2 expression vector was obtained from VectorBuilder. Cells were transfected with this plasmid and a control plasmid using Lipofectamine 3000 and selected for prominin2 expression with G418 (0.5 μg/mL) for ten days.

Immunofluorescence Microscopy

For adherent cells, 8 well chamber slides were coated with 1 μg/mL laminin. Cells (5.0×10^4 per well) were plated overnight and then treated for 1 h with either DMSO or RSL3, fixed in 4% paraformaldehyde and permeabilized in 0.1% Triton. Slides were blocked in 0.5% BSA, incubated in antibody overnight at 4°C, washed in PBS and incubated in secondary antibody for 1 h at room temperature. Slides were washed and mounted in Vectashield with DAPI. For ECM-detached experiments, cells were trypsinized and plated (5.0×10^5 per well) in 60 mm low-adherent plates for 2 h, collected and spun down prior to being fixed and stained as described above. Slides were imaged on a Zeiss or a Nikon A-1 confocal microscope.

Exosome Isolation

Cells were cultured for 24 h in their respective media containing extracellular vesicle (EV) free serum and treated with RSL3 for 24 h. Culture supernatants were centrifuged at 4°C at 1000 RPM for 5 min, 3000 RPM for 10 min, 4000 RPM for 30 min prior to ultracentrifugation at 22,000 RPM for 140 min at 4°C. Pellets were resuspended in cold PBS and centrifuged again under the same conditions. For immunoblotting, pellets were lysed in RIPA buffer, centrifuged at 10,000 RPM for 15 min and protein concentration was determined by Bradford Assay. For TEM, PBS was removed and 20 μL of the exosome preparation was fixed and processed. For ICP-mass spec, exosome-containing pellet was resuspended in 0.5 mL PBS and centrifuged in a speed-vac at 45°C. Samples were sent to the UMASS mass spectrometry Core where they were digested in 100 μL HNO$_3$, heated to 65°C for 20 min and diluted to 2 mL with ddH$_2$O before analysis.

Transmission Electron Microscopy

Adherent siControl and siProminin2 cells were treated with DMSO or RSL3 (5μM) for 2 h. ECM-detached siControl and siProminin2 cells were maintained for 2 h in low-adherence plates. All cells were fixed by adding 2.5% glutaraldehyde (v/v) in 0.1 M Na cacodylate buffer (pH 7.2) and processed for TEM. The samples were examined on a FEI Tecnai 12 BT transmission electron microscope using 100KV accelerating voltage. Images were captured using a Gatan TEM CCD camera.

QUANTIFICATION AND STATISTICAL ANALYSIS

Statistical comparison between only two groups were done with the unpaired Student's t test. Multiple group comparisons were completed using one-way analysis of variance (ANOVA). Statistical tests were carried out using GraphPad Prism version 8.0 and a p value of less than 0.05 was considered significant. The bars in graphs represent means ± SEM. *, $p < 0.05$; **, $p < 0.01$;

CellPress

***, $p < 0.005$. Three independent experiments were performed for each experiment except for transmission electron microscopy experiments in Figures 3C and 7C which were performed once.

DATA AND CODE AVAILABILITY

The RNA sequencing data are available through the GEO database using the identifier GSE115059. All other data are available by reasonable request.